RIVAS

Railway Induced Vibration Abatement Solutions

Collaborative project

Description of the vibration generation mechanism of turnouts and the development of cost effective mitigation measures

Deliverable D3.6

Submission date: 28/02/2013

Project Coordinator:

Bernd Asmussen

International Union of Railways (UIC)

asmussen@uic.org

Title	Description of the vibration generation mechanism of turnouts and the development of cost effective mitigation measures
Domain	WP 3.3
Date	28.02.2013
Author/Authors	Roger Müller, Brice Nelain, Jens Nielsen, Samir Said, Werner Rücker, Estelle Bongini
Partner	SBB, VTC, Chalmers, BAM, SNCF
Document Code	RIVAS_UIC_ WP3-3_D3_6_V02
Version	2
Status	Final

Dissemination level:

Project co-funded by the European Commission within the Seventh Framework Programme		
Dissemination Level		
PU	Public	X
PP	Restricted to other programme participants (including the Commission Services)	
RE	Restricted to a group specified by the consortium (including the Commission) Services)	
CO	Confidential, only for members of the consortium (including the Commission Services)	

Document history		
Revision	Date	Description
1.4	15/12/2012	First draft
2	28/2/2013	Second draft

EXECUTIVE SUMMARY

Within the frame of the EU FP7 project 'Railway induced vibration abatement solutions (RIVAS)', abatement measures for ground-borne noise and vibrations for tracks at grade are studied. Workpackage 3.3 of RIVAS focuses on railway infrastructure based vibration reduction technologies for curves and turnouts. For the curve three different types of soft under sleeper pads are studied, for the turnout at least two mitigation measures are tested. These two options are studied with measurements for an existing railway line and their effective reduction will be measured in field tests.

The present report is a state-of-the-art of ground borne vibration issues in railway turnouts and describes the possible generation mechanisms and possible cost-effective mitigation measures, some already characterized in terms of insertion loss for ground vibration.

In Chapter 2 of the report, a literature survey based on papers and vibration measurements of SBB is described. The main excitation mechanisms are described and analysed, and ground vibration mitigation measures tested numerically or experimentally are presented. The mitigation measures found in the literature were mainly aimed at reducing the dynamic wheel-rail contact force. From differences in vibration turnout-amplifications it could be concluded that there are possibilities to improve the crossing nose part of a turnout. The wheel transition over a turnout shows that geometry is important for optimum and low energy impacts at the crossing nose. There is an influence of vertical and horizontal geometries.

In Chapter 3 vibration measurement studies on mitigation measures for turnouts are described. So far it is not possible to draw definitive conclusions from the existing tests outside of RIVAS which solution could be a cost-effective mitigation measure for a turnout. A chance to improve the vibration excitation of a turnout lies in softening the USP for better track behavior (unfortunately, it is unclear why softer USP should be better for track geometry than stiffer USP), to improve the turnout design (material and geometry of frog and geometry of turnout) and to soften the rail pad.

In Chapter 4 the first RIVAS test campaign using stiff under sleeper pads for four turnouts and its results (comparison to four normal turnouts) are presented. The vibration measurement results of Le Landeron and even more for Rubigen seem to be influenced by turnout condition and ground condition. The influence is too big to determine effects of USP in the low frequency range. Therefore conclusions cannot be obtained so far: there is a need of properly defining the turnout status that means direct correlations of turnout parameters with vibration emission measurements. A first option could be the DB measurement method for turnout quality, the second is axle box acceleration measurements (see DB measurement car CTM in Chapter 2). In Rubigen a turnout showed low vibration impact on the frog and in total two turnouts showed low turnout-amplification. These could be "ideal" turnouts, but the parameters to result in such an ideal turnout have to be investigated.

In Chapter 5, what appear to be the most promising mitigation measures are presented. The best approach to improve the turnout-amplification is a system-approach where different parameters are

changed and interact in a harmonic way. The SBB innovation “turnout 2015” could be such an approach and should be tested in 2013. From these tests also indications should follow if further improvements are possible and needed for vibration mitigation (such as rail profiles, geometry, soft layers). Another approach could be to find out what is the difference between a good turnout behavior (“ideal turnout”, see Rubigen turnout nr. 11 and 12) and a turnout with high impacts.

It is important to identify the parameters provoking an ideal turnout. Further modeling is needed to understand the wheel transition over the crossing nose and to see geometry parameter effects on this wheel transition. Further tests are needed to define the relevant geometry parameters influencing the turnout-amplification. If an improvement of the interaction of wheel transition and rail geometry can be obtained, then the turnout-amplification as well as the frog maintenance are improved. The following next steps are concluded:

Next steps:

Chalmers will simulate wheel–rail contact forces in turnouts and aim for an optimisation of crossing geometry that is robust for a range of nominal and worn wheel profiles. The magnitude and frequency content of the impact load at the crossing will be investigated. Sleeper velocities and/or forces in discrete springs modelling the ballast/subgrade stiffness could be predicted as an indication of the influence of crossing geometry on ground vibration.

End 2012, SNCF carried out a test campaign on a turnout trying to establish the contribution of each part of the turnout (joints, switch end, frog) and therefore of each excitation mechanism (impact load at the different joints and frog, parametric excitation) to the ground vibration velocity produced in the surrounding ground. First correlations will then be drawn between the excitation mechanisms, the contact force evolution along the turnout and the ground vibrations generated. Some parts of the measurement campaign will also allow validating Chalmers turnout-model. Results are planned to be delivered mid 2013.

The geometry influence on vibration excitation shall be studied for a few interesting turnouts by existing axlebox acceleration measurements over time (some years; SBB or DB has such data). This avoids an influence of differences in ground condition, turnout-type, passby direction, train velocity when looking at time histories. Correlations of the influence of frog geometry (maintenance status) with accelerations of wheelsets should be elaborated.

The new mitigation measure (SBB “Turnout 2015”) which is recently installed in Wichtrach between Bern and Thun shall be validated by ground vibration measurements if axlebox measurements in Spring 2013 indicate a positive geometry in comparison to normal turnouts on the same line.

TABLE OF CONTENTS

1. INTRODUCTION

It is the aim of the EU to have cost effective mitigation measures for as many people as possible for vibration protection. Because of the additional vibration impact, turnouts are a problem in the vicinity of populated areas. Often they are the cause to exceed limit values. A study of complaints at SBB showed that around 32% of all complaints in terms of vibration are due to turnouts (new and old ones). Until now, there is a lack of international studies about causes of vibration at switches as well as their mitigation measures.

There is no existing model in use to assess vibrations caused by a train running over a turnout. Modelling of a turnout is difficult because a turnout is a special inhomogeneous object (point source) which shows a disturbed overrun by a wheelset.

It is difficult to find cost-effective mitigation measures because the problem for turnouts can often be found in the frequency range of 16 Hz to 31 Hz and most of the mitigation measures (as under ballast mats, soft under sleeper pads) mitigate higher frequencies (normally higher than 40 Hz). Turnouts normally cause higher vibration levels by a factor of about 2 compared to a straight line situation.

The turnout vibration emissions also normally increase on the long-term because of degradation of the maintenance status. So far it is not known how to characterize a turnout with respect to vibration emissions. This question will be discussed in WP2.

For the last 15 years, SBB did not find a cost-effective vibration mitigation measure. Today, SBB is still running a test of hard under sleeper pads (USP) which have the potential as a cost-effective mitigation measure. The first results measured before the RIVAS Project showed promising results.

In the first part of the RIVAS turnout project, additional test sites of turnouts with USP and reference turnouts (without USP) were measured to validate the mitigation effect and to improve the understanding of turnout emissions.

In this report a State of the Art is given in Chapter 2. Tests of mitigation measures for turnouts will be summarized in Chapter 3. These two chapters summarize the knowledge before the RIVAS project. Chapter 4 will show the results so far from RIVAS from measurements at 8 turnouts in Switzerland which gives a hint of the influence of under sleeper pads as a mitigation measure and shows 8 turnouts and their turnout-amplification. Chapter 5 will show the most promising mitigation measures. Some of them will be studied in the next phase of this RIVAS-project. This report builds up the basis to decide upon the future mitigation measures to be tested and which measurements should be used to characterize the turnout.

The SNCF is carrying out a measurement campaign, at the end of 2012, on a turnout to establish correlation between turnout parameters and vibrations and also to provide input for numerical simulations. It would therefore be possible to correlate interaction force to ground borne vibration and then give instructions for the development of dedicated mitigation measures.

The strategy for assessing the effect of turnouts and their mitigation measures on the vibration level and to optimize the switch measures is presented in the Figure 1.1 below.

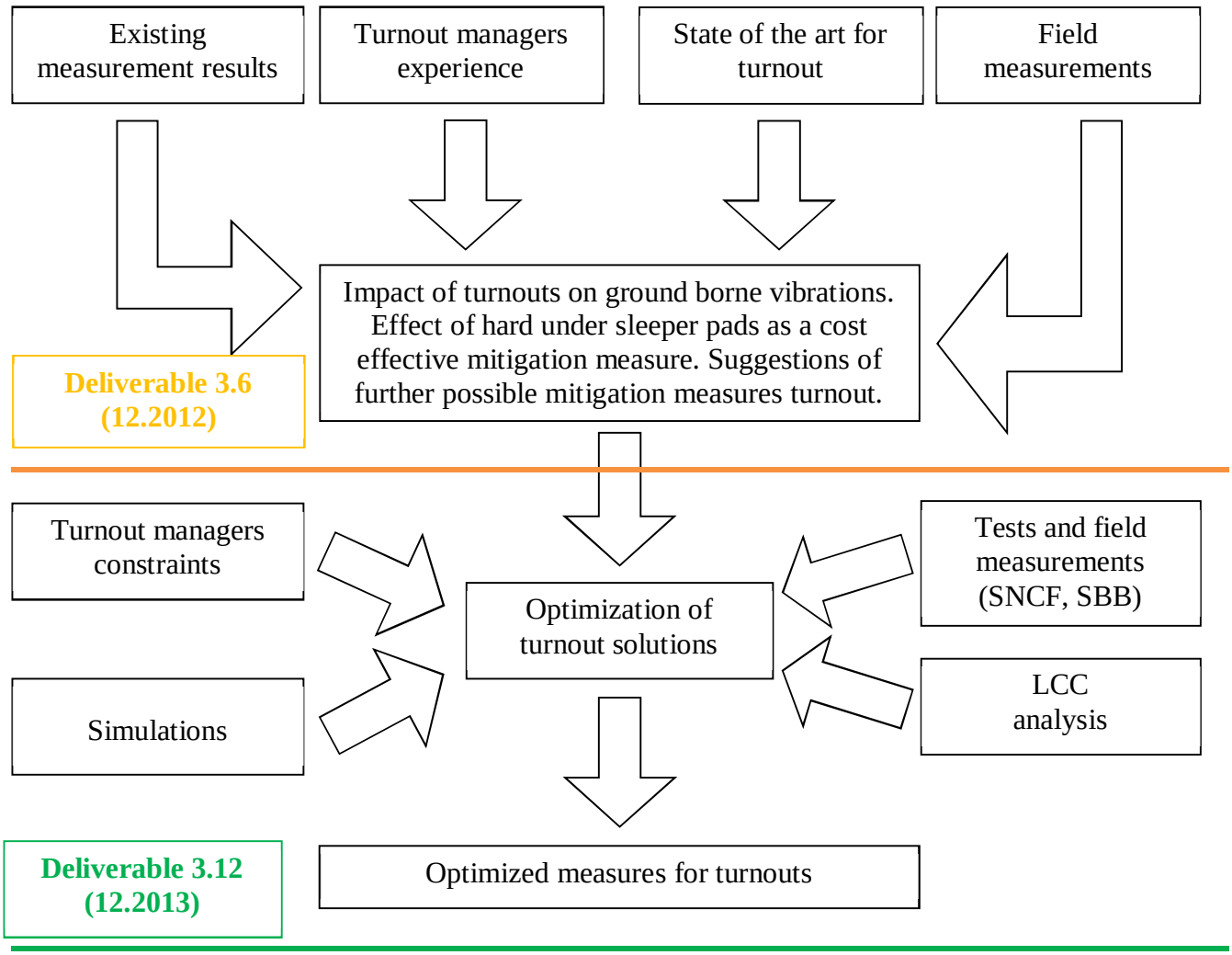

Figure 1.1: Strategie for WP3.3 turnout project.

2. LITERATURE SURVEY

Most of the inputs used to compile this state-of-the-art come from the INNOTRACK EU FP6-project and SBB previous tests. Some papers on modelling of turnout excitation mechanism can be found as well as a few mitigation measures for a turnout (Austria, Belgium). Numerical models were developed to compute the contact force at the wheel-rail interaction point, but at the moment no model to predict ground vibration induced by a turnout including soil was developed.

This literature review starts with general description of a turnout and how it can be described as source of excitation for ground-borne vibration. In fact, several mechanisms of excitation are involved in the generation of vibrations due to a turnout. The studies presented in this chapter do not contain vibration mitigation measurements. For this analysis see Chapter 3.

2.1 TURNOUT DESCRIPTION

Switches & crossings (S&Cs, turnouts) contain a switch panel and a crossing panel that are connected by a closure panel, see Figure 2.1. Dynamic interaction between vehicle and track is more complex in S&Cs than on tangent or curved tracks. For example, wheel–rail impact loads with large magnitudes and significant contributions from high-frequency vehicle–track interaction are generated when the nominal wheel–rail contact conditions are disturbed at various locations in the S&C, such as at wheel transfer from wing rail to crossing nose [1] (facing direction). The impact load at the crossing may be a significant source to ground vibration and noise.

The switch panel and the crossing panel are the most important for ground vibration as they feature changes in rail cross-section, track curvature, track irregularities and track stiffness variations [2].

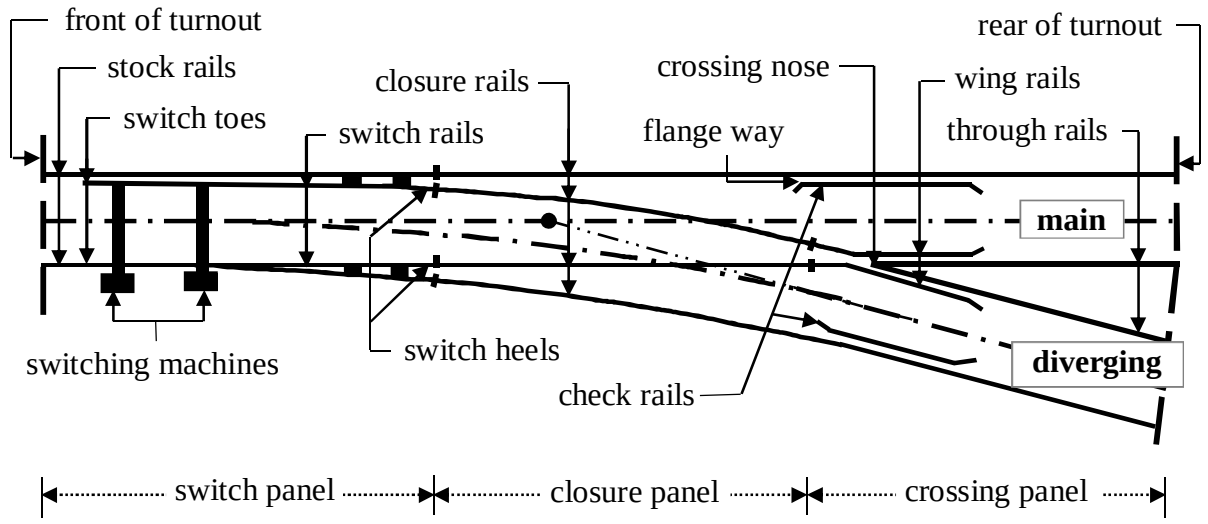

Figure 2.1: Components of an S&C with main (through) and diverging routes. From [1]

2.2 SCHEMATIC DESCRIPTIONS OF WHEEL TRANSITION OF CROSSING/SWITCH

It is important to explain the wheel transition in connection with vibration turnout-amplifications see [3] and partially [4]. The following explanations in this chapter show in detail the transition of a wheel over a frog with a fixed frog to explain the turnout-amplification. Further details of wheel transition for a flexible frog can be found in [3]. An overview is given in [5].

2.2.1 Schematic Crossing Nose Layout, Wheel Profile, Rail Profile

The following layout (Figure 2.2) is the basis structure of a frog. For the frog with fixed point there is a need for channels to have an undisturbed wheel transition but show interruption in the rail bearing surface and in the gauge line (running edge).

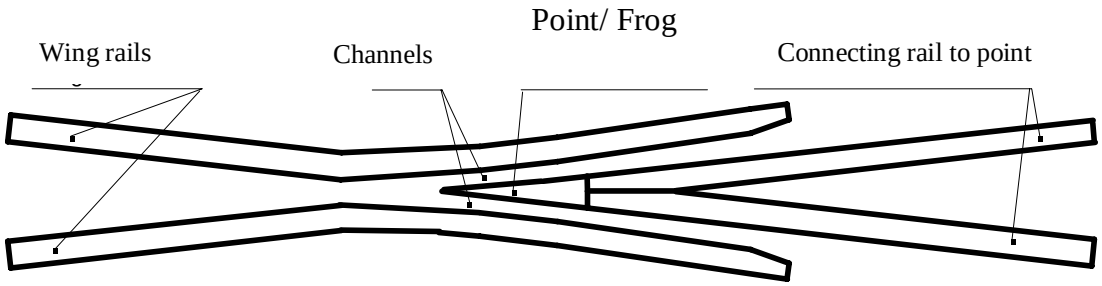

Figure 2.2: Layout for crossing nose with fixed frog.

For the following explanations it is taken as a basis (see Figure 2.3):

- Frog and form of rail head are considered as newly installed
- Wheel profile corresponds to a new wheel and worn (hollow)
- Train direction is against the frog (from left to right).

Not every possible wheel transition is covered.

On the one hand the rail head worn is not included for simplicity. It is the case for longer radius turnouts where nearly only vertical wear of rail head form occurs, which is not big, so no big influence on vibration emission is assumed.

On the other hand the wheel transition in the other direction is not shown, as the influence for vibration and noise has similar amplitudes as for the direction to the frog.

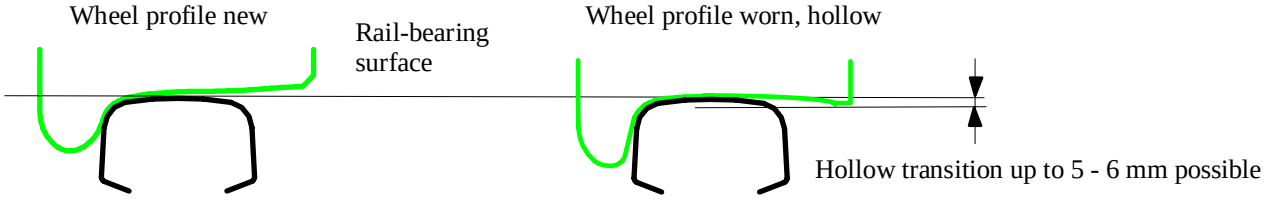

Figure 2.3: Wheel profile new and worn

Figure 2.3 shows the wheel profile new and worn/hollow with new rail head form. For the worn, hollow wheel profile it is especially important for the wheel transition that the tread surface can be 5 – 6 mm below the rail bearing surface.

2.2.2 Wheel Transition for the Frog

In Figure 2.4 it can be seen on the sketch on top that the point (frog) is dropping. In the sketch below different positions of a wheel transition over a turnout are defined.

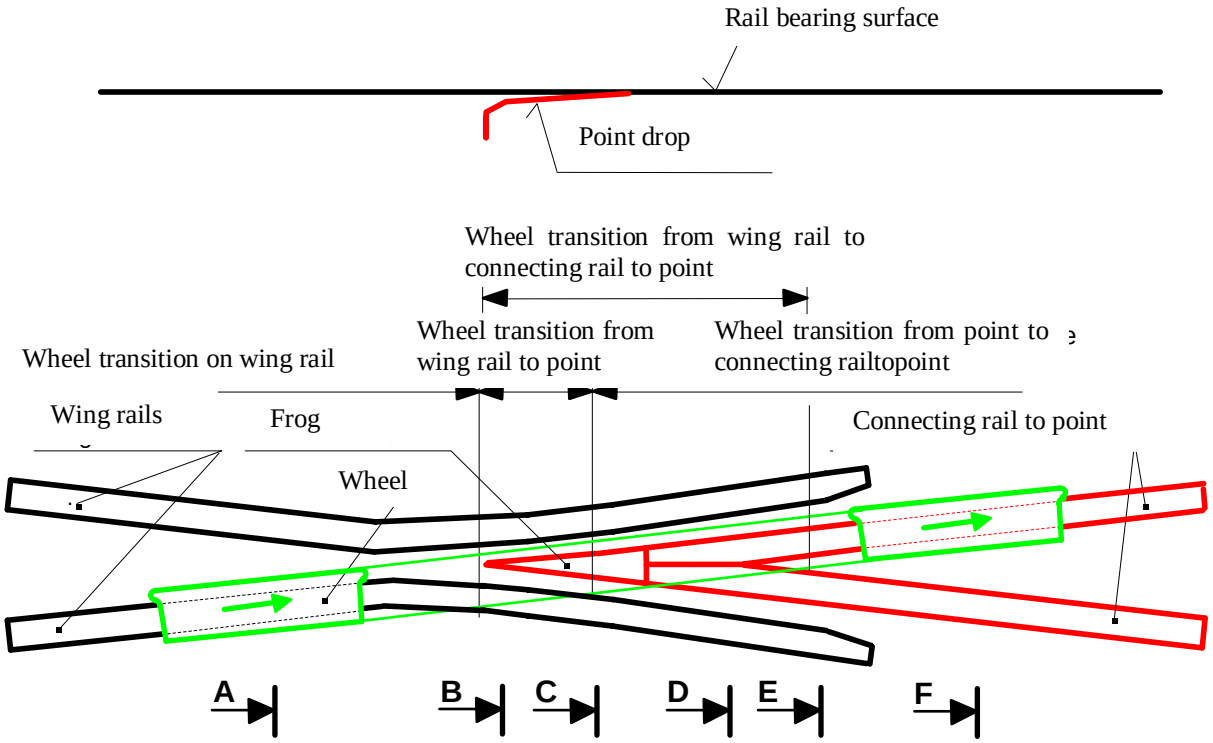

Figure 2.4: Switch nose with fixed frog

Section A in Figure 2.5 shows the position of the wheel on the wing rails, before the wheel transition from the wing rail on the frog. The situation for a new and a worn/hollow wheel profile are optimum and nearly identical that means no relevant difference in vibration excitation for these wheel profiles.

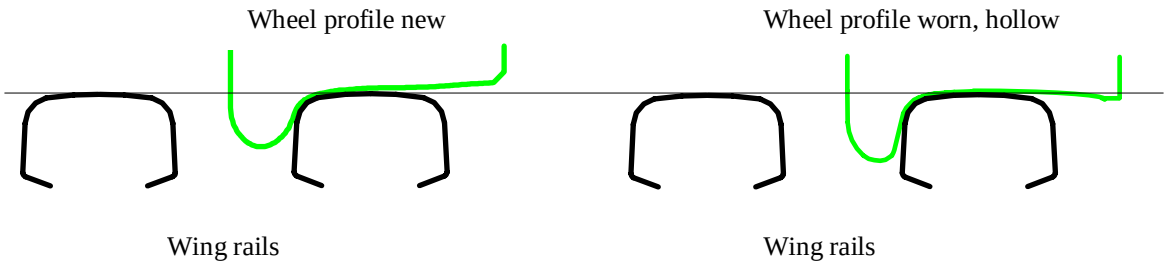

Figure 2.5: Section A

Section B shows the position of the wheel in the transition from wing rail to frog. During this transition the wheel has to pass the channel (see Figure 2.2), which implies an impact. **The new wheel profile is supported by the wing rail and, with a point thickness of about 20 mm, some part is taken by the frog.** The worn/hollow wheel profile is supported only by the wing rail and is vertically moving (up and down) dependent on the degree of the hollowness because the wheel has a horizontal movement over the wing rail (the wing rail is not straight here). The situation of the worn/hollow wheel on the rail is not ideal and this is the case until and including section E!

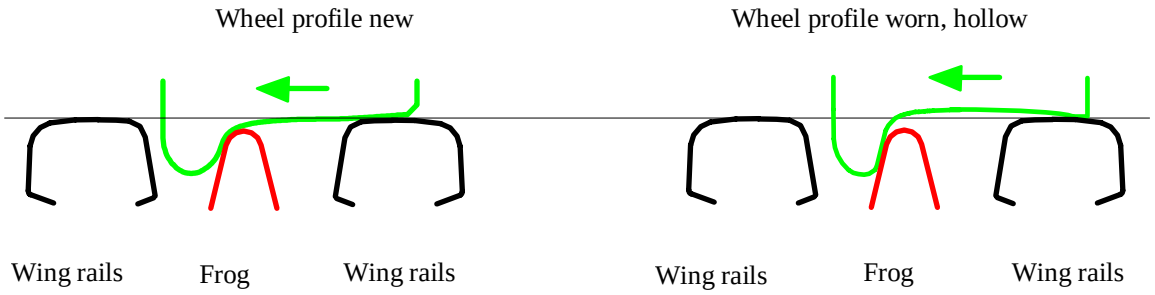

Figure 2.6: Section B

Section C shows the position of the wheel at the end of the transition from wing rail to frog. For the new wheel profile the wheel transition is already finished. For the worn/hollow wheel profile the wheel transition is in the final phase. The wheel profile is lifted and will fall with an impact after further horizontal movement.

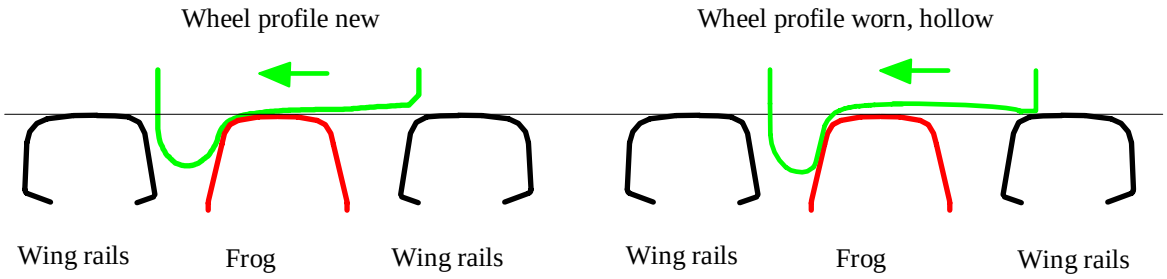

Figure 2.7: Section C

Section D shows the position of the wheel on the connecting rail to point. The new wheel profile is fully running on the left connecting rail to point. The worn/hollow wheel profile is lifted on the right connecting rail to point and runs in the further transition transversal over the connecting rails to point with additional vertical movements.

Figure 2.8: Section D

Section E shows the position of the wheel on the connecting rail to point. The new wheel profile is fully running on the left connecting rail to point. The worn/hollow wheel profile has been lifted up by running over the right connecting rail to point and falls with an impact on the left connecting rail to point.

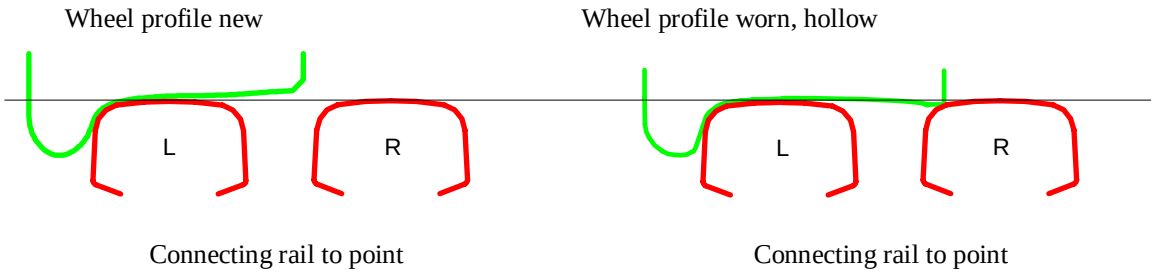

Figure 2.9: Section E

Section F shows the position of the wheel on the left connecting rail to point after crossing the right connecting rail to point. The situation for a new and a worn/hollow wheel profile are optimum and nearly identical.

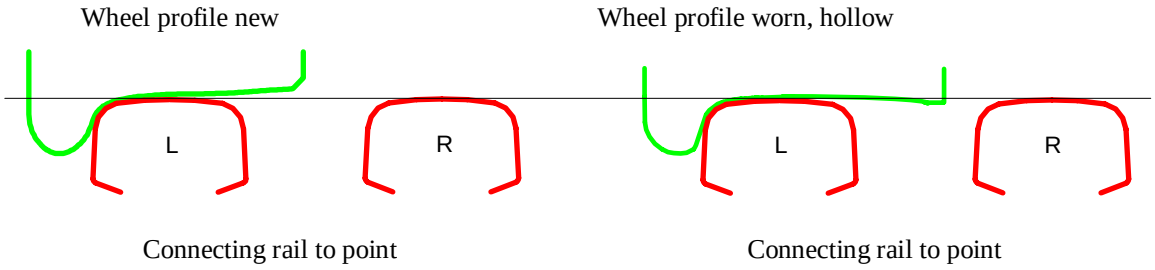

Figure 2.10: Section F

2.2.3 Wheel Transition for the Switch Part

A sketch of a wheel transition over the switch part of a turnout is shown in Figure 2.11 [4].

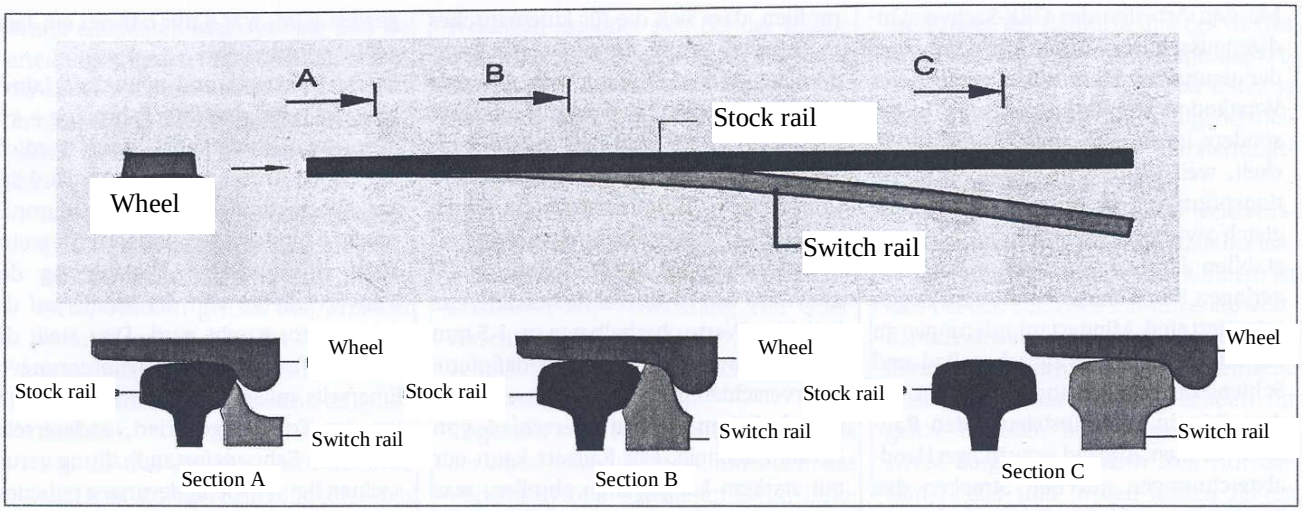

Figure 2.11: Transition of a wheel from stock rail to switch rails

To avoid an impact by the wheels in diverging direction, the switch rails and the stock rails should adapt as good as possible. So in section B the switch rail is somewhat above the head of the stock rail (further discussions see [4]).

2.3 MECHANISMS OF EXCITATION

In addition to the wheel and rail unevenness, which is the predominant excitation in straight lines, a train rolling on a turnout is subjected to track geometrical irregularities (sudden change in track vertical or lateral alignment, implying changes in contact point location and number), as well as track stiffness variation (due to rail cross section variation and stiffness variation of the different components along track e.g. wing rail, crossing nose, sleepers …).

These phenomena are combined in the contact force resulting from the wheel - rail interaction as illustrated Figure 2.12. Notice that in this figure, the wheel and rail unevenness is not represented, but it is also present in turnouts. The repetitive high forces generate rail surface damage (Figure 2.13) which in turn gives rise to higher impact load. This loop is also illustrated in Figure 2.12.

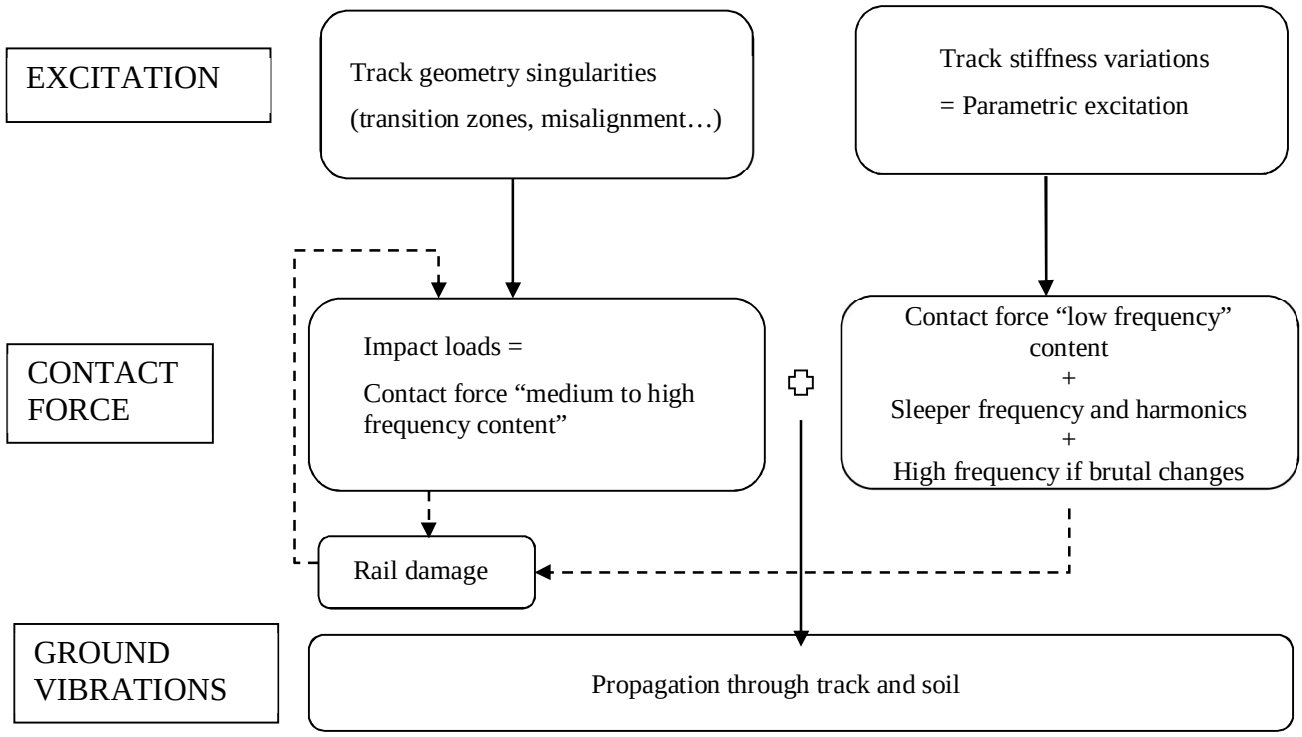

Figure 2.12: Generation and propagation of ground vibration in railway turnouts

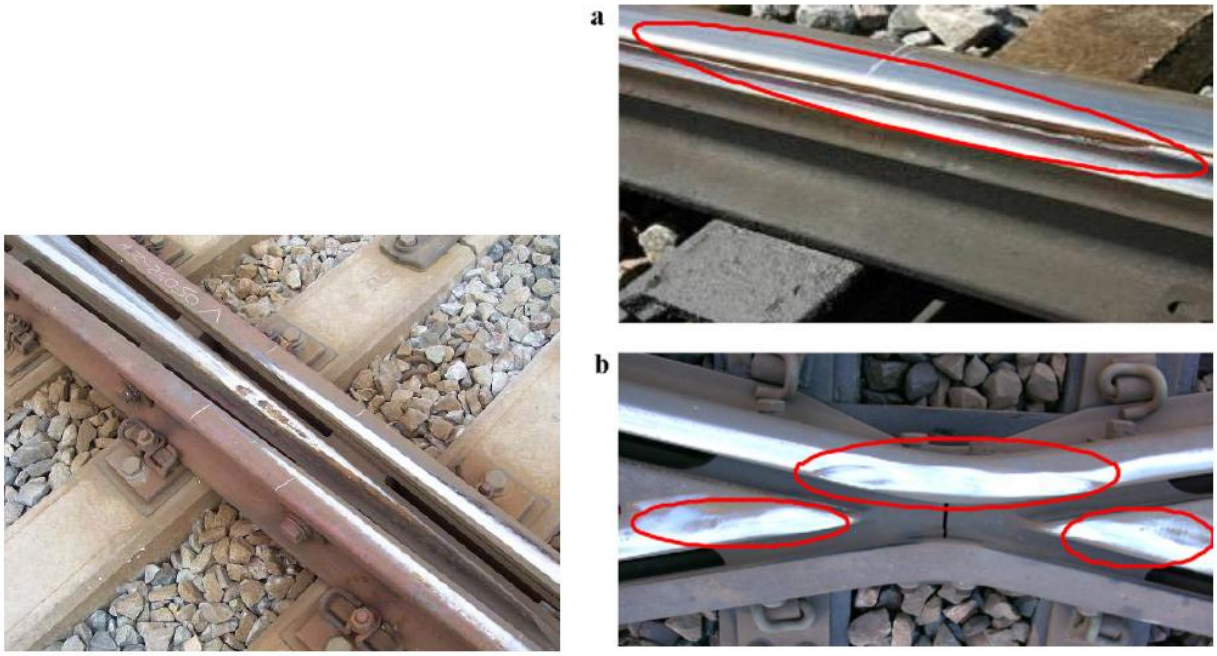

Figure 2.13: Rail surface damage – left [6], Damage due to RCF (Rail contact fatigue) – right [2]: Detached material from the rail (a), plastic deformation (b)

Track geometrical irregularities are especially located at the switch panel and the crossing panel, where the wheel jumps from one rail to another. **Optimization of these transition zones to reduce**

contact force is achieved by smoothing the wheel trajectory at the transition, for example by minimizing the slope and step depth of the transition (Figure 2.14).

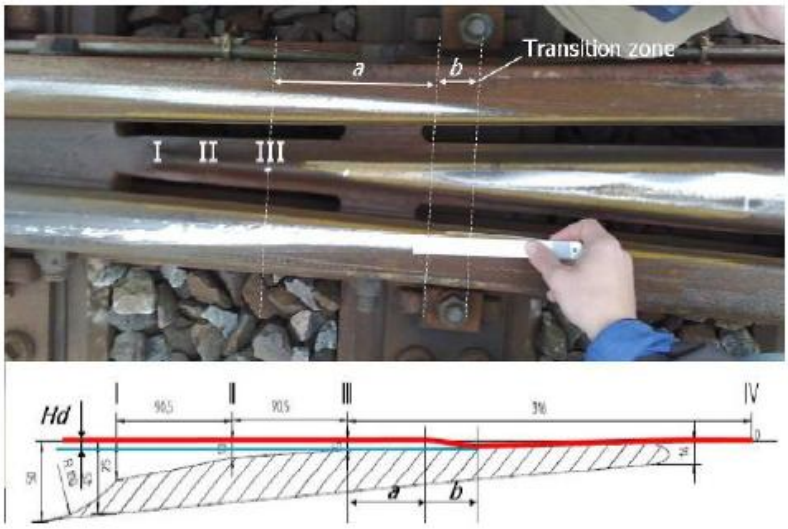

Figure 2.14: Track misalignment in the transition zone [6]

S&C also involves changes of stiffness when rolling over the switching part and the frog, illustrated by measurements in Figure 2.15. In the example turnout studied in Figure 2.15, at the entry of the turnout (0 m), the track stiffness drops down to 40 kN/mm (due to poor tamping of the ballast, leading to hanging sleeper) and suddenly reaches a peak at 100 kN/mm, two meters away. The figure also shows the influence of the rail pads (stiff, soft, medium stiffness) on the track stiffness in the switch and crossing panels. In this article [7], it is shown that the use of softer rail pads constitutes a mitigation measure to reduce contact force.

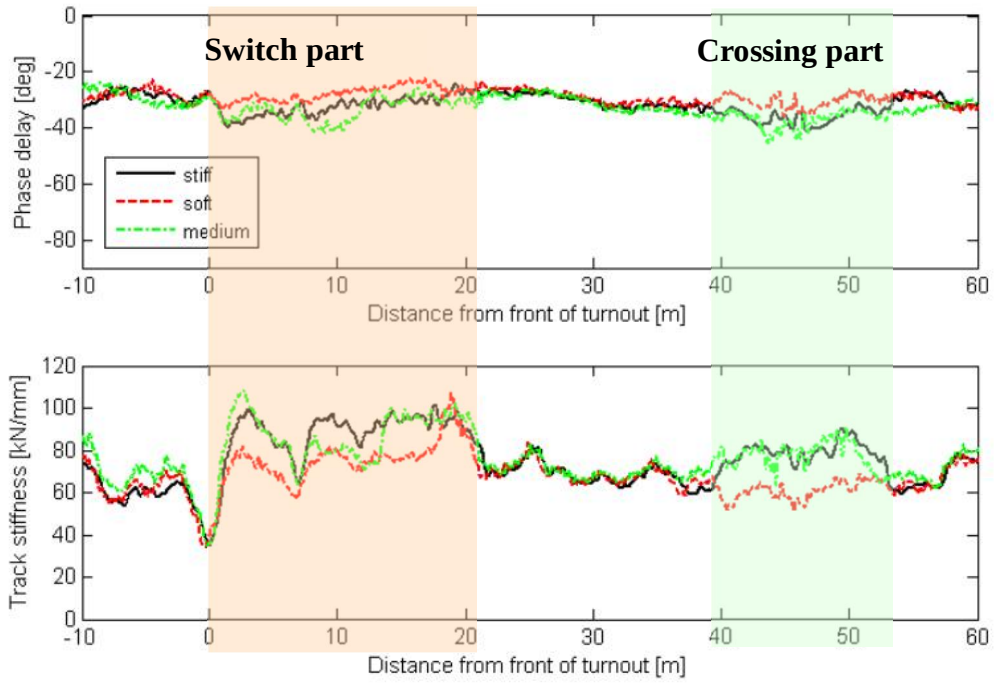

Figure 2.15: Track stiffness measurements (10 Hz) S&W for 3 kinds of rail pads [7]

The impacts due to geometrical changes feature two main frequency peaks, that are named P1 and P2 peaks, illustrated in Figure 2.16. The P1 peak has high amplitude in the frequency range above 200Hz, and therefore is not relevant for ground-borne noise and vibration issues. However, this peak is responsible for rolling contact fatigue damage of the rail and the wheel and is an indirect cause of vibration.

The P2 peak is related to the response of the train-track system, with frequency range close to the resonance frequency of the unsprung mass on the track stiffness (in the range [50 Hz-80 Hz] for standard tracks and trains – a lower frequency range for softer tracks, such as USP or soft soil conditions).

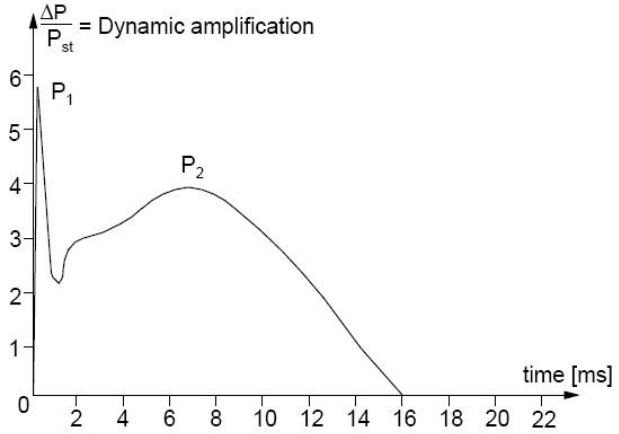

Figure 2.16: Scheme of vertical impact load at the crossing nose [6]

Vertical contact force (Q-force) was measured by Pålsson for different rail pads [7], showing the impact at the crossing part of the turnout. From the figure, the frequency of the main resonance is at about 80 Hz.

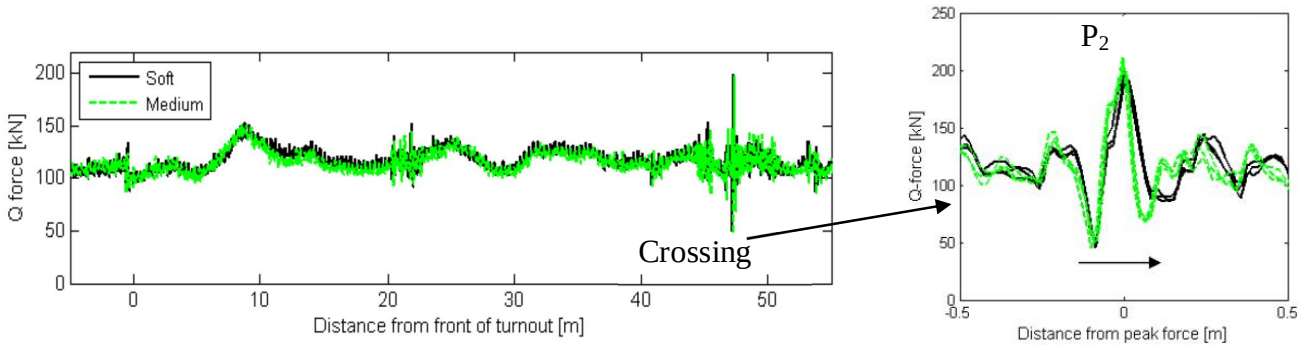

Figure 2.17: Vertical contact force measurements throughout a turnout – train speed 70 km/h

The relative dominance of these mechanisms of excitation is not fully understood, but some hints are indicating that the amplitude of the impact related to the track geometry variation is more important than the impact due to track stiffness variation.

Figure 2.18 illustrates this assumption: at 0 m, the most brutal change of stiffness is measured in the switch part, while the highest contact force is measured at about 48 m, where the train rolls on the crossing part of the turnout (impact due to geometrical variation).

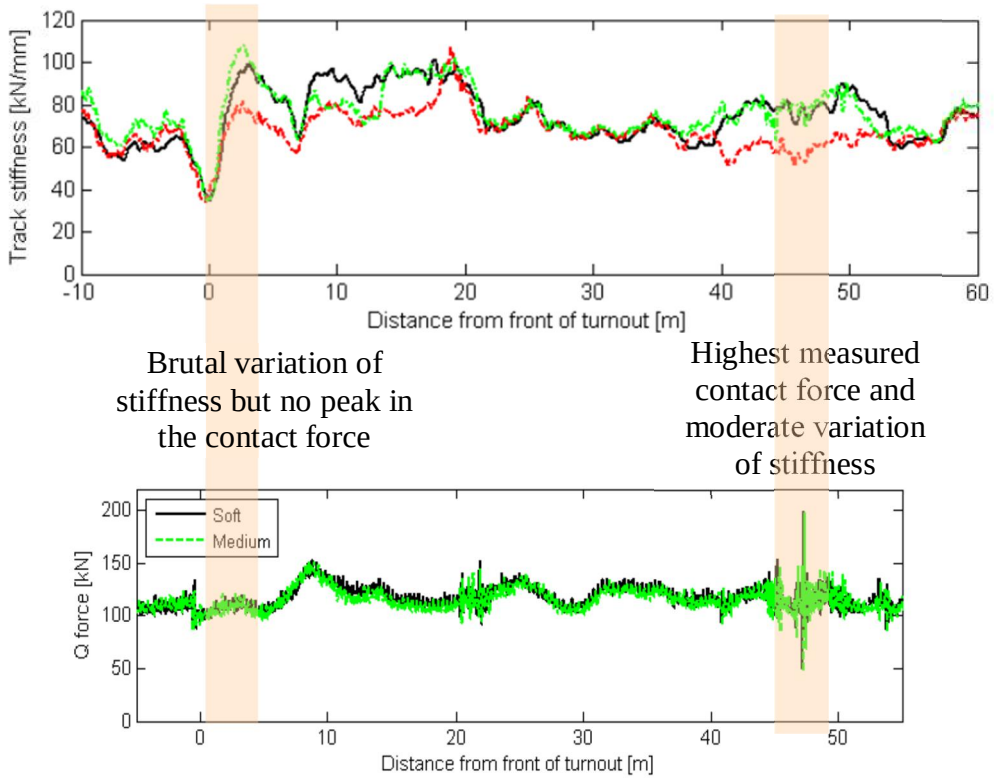

Figure 2.18: Vertical contact force and track stiffness measurement

Further impact load measurements:

Härad, Sweden

In the CHARMEC project TS7, an extensive field test was performed in a 60E1-760-1:15 (curve radius 760 m and crossing angle 1:15) S&C near Härad between Södertälje and Eskilstuna in Sweden. The field test was performed in May 2006. Lateral and vertical wheel–rail contact forces were measured by a wheelset instrumented with strain gauges on the wheel discs. The sampling frequency of the contact force measurements was 9.6 kHz. The measured force signals were then low-pass filtered with a cut-off frequency of 1.0 kHz.

The test vehicle with Y25 freight vehicle bogies and an axle load of 25 tonnes passed through the S&C in the main (through) and diverging routes and in both facing (from switch panel to crossing panel) and trailing (from crossing panel to switch panel) moves. The influences of vehicle speed, route and move on the maximum vertical contact force Q_{max} at the crossing are illustrated in Figure 2.19. For all vehicle routes, an increase in Q_{max} with increasing vehicle speed was observed. However, the increase in impact load was considerably higher for the diverging route compared to the main route. In the main route, the contact force increased by a moderate 15 % when vehicle speed increased from 10 km/h to 80 km/h. The corresponding increase in the diverging route was about 40 %. The influence of moving direction (from wing rail to crossing nose in the facing move or vice versa in the trailing move) on Q_{max} was relatively small for both the main and diverging routes.

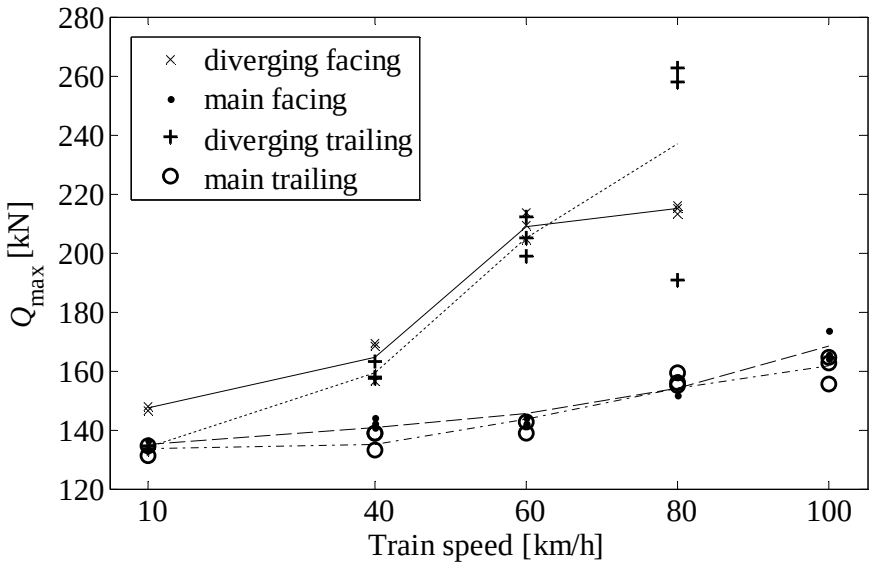

Figure 2.19: Measured maximum vertical contact force Qmax when the train (axle load 25 tonnes) was moving in the main and diverging routes and in both facing and trailing moves. The lines are least square fits to the measured values. From [1]

Eslöv, Sweden

In the EU FP6 project INNOTRACK, another extensive field test was performed in a 60E1-760-1:15 S&C at Eslöv (switch 413) in the south of Sweden. The field test was performed in December 2009. The measurements were repeated using standard and soft rail pads. According to the S&C manufacturer, the static stiffness of the standard rail pad in the crossing panel was 120 kN/mm (dynamic stiffness 180 kN/mm). The corresponding stiffness of the soft rail pad in the crossing panel was 80 kN/mm (dynamic stiffness 120 kN/mm)[1]. Lateral and vertical wheel–rail contact forces were measured by a wheelset instrumented with strain gauges on the wheel discs. The sampling frequency of the contact force measurements was 1.2 kHz. The measured force signals were low-pass filtered with a cut-off frequency of 250 Hz.

The test vehicle with Y25 freight vehicle bogies and an axle load of 22.5 tonnes passed through the S&C in the main (through) and diverging routes, and in both facing and trailing moves. The influences of vehicle speed, route and rail pad stiffness on the maximum vertical contact force in the crossing panel are illustrated in Figure 2.20a,b. It is observed that a significant reduction in impact load at the crossing can be achieved by using softer rail pads. Measurements in a reference turnout with standard rail pad stiffness confirmed these results.

[1] Note that the corresponding rail pad stiffness in the turnout at Härad is in the order of 1000 kN/mm

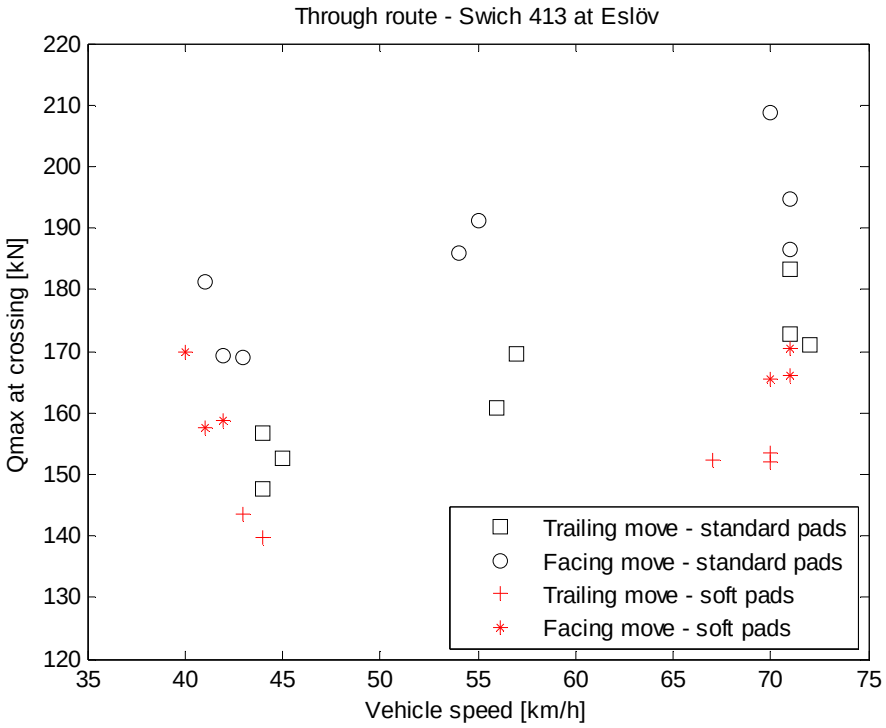

Figure 2.20a: Measured maximum vertical contact force Qmax when the train is moving in the main (through) route and in the facing and trailing moves. Two different rail pad stiffnesses. [2]

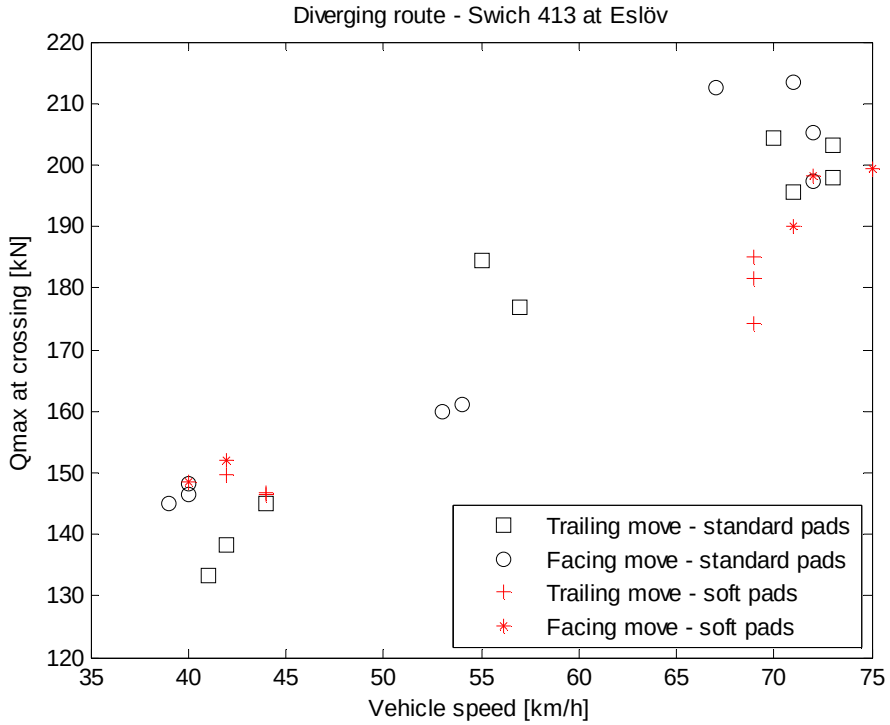

Figure 2.20b: Measured maximum vertical contact force Qmax when the train is moving in the diverging route and in the facing and trailing moves. Two different rail pad stiffnesses. [2]

Testelt, Belgium (artificial source)

USP tests in Belgium [8] for turnouts with and without USP showed for a weight dropping of 60 kg a shift in frequency from the excitation at rail and sleeper to lower frequencies at the 4 m, 10 m and 15 m measurement points (see Figure 2.21). It is obvious: the closer to the source, the higher the frequencies in the response. The wave propagation speed is about 180 m/s. The force reaches a peak value of approximately 50 kN during 10 milliseconds. On the rail and on the sleeper peak accelerations of 5 g were measured, while next to the track the acceleration is smaller than 0.1 g.

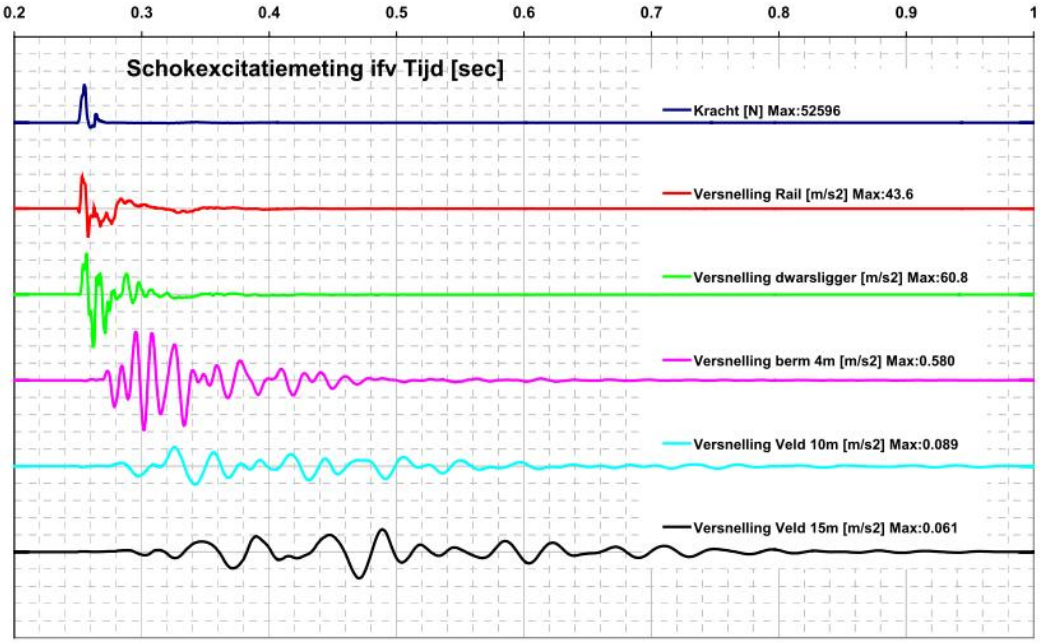

Fig. 10. Shock excitation measurements in function of time [sec] for original, non-isolated turn-out; Excitation force [N], Acceleration Rail [m/s²], Acceleration Sleeper [m/s²], Acceleration field 4m [m/s²], Acceleration field 10m [m/s²], Acceleration field 15m [m/s²]

Figure 2.21: Test at Belgium test site by 60 kg weight dropping on the frog.

First conclusions for mechanisms of excitation: The total contact force contains components in a wide frequency range, which will be transferred differently through the track and propagate into the soil. The propagation in the ground will be different depending on the frequency range but also on the nature of the excitation: point or linear sources.

For the moment, the relationship between contact force and ground borne vibration is not clarified for turnouts, as it is more complex than for straight line. More investigations are required in this domain.

As presented, measurements of contact force show amplifications in the frequency range [50-80] Hz, corresponding to the resonance of the vehicle un-sprung mass on the track stiffness.

Ground vibration measurements from SBB show vibration excitation, the turnout-amplification, in lower frequencies [16-40 Hz] (See Figure 2.29a). This might be due to lower track stiffness, for instance in soft soil conditions or presence of under sleeper pads.

2.4 OPTIMISATION OF GEOMETRY AND TRACK STIFFNESS

One objective of INNOTRACK SP3 was to optimise the transition geometry and stiffness of resilient elements in the crossing panel to reduce material degradation (wear and plastic deformation) of the rails, see [9], [10].

Simulations of vehicle dynamics in the S&C were carried out by DB Systemtechnik using the multi-body dynamics software SIMPACK. Only the main (through) route of a German standard crossing EH 60-500-1:12 was studied.

The simulations were performed with complete three-dimensional vehicle models of a Loco BR 101 and of an ICE-T coach (BR 411), representing two different static wheel loads (Loco BR 101: Q_0 = 107 kN, ICE-T coach: Q_0 = 67 kN). Three different wear states of the wheel profiles were used: nominal S1002, medium-worn and hollow worn. The S&C track flexibility was represented by a finite element model consisting of elastic rails and elastically supported elastic sleepers.

2.4.1 Control of Crossing Geometry

Regarding the optimisation of the transition geometry of rigid (non-movable) crossings, two general design approaches were discussed. The first one was to prevent the wheel from making contact with the crossing nose at a rail section being too weak to withstand the impact loads. The second approach aimed at smoothing the vertical wheel trajectory during the transition between wing rail and crossing nose to reduce the magnitude of the impact loads. Based on these two approaches, three designs were investigated by numerical simulations:

- Reduction of the flangeway width between crossing nose and wing rail in order to delay the transition area to a thicker cross-section of the crossing nose;
- Modified profiling of the crossing nose by using a kinked ramp to decrease the gradient of the wheel trajectory after transition to the crossing nose (optimisation for facing move);
- Superelevation of the wing rail and profiling with a negative wheel shape to reduce the vertical wheel movement (MaKüDe).

Examples of improved vertical wheel trajectory compared to what is obtained for the nominal geometry are shown in Figure 2.22. The figure also shows the result for a shorter version of the kinked ramp which has a similar effect on the impact loads in the transition area as the longer version.

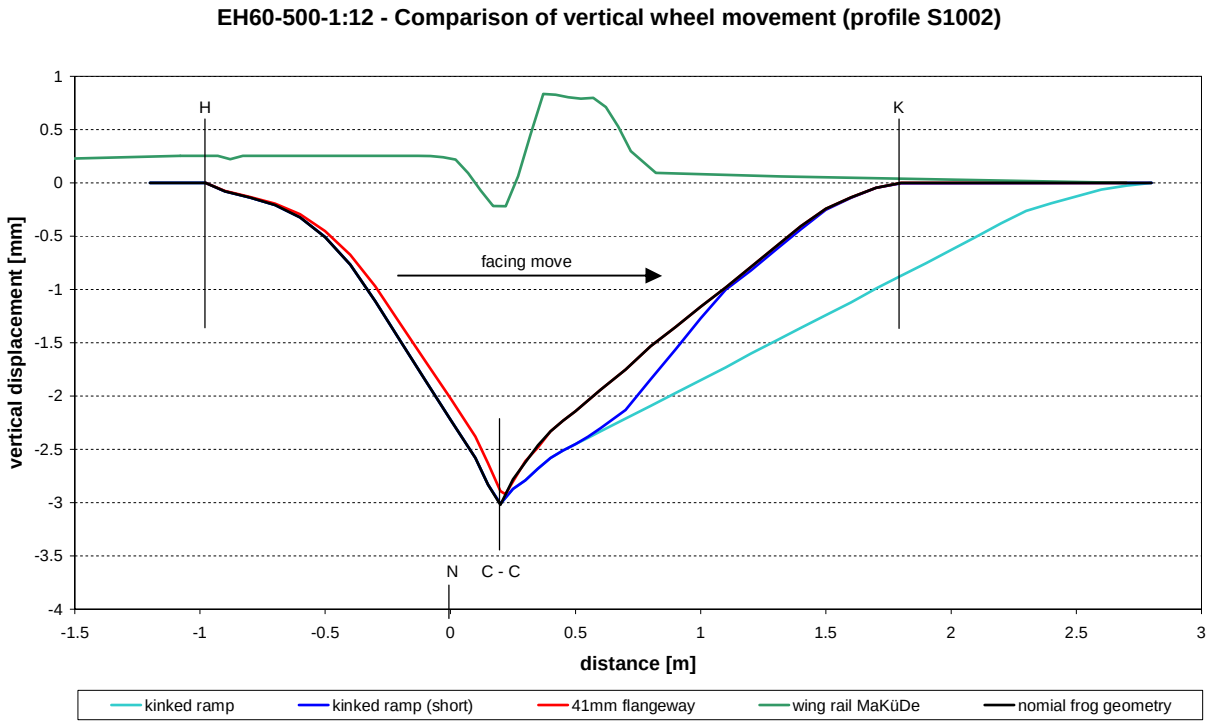

Figure 2.22: Influence of geometric crossing (crossing nose and wing rail) design on vertical wheel movement (trajectory) with point N marking the tip of the crossing nose (s = 0 m). From [9]

Simulation results from INNOTRACK SP3 of maximum normal contact forces and maximum equivalent stresses for the alternative crossing designs are presented in Figure 2.23. For the nominal S1002 wheel profile, the largest contact force reduction (up to 50 kN) was obtained for the kinked ramp design whereas the MaKüDe design led to higher normal contact forces than the nominal design. This is caused by the steep gradient of the wheel trajectory after transition to the frog, see Figure 2.22. For worn wheels, the effect is inverted. Here the MaKüDe design leads to the lowest normal contact forces. For the medium-worn wheel profile, the MaKüDe design leads to a reduction in impact load of nearly 50 %.

These simulation results illustrate that it is difficult, if not impossible, to find a solution which leads to a contact force reduction for all wheel profiles occurring in service. Nevertheless, **the MaKüDe design developed by DB Systemtechnik showed the best performance especially for mean worn wheel profiles and for both facing and trailing moves. In connection with reduced support stiffness (e.g. elastic rail pads), this crossing design could lead to a significant reduction of the impact loads and possibly provide a potential for reduction of ground vibration.**

Note that the maximum stress in the crossing may occur at a different location than the maximum contact force and that small changes of contact conditions (contact radii) may lead to large variations in contact stresses. This needs to be considered in the optimisation of crossing geometry. Further, it also needs to be considered that softer rail pads will increase the risk for fatigue of the rail foot induced by rail bending.

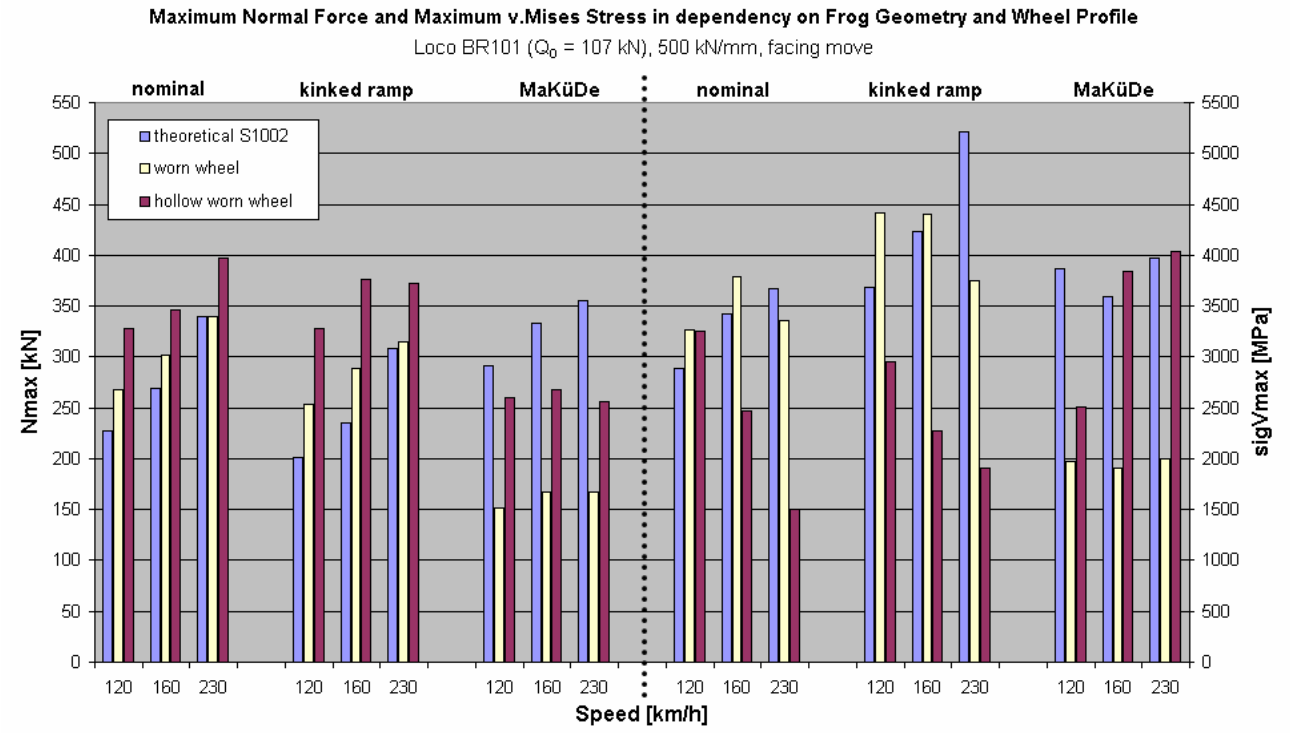

Figure 2.23: Influence of transition geometry and wheel profile on maximum normal contact force and equivalent stress. From [9]

2.4.2 Soft Rail Pads

Soft rail pads were also used to reduce contact force.

Markine [6] numerically showed that the use of soft rail pads and under sleeper pads can induce a reduction of the P1 peak by up to 20 %, and a reduction of the force transmitted to the sleeper by more than 60 %.

The influence of track stiffness on impact load at the crossing is illustrated in Figure 2.24. By the use of softer rail pads, a reduction of track stiffness from 500 kN/mm to 85 kN/mm leads to significantly lower impact loads and an increasing effect with increasing speed. Also for the case with one unsupported sleeper below the transition area of the crossing, slightly reduced impact loads can be observed. For the unsupported sleeper case, the support stiffness was reduced in the transition area. The reduced stiffness values were chosen so that the simulated crossing nose deflection corresponds to displacements measured on an in-service crossing with unsupported sleepers.

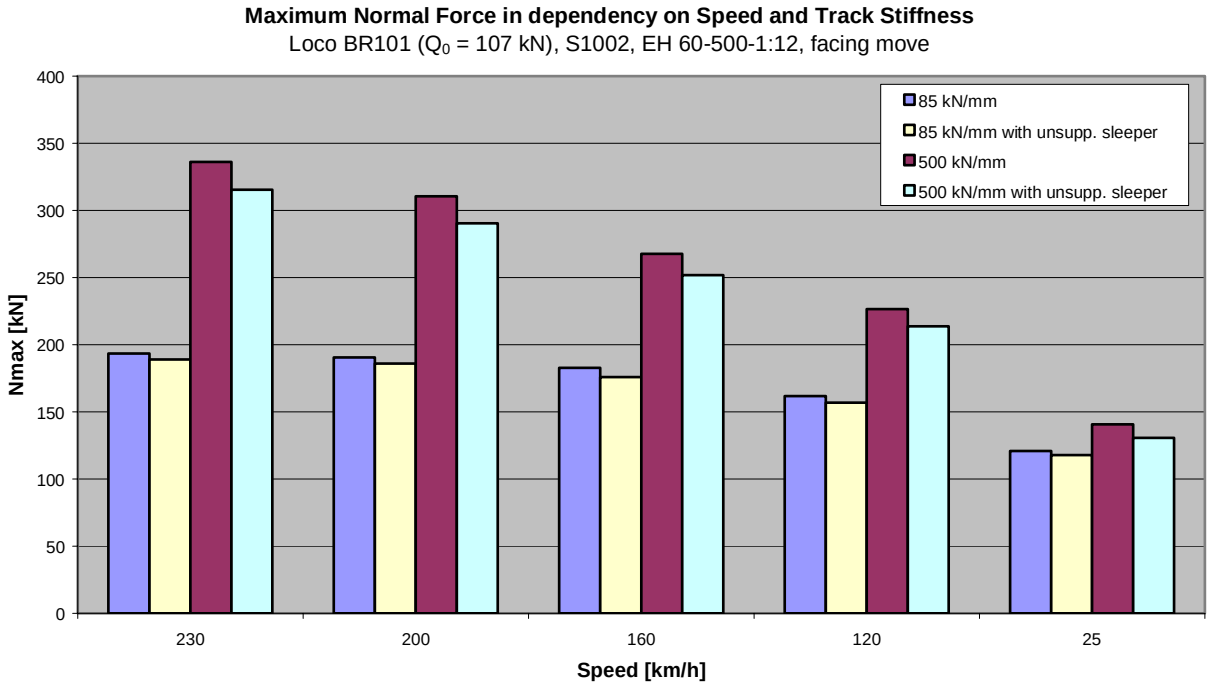

Figure 2.24: Influence of vehicle speed and track stiffness on maximum normal contact force. [9]

Palsson [7] also tested soft rail pads for reducing contact force. The experimental results presented in Figure 2.25 show that this mitigation measure's efficiency increase with train speed.

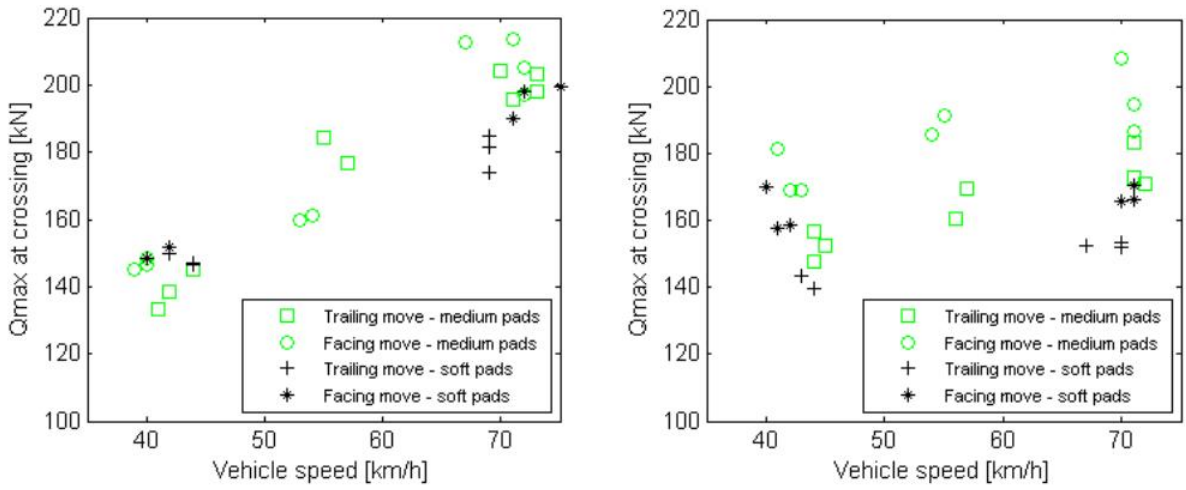

Figure 2.25: Summary of measured maximum vertical wheel–rail contact forces at the crossing as a function of vehicle speed for all test runs in turnout: (left) diverging route, (right) through route

Zhu mounted elastic slide base plates under the switch rail [11] to reduce the contact force. The reduction was experimentally and numerically studied (see Figure 2.26 and Table 2.1).

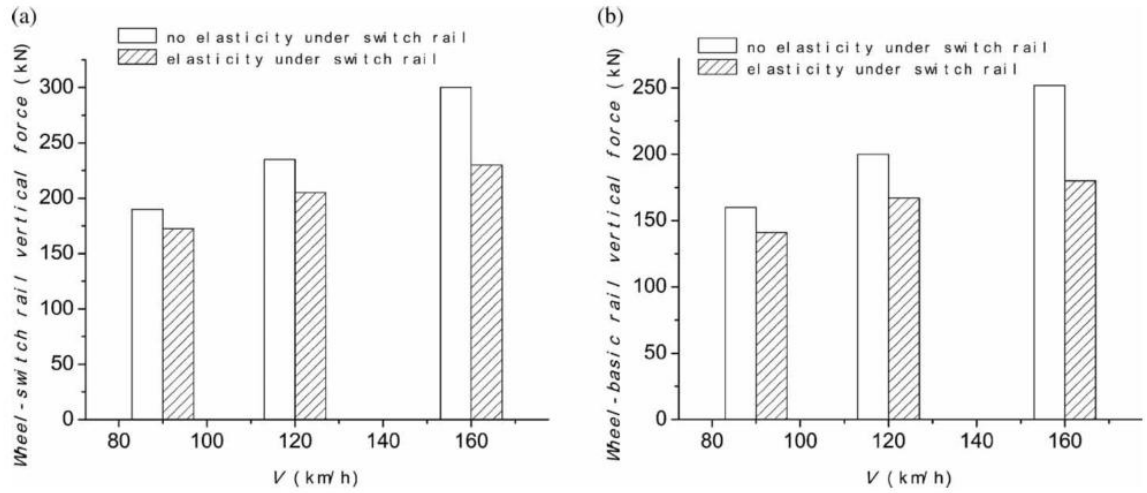

Fig. 4 (a) Wheel–switch rail vertical force. (b) Wheel–stock rail vertical force

Figure 2.26: Reduction of contact force using elasticity under switch rail

Table 2 Experimental comparison after the switch rail is laid elastically

		After the switch rail is laid elastically		Before the switch rail is laid elastically	
Test items	Test position	Freight train	Passenger train	Freight train	Passenger train
Wheel–rail vertical force (kN)	Stock rail	197	172	213	194
	Front switch rail	150	130	175	137
	Stock rail	104	182	133	203
Rail acceleration (g)	Front switch rail	97	240	140	298
	Stock rail	94	106	144	150
Slide base plate acceleration (g)	Anterior switch rail	125	240	155	298
	Middle switch rail	123	148	146	200

Table 2.1: Experimental results – introduction of elasticity under switch rail

2.4.3 Influence of Wheel Profile – Instructions for Optimization of Rail Profile

Using the multi-body dynamics software GENSYS, the influence of wheel profile on vertical contact force and contact position at the crossing have been studied in the CHARMEC project TS13, see [12]. Based on a sample of measured wheel profiles, it has been shown that wheels with hollow worn tread profiles make a significantly later contact with the crossing than most other wheel profiles, see Figure 2.27a. This is because the “false flange” at the field side of the hollow worn wheel profile makes contact with the wing rail, and this contact continues until the wheel loses contact with the gauge corner of the wing rail and essentially falls down on the crossing as can be observed in Figure 2.27b at around 47.5 m. The wheel profile with the hollowest wear generated the highest normal contact force at the crossing section as is displayed in Figure 2.27c.

Continued work by Chalmers on optimising the rail profiles at the crossing will be performed in RIVAS WP3 based on an approach similar to the one applied in [13].

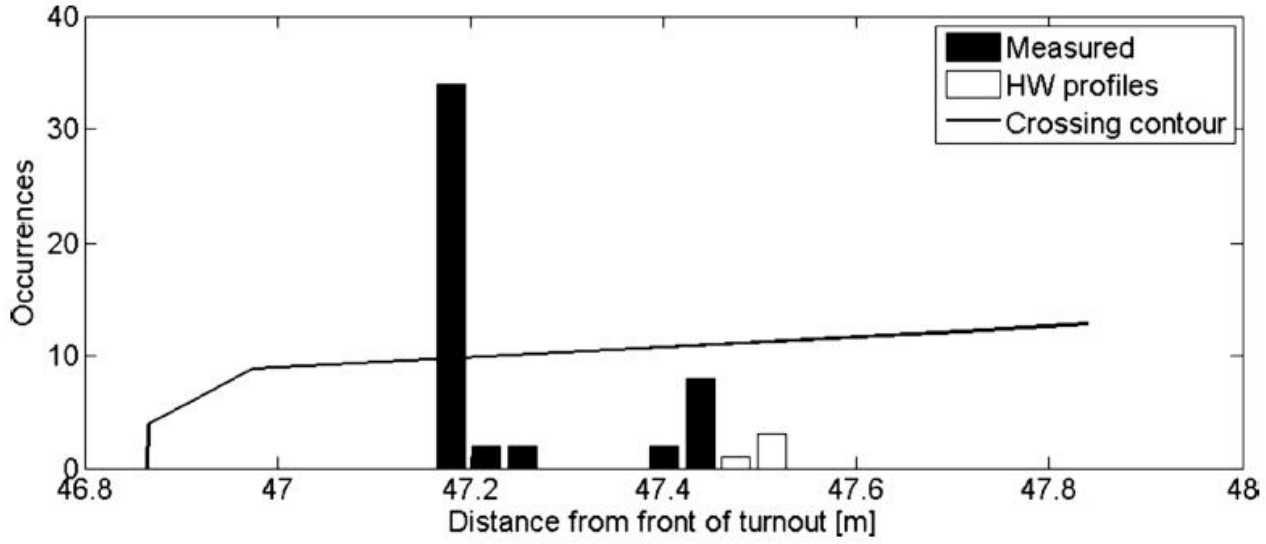

Figure 2.27a: Histogram of position for initial crossing nose contact. Numerical simulations in GENSYS based on a sample of measured wheel profiles. From [12]

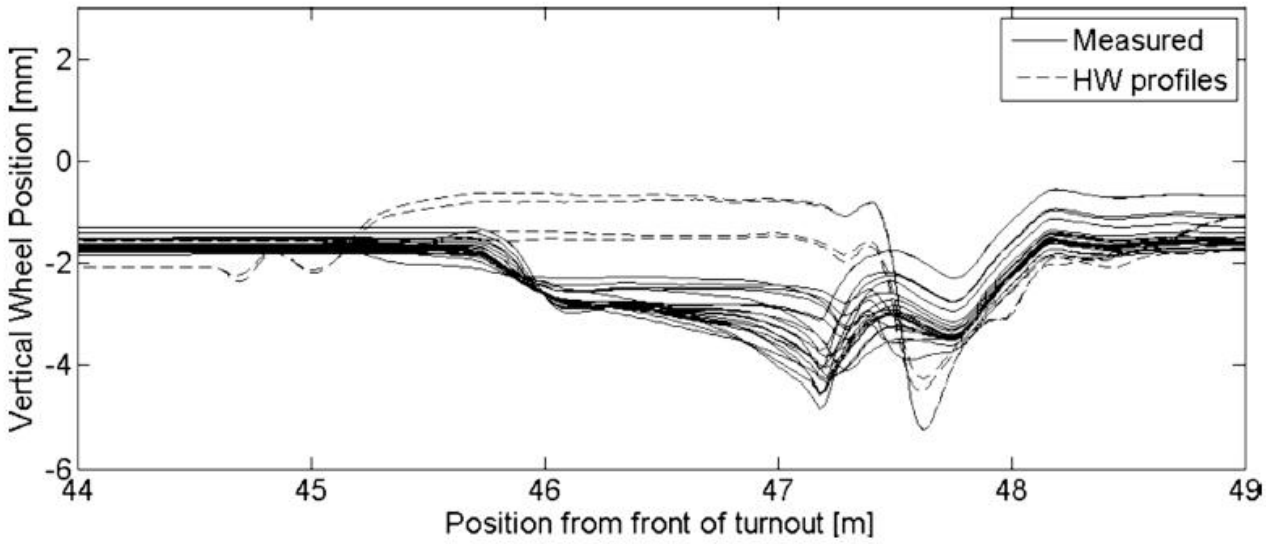

Figure 2.27b: Vertical wheel trajectory during crossing transition. Numerical simulations in GENSYS based on a sample of measured wheel profiles. From [12]

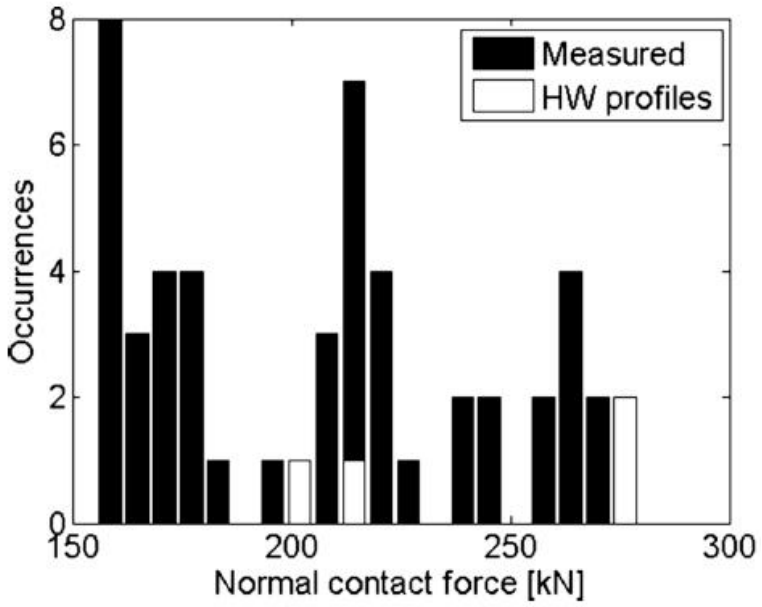

Figure 2.27c: Histogram of maximum normal contact force at the crossing section. Numerical simulations in GENSYS based on a sample of measured wheel profiles. From [12]

2.5 NUMERICAL MODELS OVERVIEW

Numerical models were developed to compute the contact force at the wheel-rail interaction point, but at the moment no model of turnout including soil was developed. The main reason is that turnout computations require time domain solving, while soil models are developed in the frequency - wave number domain [14].

Coupling of TRAFFIC software (vehicle-track-soil in frequency-wave number domain) with DIFF model (vehicle-track in time domain) was however already performed in RIVAS [15], but it is not achievable for turnouts, because of the underlying assumption of invariant properties along the track direction, in TRAFFIC software, which is not compatible with the turnout design.

The developed numerical models for contact force computations in turnout are in reasonably good agreement with physical measurements, as it is shown by the following Figures 2.28a and 2.28b.

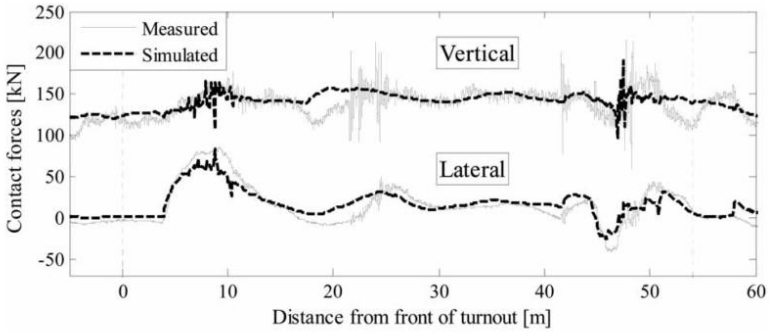

Figure 7. Vertical and lateral wheel-rail contact forces on the left (outer) wheel of the leading wheelset in the leading bogie. Facing move in the diverging route. Train speed 80 km/h.

Figure 2.28a: Measured and simulated contact forces in a turnout [16].

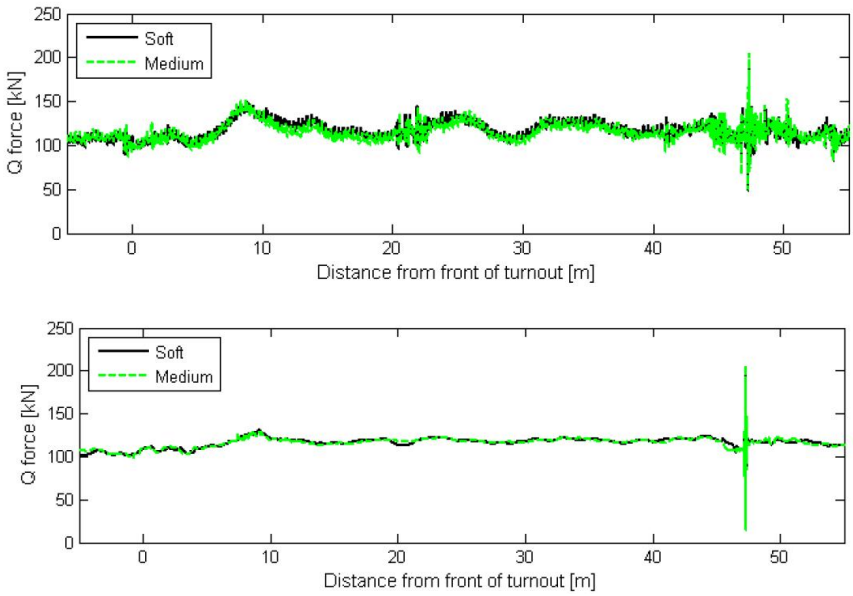

Figure 2.28b: Measured (upper) and simulated (lower) contact forces in a turnout [2].

These models require consequent measurements for set-up and tuning purposes. The turnout is dynamically described if at least the following parameters are known:

- 3D geometrical description of the turnout (especially in switch and crossing panels),
- Track dynamic stiffness measured along the turnout with RSMV (Swedish Rolling **Stiffness** Measurement Vehicle) for several frequencies
- Rail roughness (or rail unevenness)
- Dynamic properties of the track component

Investigations on transfer functions from contact force to ground vibration are still required in order to validate the models for ground vibration prediction.

2.6 VIBRATION MEASUREMENT RESULTS OF TURNOUTS

Many measurements are performed at SBB and some at other railway companies during the last years about the turnout vibration amplification.

2.6.1 Turnout-Amplification

The turnout-amplification shall be defined as the amplification (normally frequency dependent) of the measured vibrations at the turnout in comparison to the reference track (in dB: subtraction, in mm/s: division of values). The turnout-amplification depends on the turnout type, the quality of the turnout-geometry and the maintenance state of the crossing (frog).

a) An analysis of SBB [17] in 1998 about VIBRA-3 data from building measurements showed that the vibrations are amplified especially in the frequency range 16-40 Hz (mean maximal value at 25 Hz of 16 dB) from 0 to 8 m distance and in the frequency range of 16-32 Hz (mean maximal value at 25 Hz of 6 dB) from 8 to 16 m distance.
b) In the USA (FTA-Federal Transit Administration, Transit noise and vibration impact assessment, 1995) the turnout-amplification is suggested + 10 dB (Factor 3.16)
c) Krüger is suggesting estimate values for octave-bands [18]:

Hz	8	16	32	63	125	250
dB	5	5	10	15	10	5
Factor	1.8	1.8	3.16	5.6	3.16	1.8

Table 2.2: Estimation values for turnout-amplification

d) For the turnout-amplification several special vibration measurements were performed at SBB [e.g. 19,20,21]. An overview of frequency dependent emissions for several switches is given in Fig.2.29a. It shows the importance of having mitigation measures for frequencies lower than 40 Hz. The measurements of turnouts in Switzerland show a substantial increase of vibration compared to a normal track, in particular in proximity to the frog. **The highest increase of vibration in average appears from 16 - 40 Hz.** These frequencies are often the most important resonance frequencies of wooden floors, so that buildings adjacent to the turnout are subjected to a substantial amplification of vibration.

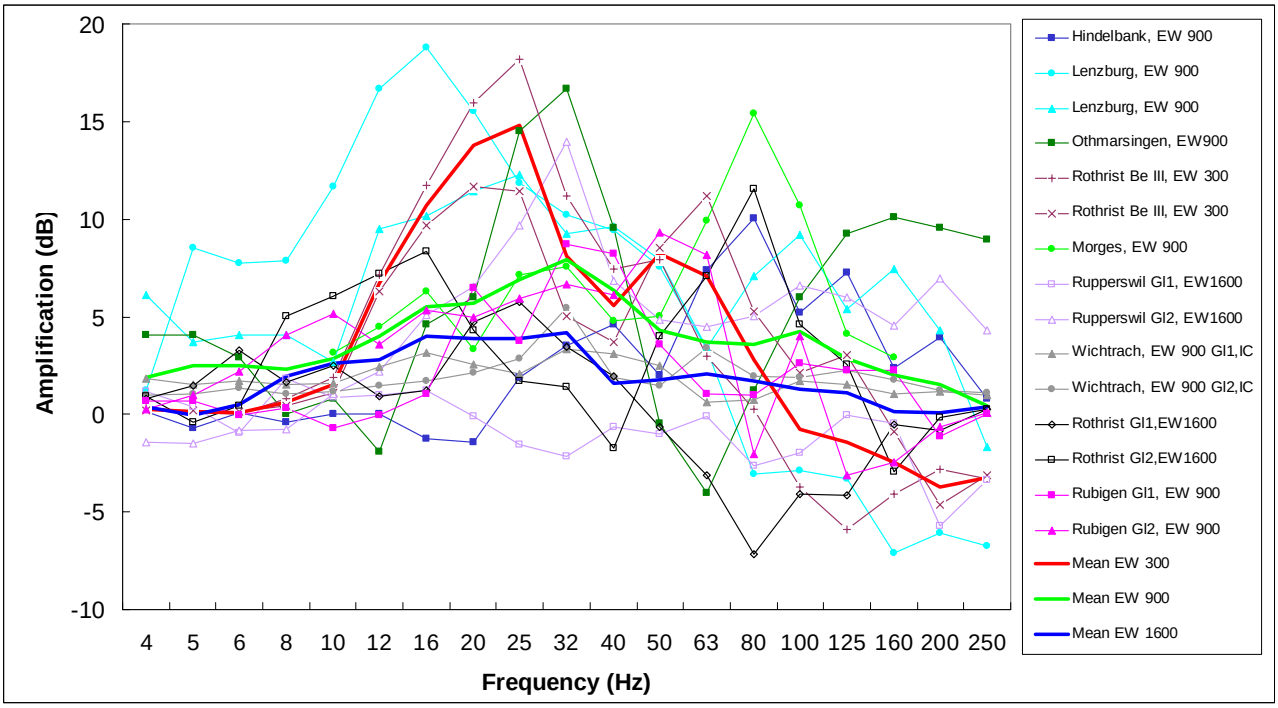

Figure 2.29a: Amplified vibration of turnouts compared to track at grade in about 8 m distance to the open line near the unmoving frog. The numbers after "EW" indicate curve radii of the switch in deflection (e.g. EW 300 = radius 300 m).

Figure 2.29b shows significant differences in terms of amplification for different turnout radii. **It is visible that the smaller the radius of a turnout the higher the amplification of the frog part between around 12 Hz up to 60 Hz.**

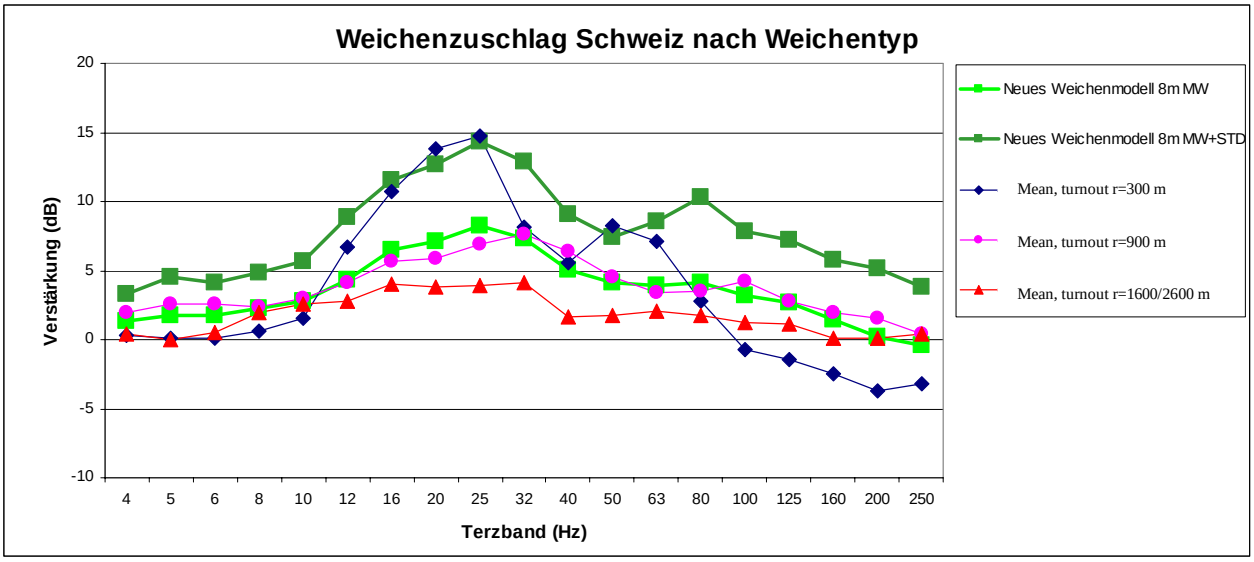

Figure 2.29b: Turnout-amplification classified in dependency of turnout type (radius)

In Figure 2.29c a strong variation of turnout-amplifications is visible for the same type of turnout (EW 900, r=900 m). This implies that parameters such as turnout geometry, maintenance status and geology also have strong influence on the turnout-amplification. Differences of 10 dB (Factor 3) ore even higher occur in several 1/3 octave bands.

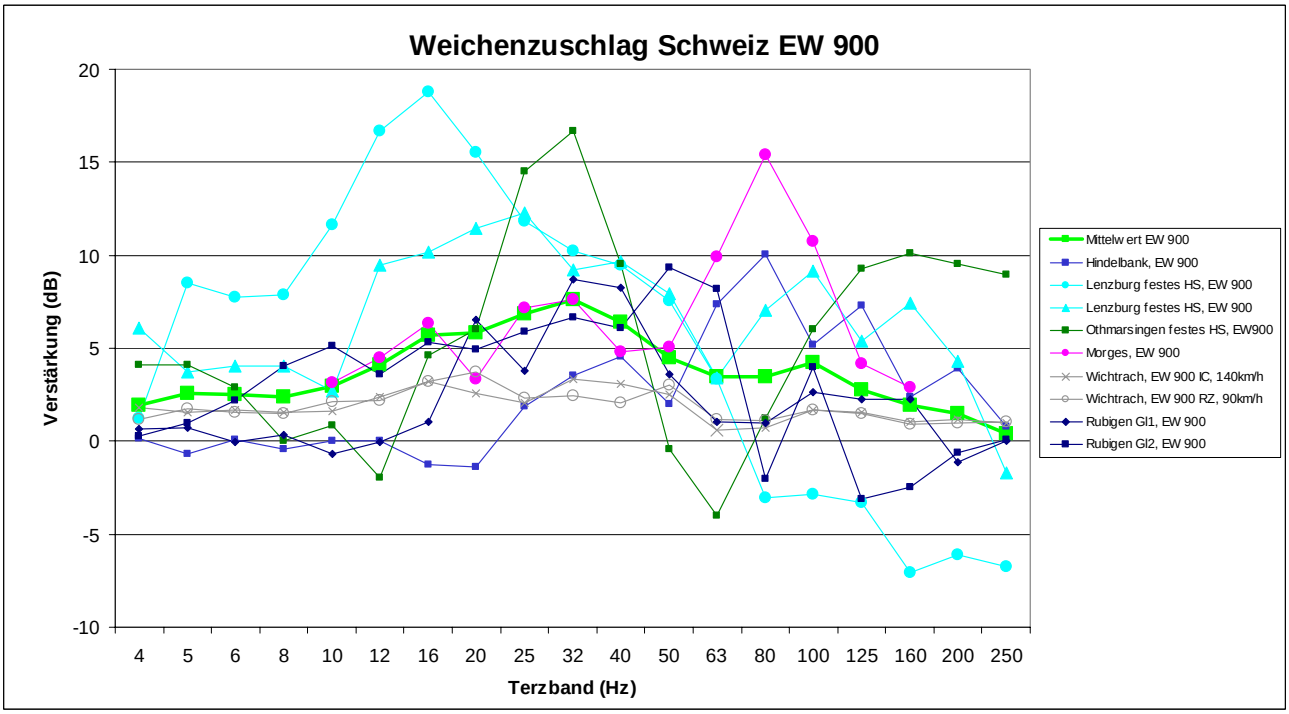

Figure 2.29c: Turnout-amplification of EW 900 given from different measurements. (Rubigen Gl1 and Gl2 are turnouts with hard USP).

2.6.2 Turnout-Amplification and Distance Influence

The turnout-amplification is dependent on distance (see Figure 2.30) as the turnout (frog) is a point source in contrast to the reference track which is considered as a line source.

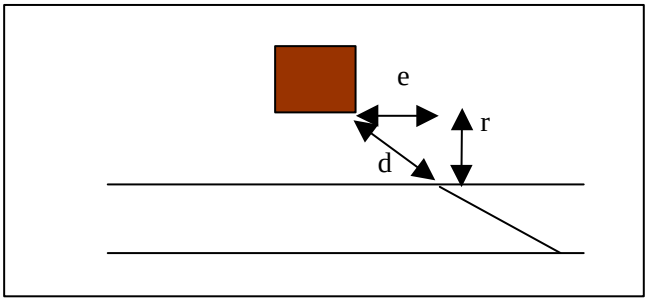

Figure 2.30: Distances to the frog (crossing)

A simple linear formula could describe the distance influence and comparisons are shown in figure 2.31 and 2.32

$$F = 1 - d/50$$

where F is a factor that takes into account the influence of the distance on the amplification factor due to a turnout. It is defined in these formulas that over 50 meter distance no more turnout-amplification is seen, d is distance, Pi is the circle-number 3.141592654.

F is used in the formula below (V is in linear values, mm/s, TA is the turnout-amplification at 8m distance to the frog):

$$V_{Turnout} = V_{without\ turnout}\ (1+ F * (TA_{Turnout\text{-}amplification\ at\ 8\ m} -1))$$

a) Distance influence perpendicular to track

If the transmission is perpendicular to the track d = r. In Figure 2.31, it can be seen clearly, that different turnouts have different turnout-amplifications, but the distance relationship for the turnout-amplification is quite similar (around 1 dB per 10 m). Only the measurements in Wichtrach, with nearly no amplification, show a smaller decrease.

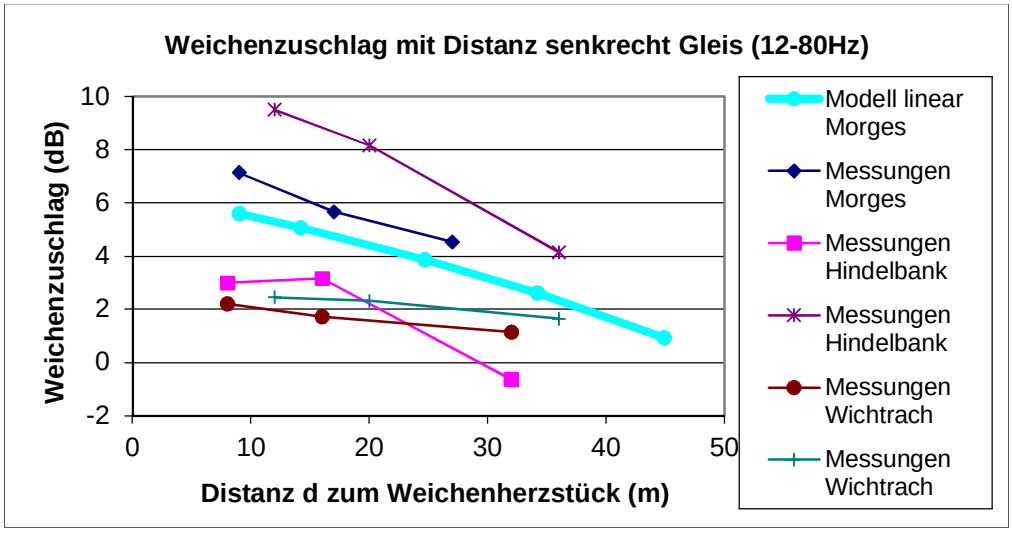

Figure 2.31: Dependency of turnout-amplification with distance perpendicular to track (d=r)

b) Distance influence parallel to track

Figure 2.32 shows a decrease of the turnout-amplification with bigger distances to the frog. It is noticeable that the switch part in Morges has nearly no influence but in Rupperswil at 65 m shows big amplification levels. The formula above match the turnout-amplification distance dependency (~0.12 dB/m) quite well. The measurement at Rupperswil Track 2 (Gl2) perhaps shows other effects than only the frog of the turnout.

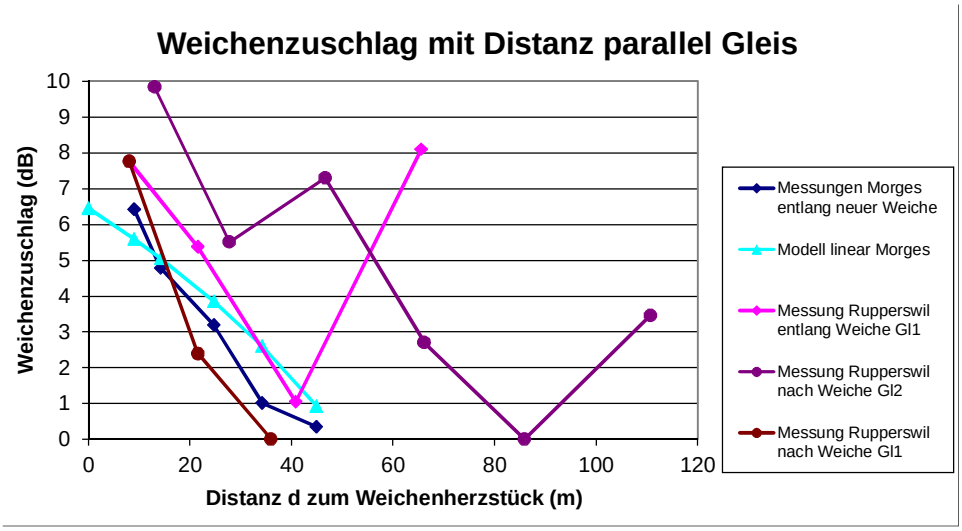

Figure 2.32: Influence of distance d parallel to track on turnout-amplification

c) The turnout-amplification at the switch part

The measured amplification of the switch part of EW 900 is shown in Figure 2.33. The amplification is smaller but still significant.

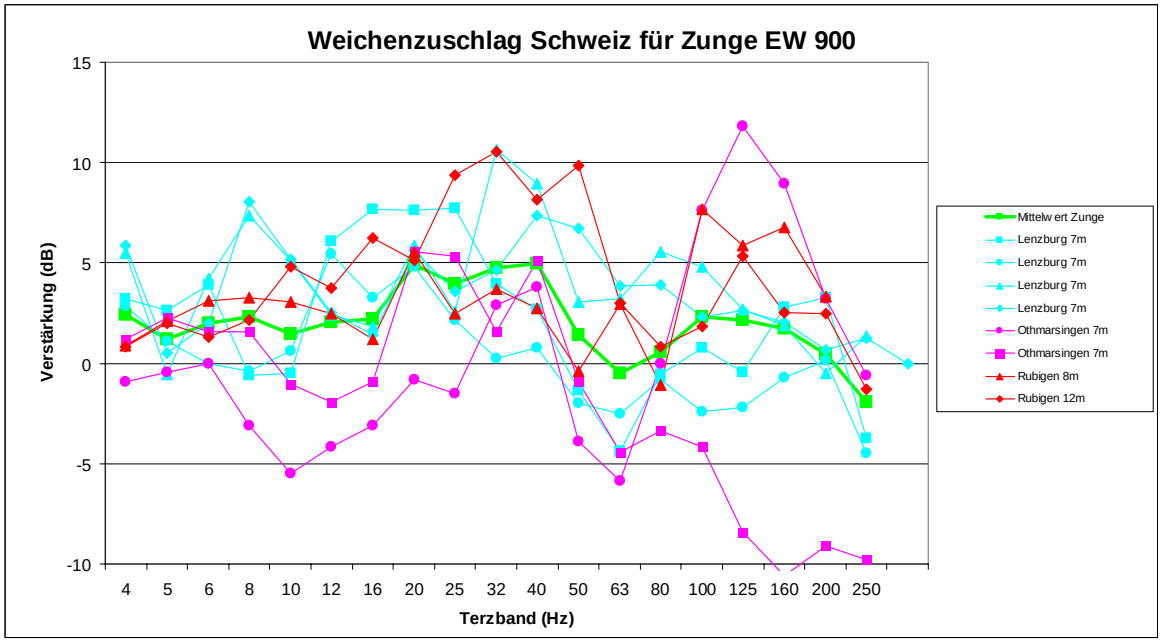

Figure 2.33: Turnout-amplification for switch part of turnouts (all turnouts EW 900)

2.6.3 Velocity Dependency and Train Direction Dependency

Measurements in Rothrist [22] for turnouts with/without under ballast mats (see section 3.5) can be used to see the vibration excitation influence of velocity dependency as well as the train direction dependency (facing, trailing) over a turnout frog. One turnout was with (measurement points G5G6G7) and one without under ballast mats (measurement points F5/F6/F7). Both turnouts were new, but the turnouts have not been investigated on geometrical differences. The turnout without UBM (see figure 3.18) is not yet in service for deviation, because the track for deviation was not yet built. **In Figure 2.34 it can be seen that the increase in velocity is amplifying the vibrations.**

The velocity dependency is clearly visible in both diagrams of figure 2.34: at 40 km/h vibration excitation is lower from around 20 Hz to 63 Hz (around a factor 3 at 31.5 Hz). The train direction dependency is much less obvious, only the turnout without UBM (figure 2.34 left) shows lower vibration levels at 40 km/h and 80 km/h for the facing direction for a few third octave bands (80 km/h: 16 Hz/50 Hz, 40 km/h 25-50 Hz). In figure 2.34 right no direction effect is visible.

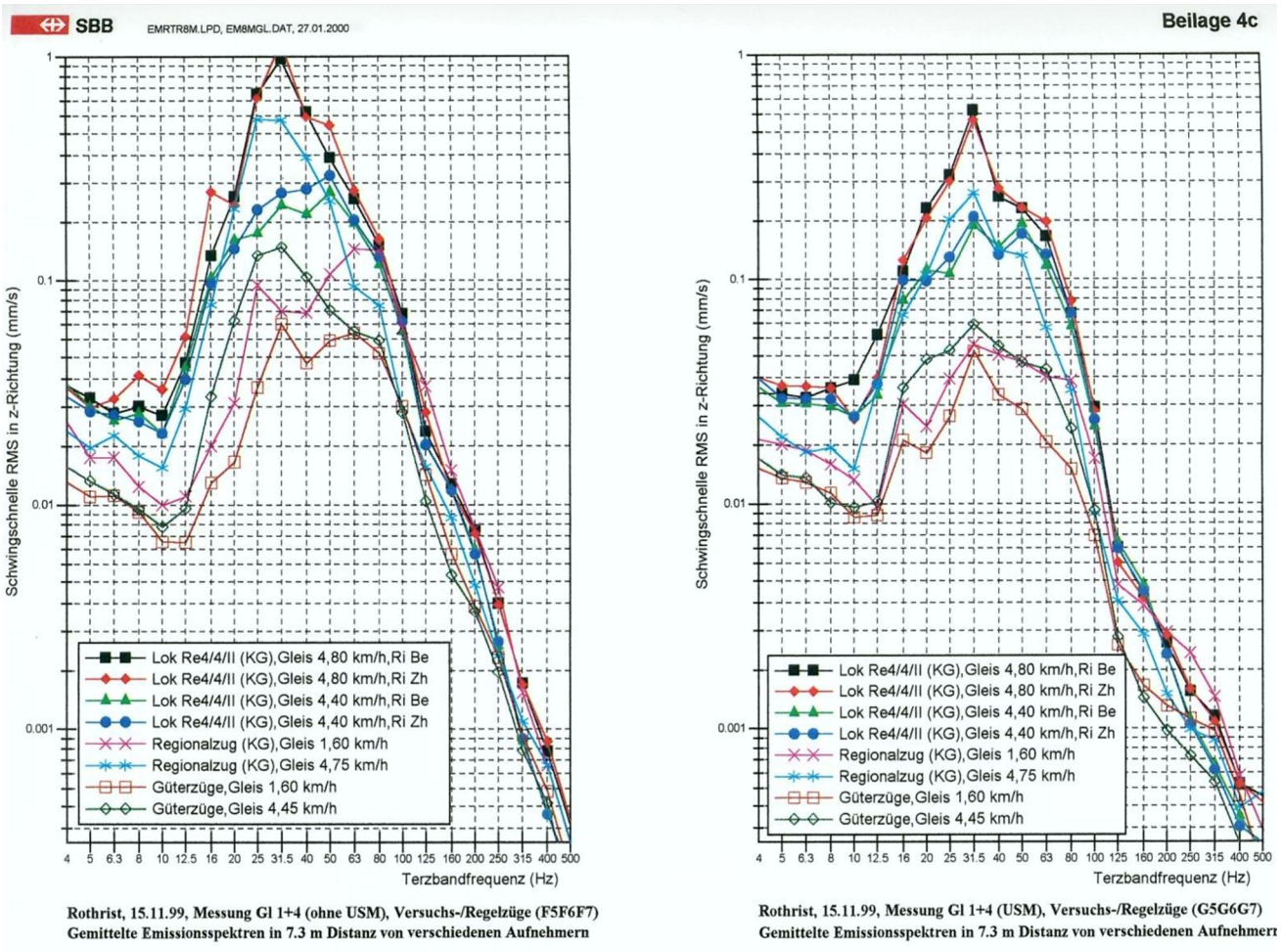

Figure 2.34: Measurements in Rothrist for 2 turnouts EW 300 in 7.3 m distance for test locomotive, regional and cargo trains [22]. Left: turnout without UBM (facing: black and green curve), right: turnout with UBM (facing: red and blue curve)

A test about velocity dependency of turnout vibration emissions was performed in Rueschlikon: the velocity was reduced from 90 km/h to 60 km/h for a certain time. The reduction of the vibrations was about 45 % as predicted by the theory, but the turnout-amplification did not change significantly.

2.7 METHODOLOGY TO ASSESS TURNOUT QUALITY FOR GROUND VIBRATION

There are yet no generally agreed procedures to assess the turnout quality for ground vibration. Appropriate measurements should be made to evaluate the cause of high vibration levels:

- Track alignment measurement car (indication for turnout geometry)
- Track stiffness measurement along the turnout (hanging sleeper)
- Rail profiles along track (wheel transition)
- Turnout quality measurement of frog (DB)
- Axlebox acceleration measurement car (DB)

DB developed a method to measure the quality of a turnout crossing nose by installing sensors on the frog and the sleepers. Results and description of method are presented in Section 3.2.

Another possibility is a measurement car equipped with accelerometers. The CTM-measurement car of DB (see Figure 2.35) is an ICE with acceleration sensors (vertical and horizontal) on axle bearings. It can measure track defects in amplitude, such as turnout quality (see Figure 2.36). The signal processing allows assessment of the track geometry (according to DB standard), the track geometry for short wavelengths (e.g. turnout, rail welds) and the track alignment. The CTM measurements include different types of turnouts (see Figure 2.37), different turnouts of the same type, consecutive runs over the same turnout (maintenance status), see Figure 2.38.

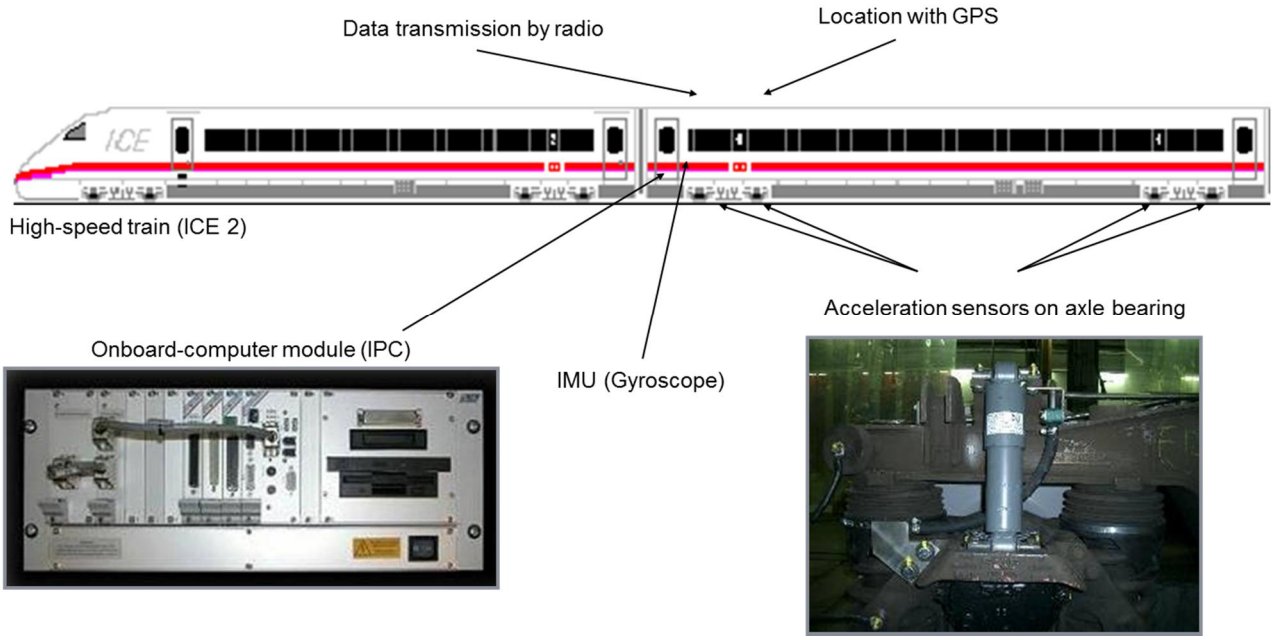

Figure 2.35: DB measurement equipment installed on a ICE which is in regular service

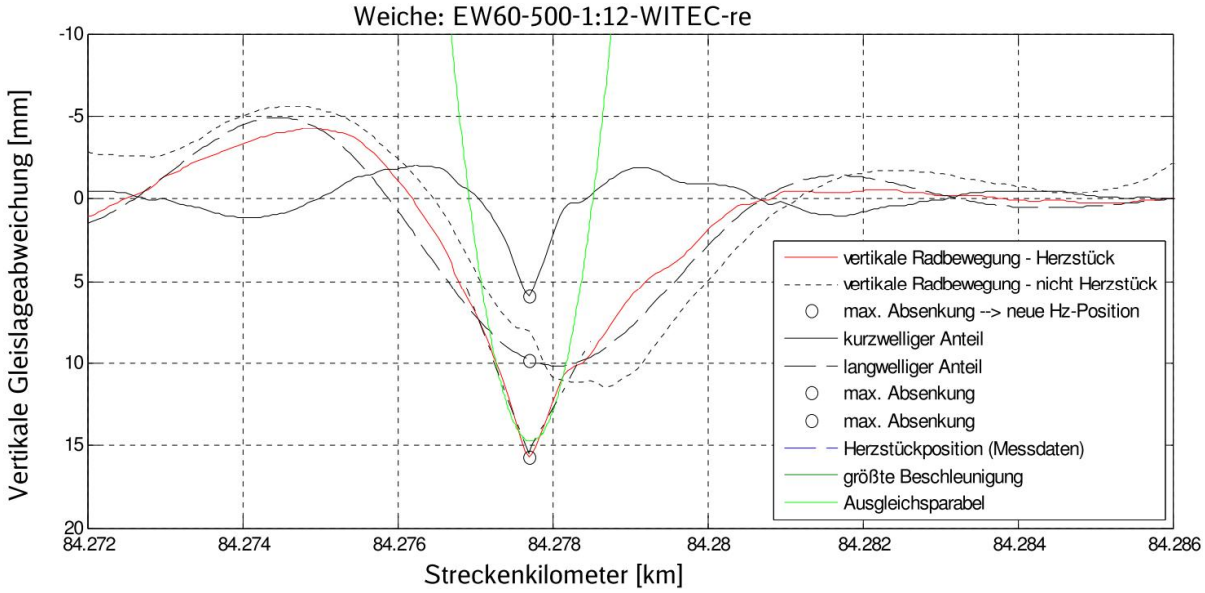

Figure 2.36: Components of vertical wheel movement over turnout

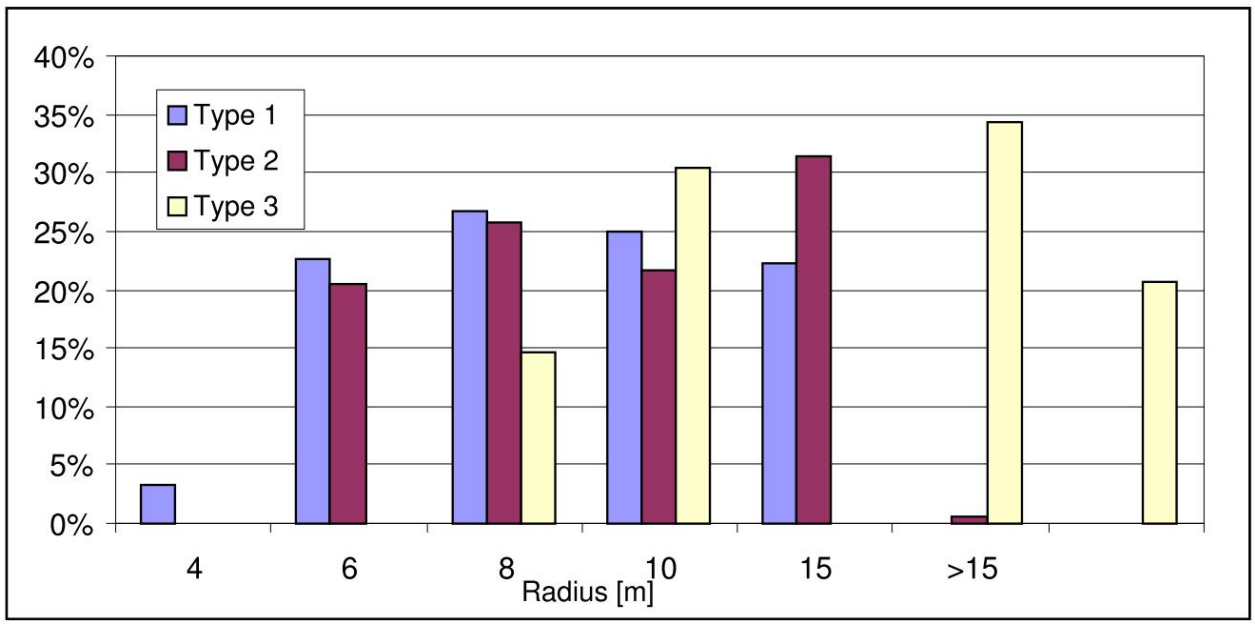

Figure 2.37: Statistical evaluation of z", Radius at lowest point and type of turnout

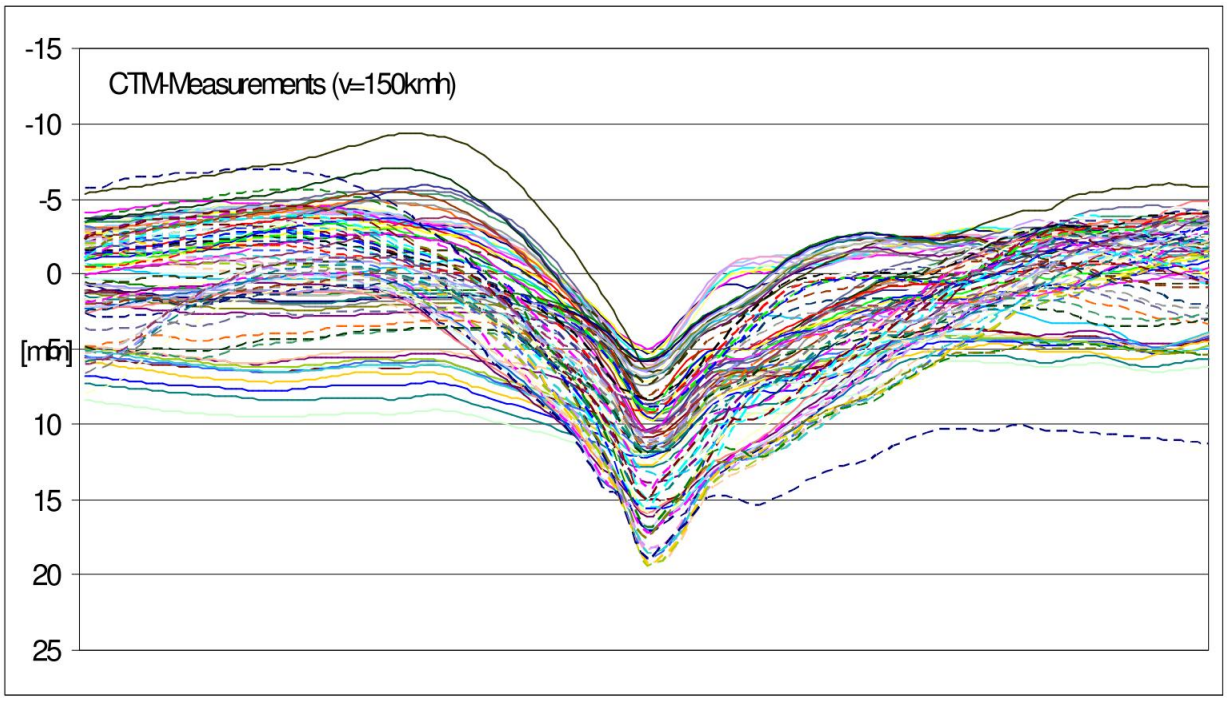

Figure 2.38: CTM-Measurements over the same turnout. y-axis: mm, x-axis in m (total length around 20 m).

For the maintenance influence see WP2, e.g. deliverable D2.3.

2.8 CONCLUSION

This first section has highlighted the complexity of the dynamic excitation when a train runs over a turnout. There are several source of dynamic excitation such as transient sources (joints, nose…) or parametric excitation (variation of track stiffness along the turnout). The contribution of each of these phenomena to the generation of ground vibration in the surrounding environment of the turnout is not yet fully mastered. Supplementary measurement campaigns, supported with numerical simulations, should allow a better understanding of the phenomena at work responsible for the generation of ground vibrations by a turnout.

Meanwhile, first instructions concerning the optimization of a turnout for reducing ground vibrations can be given from previous measurement campaigns results:

- the wheel transition over a turnout shows that geometry is important for optimum and low energy impacts at the crossing nose

- there is an influence of vertical and horizontal geometries

- There is also a big influence of the dynamic properties of the turnout elements such as rail pad stiffness or the insertion of USP.

Finally, to choose the best options for optimizing a turnout, it is important to characterize it precisely in terms of geometry and dynamic properties. The Section 2.7 proposed some measurement set-up that could be used to categorize the different turnouts.

3. REVIEW OF EXPERIMENTS FOR TURNOUT IMPROVEMENTS IN TERM OF GROUNDBORNE VIBRATION

Vibration tests of mitigation measures for turnouts will be summarized in this chapter. Only studies with vibration measurements are given.

Not shown in the results is a small study on switches in tunnels on non-ballasted tracks [23] which indicates some reduction in the turnout-amplification in comparison to ballasted track turnouts. Also not discussed in this report is a test at INNOTRACK (no vibration measurements) with a stiffened turnout (Corus track).

3.1 MOVEABLE FROGS

Figure 3.1: Moveable frog in Rueschlikon [25]

SBB tested moveable frogs (Figure 3.1) to reduce additional vibration of turnouts on open lines. A first estimation of the insulation efficiency (mitigation effect: turnout-amplification reference normal frogs minus turnout-amplification moveable frogs) of old moveable frogs for turnouts on wooden sleepers took place in Lenzburg [21] and Othmarsingen [24]. A comparison between turnouts with and without moveable frogs could be accomplished for both cases. Additionally, in the year 2004 a pilot project was executed in Rueschlikon where 2 turnouts without moveable frogs were replaced by turnouts with moveable frogs [25]. The vibration reduction is small for all moveable frogs: it allows getting a mean reduction between 0 and 3 dB for the frequency range of interest from 16 Hz to 80 Hz (see Figure 3.2). The SBB measurements demonstrate that the installation of very expensive moveable frogs is not suitable for vibration mitigation. The results tends to demonstrate that the impact load at the frog is not necessarily the only dominant excitation phenomenon for ground vibration generation due to a turnout.

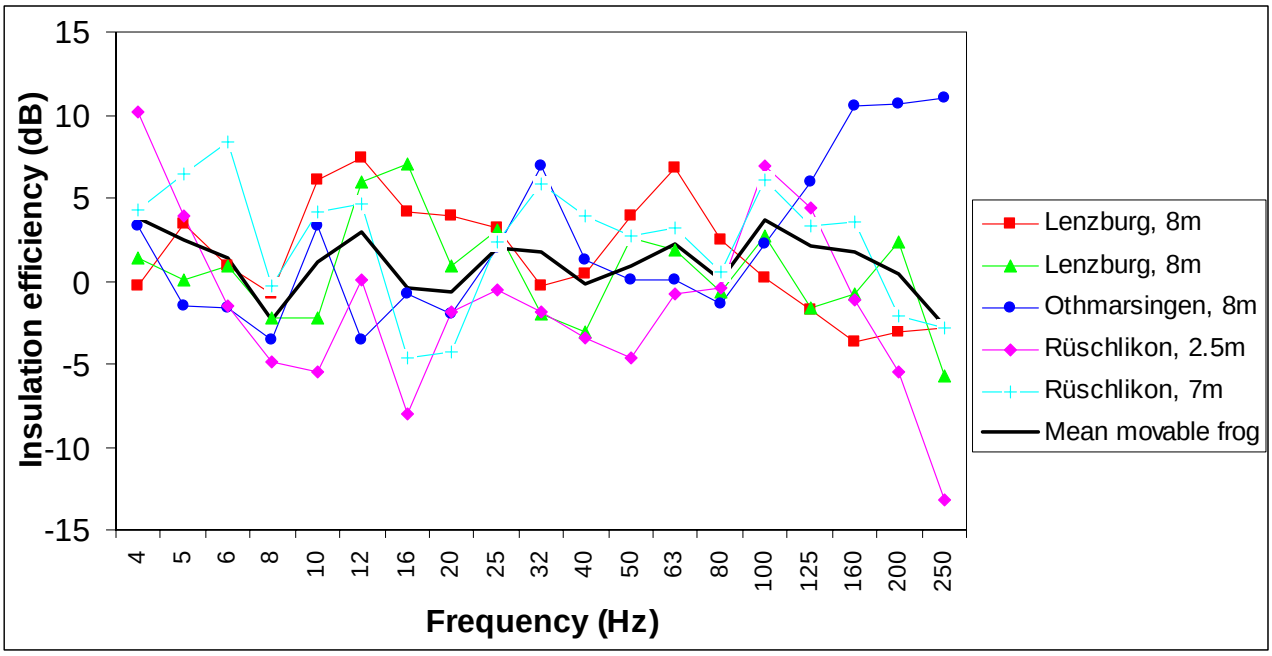

Figure 3.2: Mitigation effect (insulation efficiency) of 5 turnouts with movable frog (reference: turnouts with fixed frog)

A test site in Austria (Baden) [26], which is introduced in section 4.4 in more detail, shows a better effect for one turnout with moveable frog of about 3-6 dB insulation efficiency (see Figure 3.3) in the relevant frequency range from 8 Hz - 63 Hz. So the Swiss and the Austrian experience are not really in agreement. Maybe it depends on the maintenance status of the frogs.

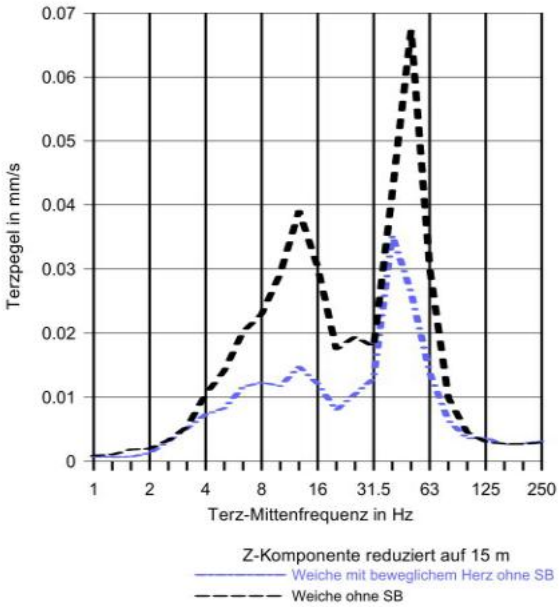

Figure 3.3: Comparison of 1/3 octave vibration velocity emissions of one switch with movable frog (blue curve) and one without (black curve). ÖBB test in Baden. [26]

3.2 IMPROVED FROG

SBB tested [27] for the first time a single casting of manganese steel on a line with heavy use (Altstetten, see Figure 3.4). The casting is treated with explosive shock hardening to increase service life and improve LCC. In March 2008 the change of the EW900 turnout was made and included 15 sleepers with USP around the frog (type SLB 2210). Vibration measurements were performed at this place and comparisons made to the second turnout of the same type just on the other track next to the test turnout.

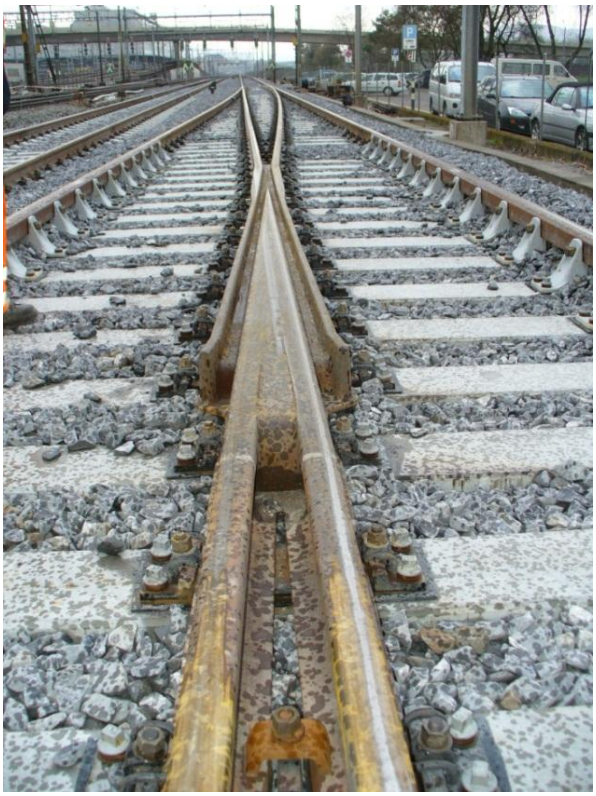

Figure 3.4: Test of frog casting for manganese steel with explosive shock hardening and 15 USP sleepers in Altstetten [27]

In Figure 3.5 the insulation efficiency of the tested frog is illustrated. From 12 to 20 Hz and from 50 Hz and above the test frog amplifies the vibration. An insulation efficiency is only visible for the important frequencies of 25 Hz and 31.5 Hz between 5 and 10 dB.

Probably the compared turnout has very good wheel transition geometry. The main emissions for both turnouts are 50 Hz and 63 Hz. From a vibrational point of view, this test was not yet successful. It would need some years of train traffic to draw conclusions.

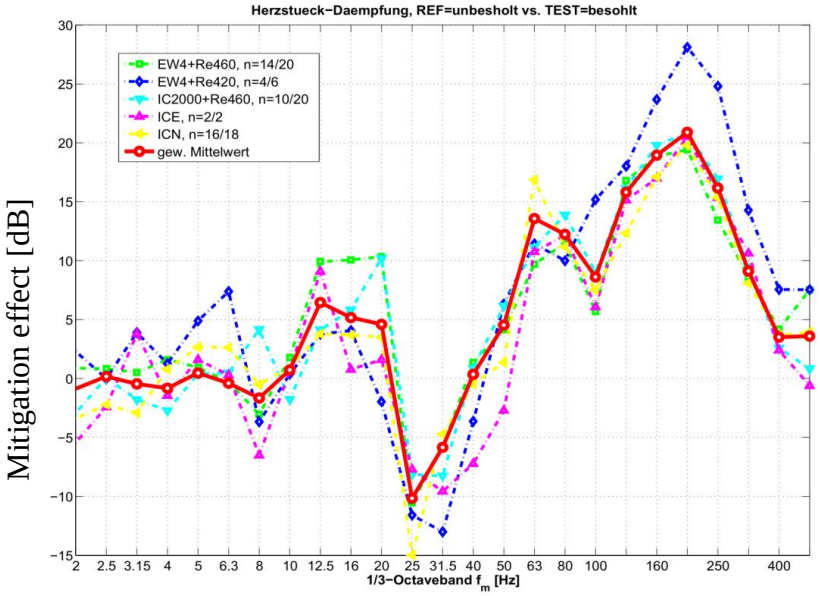

Figure 3.5: Mitigation effect of test frog in Altstetten (positive values means amplification of test frog) [27]

3.3 TURNOUT FORM

In literature ([28] p. 222) a slim turnout form is suggested as a vibration mitigation measure but no further explanations are given. Most probably the turnout geometry is concerned and larger radii should give less vibration. In section 2.5.1 SBB experience is summarized and shows that larger radii in deed have less vibration amplification. Also DB experience with the CTM measurement car (Section 2.7) shows dependencies on turnout quality in comparison to turnout types.

So far the exact reason for this behavior is not known but could probably give indications how a small radius turnout could be improved.

The exchange of a small radius turnout with a larger radius turnout as a mitigation measure is not cost effective and often not feasible.

3.4 UNDER SLEEPER PAD (USP) PRETESTS

Until now SBB did not find a cost-effective vibration mitigation measure for turnouts for open lines in the last 15 years. SBB is still running a test with hard under sleeper pads (USP) which has a potential as a cost-effective mitigation measure. The first results of different tests (SBB, ÖBB, Belgium) measured before the RIVAS Project showed promising results and are presented here.

3.4.1 Test Sites

This section gives the characterization of the turnouts.

Rubigen, Switzerland, SBB [29]
See also the test site in Chapter 4. Two turnouts and the track have been renewed in Rubigen in October 2005. Measurements have been performed before (two old turnouts) and after (two new turnouts with undersleeper pads) on open line, small embankment of 2.4 m. Traffic is of around 35'000 BRT/day. Systematic maintenance is every 3.5 years in average the last before the turnout change was about the year 2002.

Track before	Rail SBB IV, wooden sleeper, (installation type K)
Turnout before	EW-IV-900-1:19, F,H
Track after	Rail SBB VI, concrete sleeper B91, (installation type Ws)
Turnout after	EW-VI-900-1:19, F/Be with USP Getzner Typ **SLB 2210 G** (static stiffness Cstat = 0.22 N/mm^3)

Stadelhofen tunnel, Switzerland, SBB [30]
Installation of two new turnouts, change from wooden sleepers to wooden sleepers with USP for turnout. USP type Getzner SLS1010 (Cstat = 0.1 N/mm^3, in track around 0.07 N/mm^3). Heavy regional trains are passing.

Baden, Austria, ÖBB [26]
High speed track, on an embankment, concrete sleeper, two turnouts with USP type Getzner SLS 1308 G **(**Cstat = 0.13 N/mm^3, in track around 0.07 N/mm^3 : some laboratory measurements and deflection measurements show the lower stiffness).

Testelt, Belgium, Infrabel [8]
In situ measurements (deflection and ground-borne vibrations) have been performed on 2 turnouts located on SNCB-Line 35 between Diest and Aarschot near Testelt Station. The following laboratory values in Table 3.1 for the USP were obtained.

CDM-USM-H100 test conditions	Static bedding module (MN/m³)	Dynamic bedding module (MN/m³)
Flat Plate	95	181
Normalised Ballast Plate	49	94

Table 3.1: USP stiffness for flat and normalized ballast plate

3.4.2 Vibration Measurements

Rubigen

Measurements in 8 m distance (track direction Thun) and 12 m distance (track direction Berne) before and after modification of both tracks show a vibration reduction for the two new turnouts with USP (after installation). On the left of Figure 3.6 it can be seen that the turnout after modification (red bars) has not much amplification when compared to the reference.

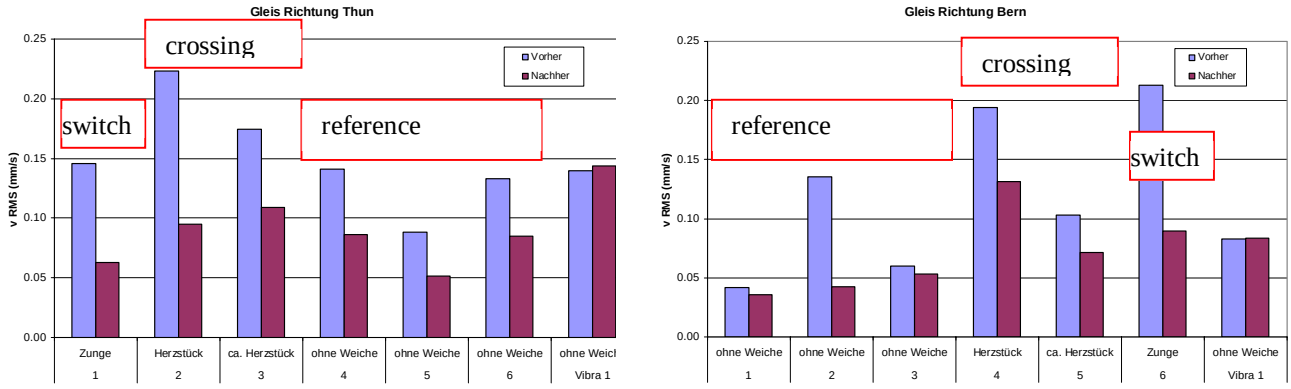

Figure 3.6: Measurements Rubigen before modification (blue bars) in comparison with measurements after modification (red bars). Left: turnout Nr. 1, for direction Thun, 8 m, right: turnout Nr. 2, for direction Berne, 12 m. [29]

The frequency dependency is illustrated in Figure 3.7. By the installation of USP it seems that in the important frequency range from 20 to 63 Hz the emissions could be reduced significantly. At 80 Hz there is no effect what could be due to the resonance frequency of the track with USP.

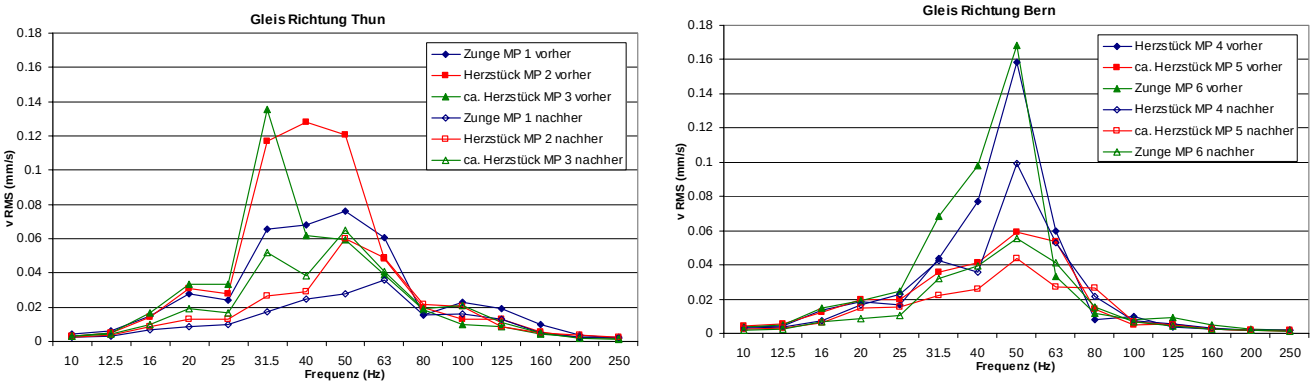

Figure 3.7: Rubigen, Frequency dependency of turnouts in 8 m (Direction Thun) and 12 m distance (direction Berne). [29]

Stadelhofen

Measurements were performed on the banket of the tunnel Museumsstrasse and in a building (Winkelwiese 6). Building: groundborne noise measurements show about the same amplitudes for the turnout with USP as for the track without USP (see Figure 3.8). One room shows more, one less groundborne noise (25-50 Hz), over 63 Hz less groundborne noise is measured.

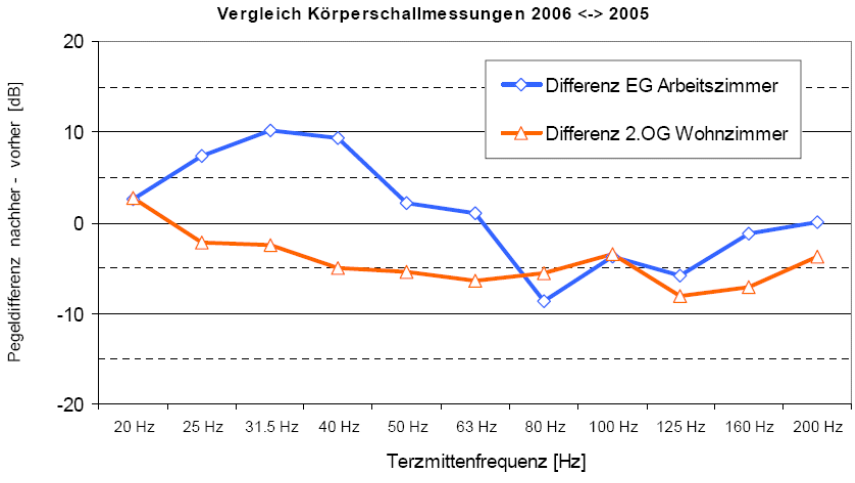

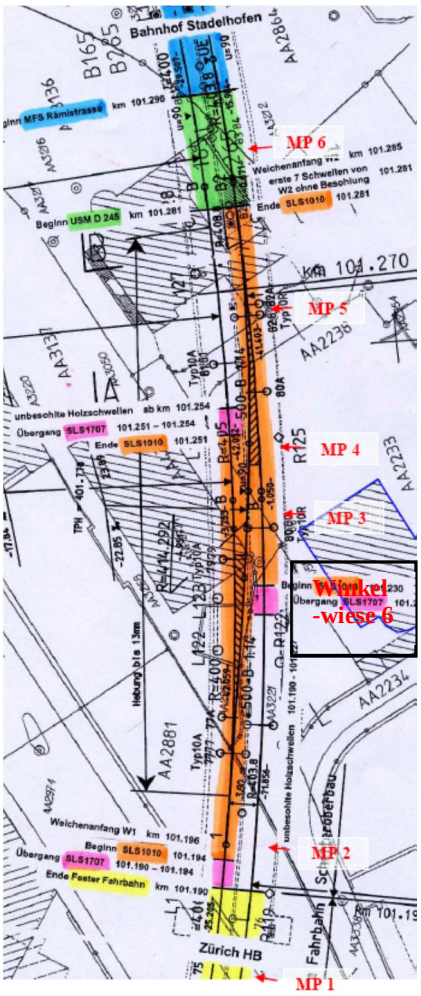

Figure 3.8: Difference in groundborne noise after (turnout incl. USP) to before installation (no turnout, no USP). Right picture: measurement positions in tunnel [30]

The frequency analysis for vibration measurements is illustrated in Figure 3.9. A comparison of turnout with and without USP is not possible here.

- Comparison track 1, measurement point MP1 and MP2 before and after show that the new track has no influence.
- Comparison track 2, measurement point 2 (MP 2) before/after shows, that USP for normal track show significant insertion loss (see green curve of right diagram of Figure 3.9).
- MP 3 before/after (both tracks) shows for tunnel that turnout with USP in comparison to track without turnout and without USP.
    - There is a lot more vibration in lower frequencies.
    - The maximum emission amplitude is in the same range => No turnout-amplification

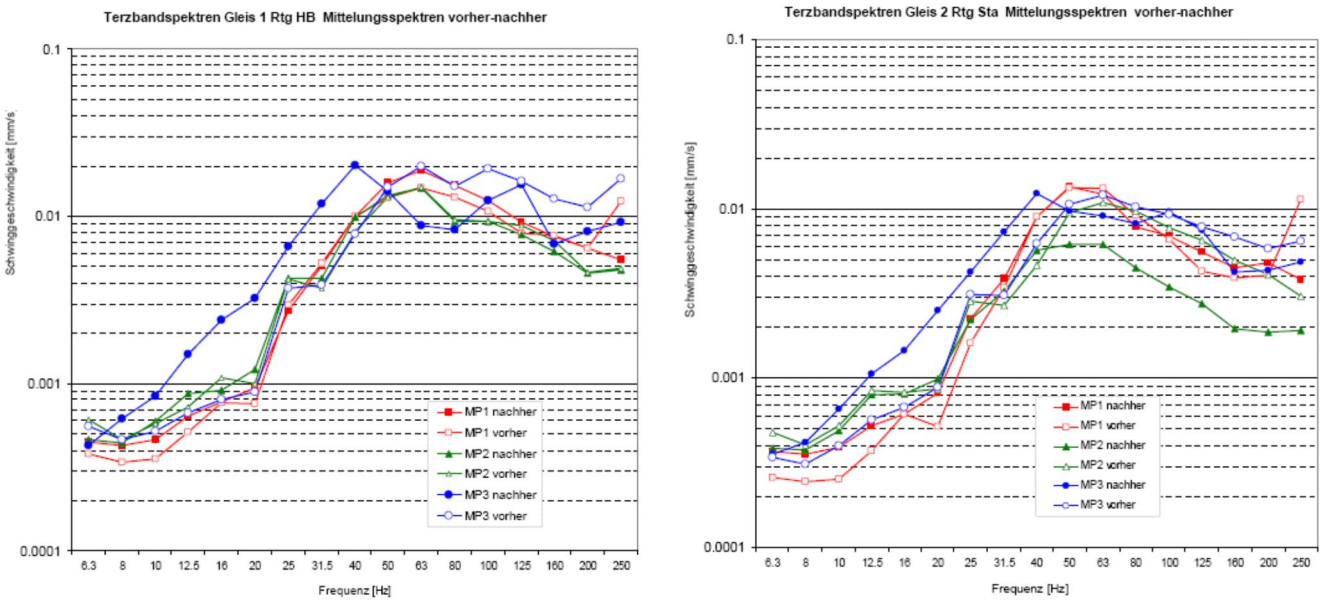

Figure 3.9: Stadelhofen, 1/3 octave emission spectra for vibration velocity on tunnel bankett. Left diagram for track 1, right diagram for track 2. MP1, MP2, no turnout, MP3 “before” no turnout, “after” with turnout.

Baden, Austria [26]

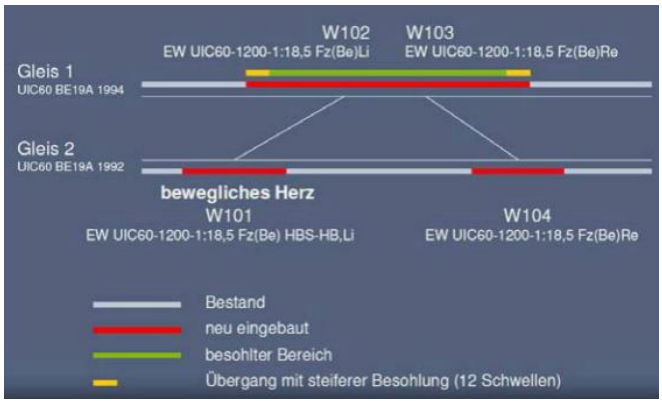

Figure 3.10: Schematic test site (moveable frog results see Section 4.1). [31]

Comparison of turnout with and without USP can be done in Baden (Figure 3.10). Measurement points on road (asphalt layer) are in distances of 28 m to 19 m to the track. The values have been normalized to 15 m by regression ($q=(d_1/d_2)^{-b}$, b defined by regression, d distance, q quotient) for every measurement profile, so that comparison is possible. Measurements are performed in one horizontal (perpendicular to track) and the vertical direction.

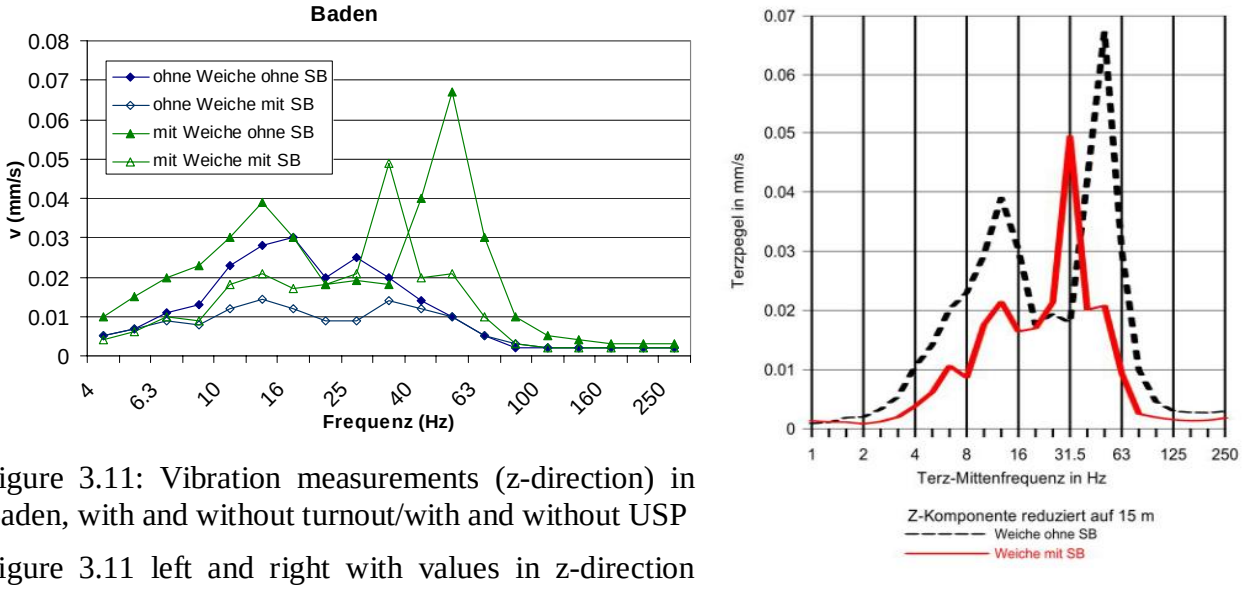

Figure 3.11: Vibration measurements (z-direction) in Baden, with and without turnout/with and without USP

Figure 3.11 left and right with values in z-direction shows a significant reduction of the most important emissions in the comparison of turnout with/without USP as well as normal track with/without USP. As for Rubigen it can be seen in Figure 3.11 left that the turnout-amplification is smaller in comparison to a normal turnout-amplification. The tracks with turnout show quite different vibration emissions in frequency than tracks without turnout for the same rolling stock.

The insertion loss of a turnout with USP (reference turnout without USP) of Rubigen and Baden is shown in Figure 3.12. It shows often relevant insertion loss for turnouts with USP. But the insertion loss curve form is not similar for the three turnouts (this is probably due to other important turnout parameters not measured: e.g. maintenance status). Therefore, it is better to look at the emission spectra directly. For all turnouts with USP it is visible that the most important emission maxima, independent of the frequency, can be reduced. The tendency that the emission spectra are moving to lower frequencies is visible.

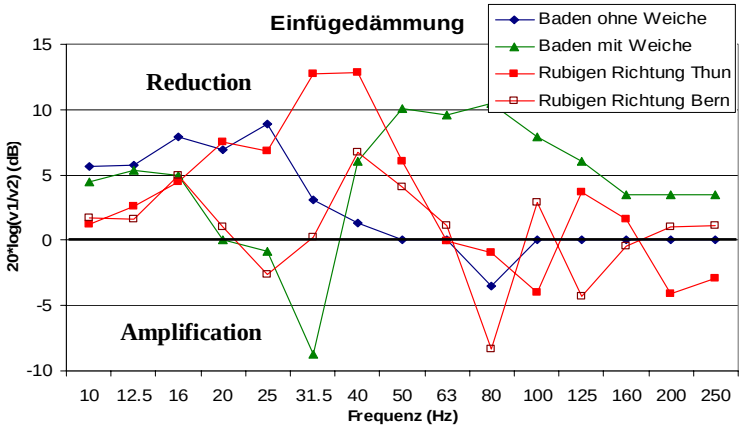

Figure 3.12: Insertion loss for turnout with USP/without USP of Baden and Rubigen, and Baden normal track with USP/without USP (blue). [29]

Possible improvement of turnout geometry quality by USP installation

Tests of geometry quality at ÖBB show improvements by installing USP for turnouts.

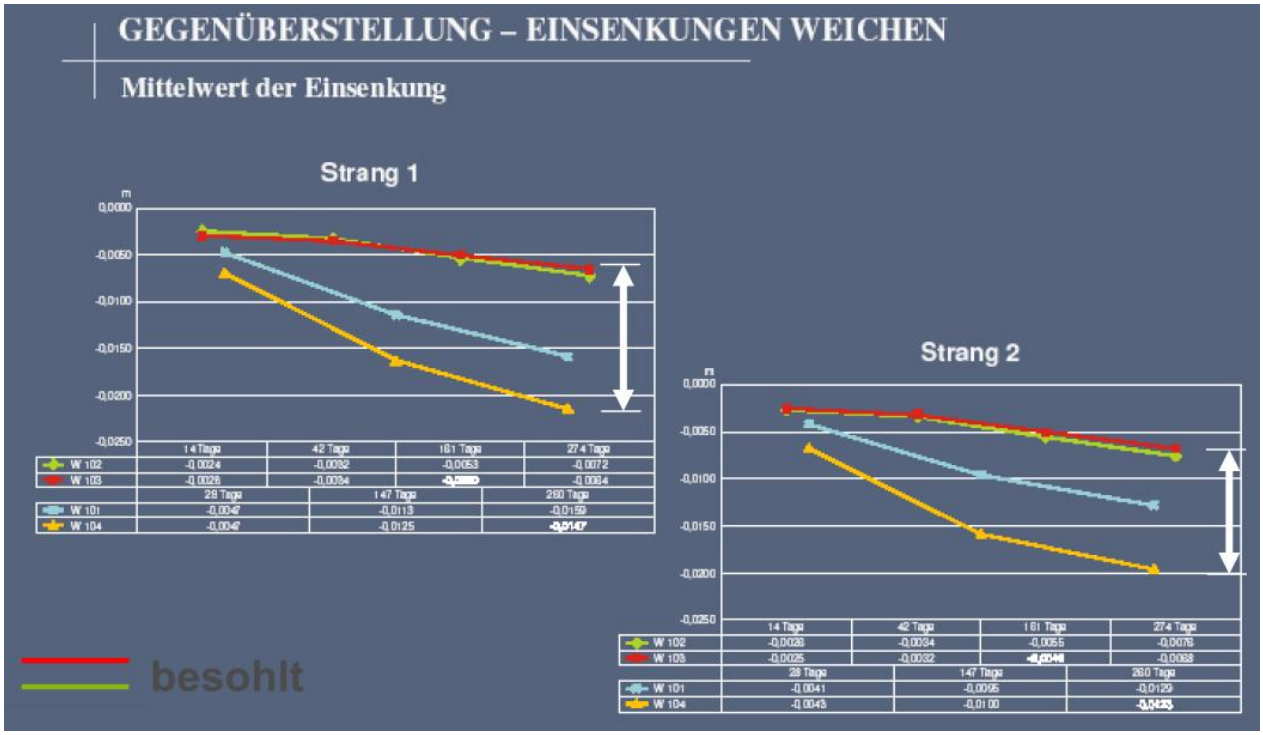

Figure 3.13: Time development of rail deflections of 4 different turnouts. The two turnouts with USP, red and green, show less geometry movements over time [31]

USP for turnouts are used for the first time in 2002. Until 2007, 87 turnouts are installed on the ÖBB network. Baden was one of the first test sections (see Figure 3.10, 3.13). The positive aspects of USP are seen also in the turnouts. The USP is preserving ballast and the higher system-elasticity leads to better track geometry quality and to less maintenance. The Figures 3.14 and 3.15 show a comparison of track geometry quality for a turnout with moveable frog and no USP and for the turnout with fixed frog and with USP. The turnout without USP shows the tendency to decrease along the turnout. The other signal ("Längshöhe") shows more disturbed vertical track geometry. The track quality at the frog is not much more disturbed (effect of moveable frog). The turnout with USP shows, due to less deflection (see Figure 3.13), a better track quality ("Überhöhung" and "Längshöhe").

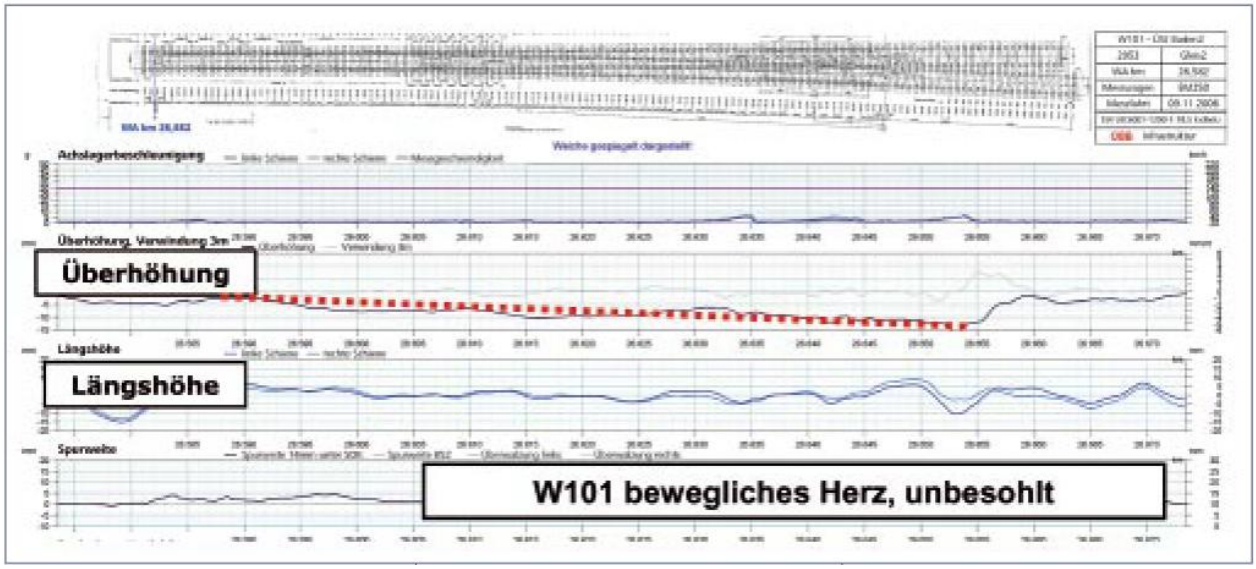

Figure 3.14: Track geometry for turnout with moveable frog [31]

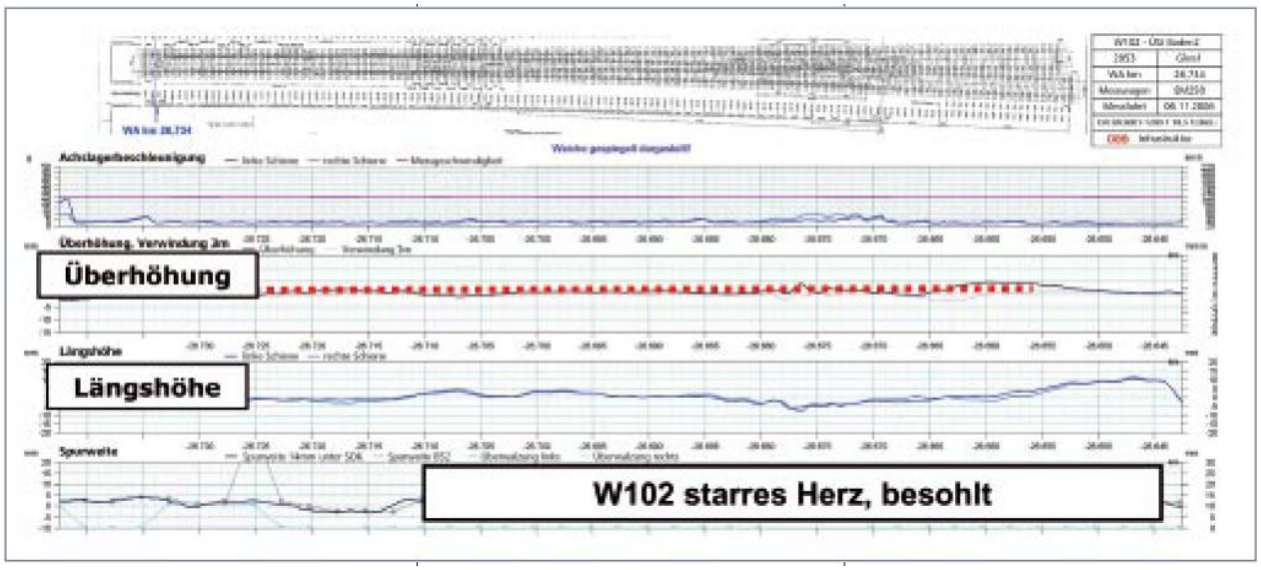

Figure 3.15: Track geometry for turnout with USP [31]

Testelt, Belgium

The introduction of under sleeper pads was experimentally tested during renewal of a turnout [8]. Figure 3.16 shows measured ground vibration insertion loss. An attenuation of up to 14 dB is achievable for the USP turnout. A turnout renewal does show only small influence on insertion loss. Figure 3.17 shows that the USP is very soft (0.095 N/mm^3): the mean additional deflection is more than 1 mm and small amplitude maxima (wheel out of roundness?) show additional amplitudes of around 5 mm.

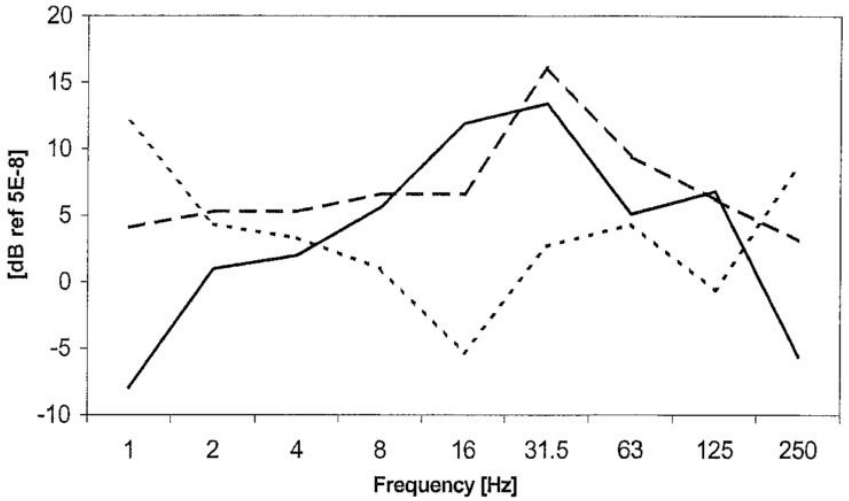

Fig. 15. — Effect of USM treatment only (difference between vibration reduction for case B and case A), --- vibration reduction for case A (turn-out renovation), – – – vibration reduction for case B (turn-out renovation + USM)

Figure 3.16: Effect of USP (here named USM) on ground borne vibrations [8]

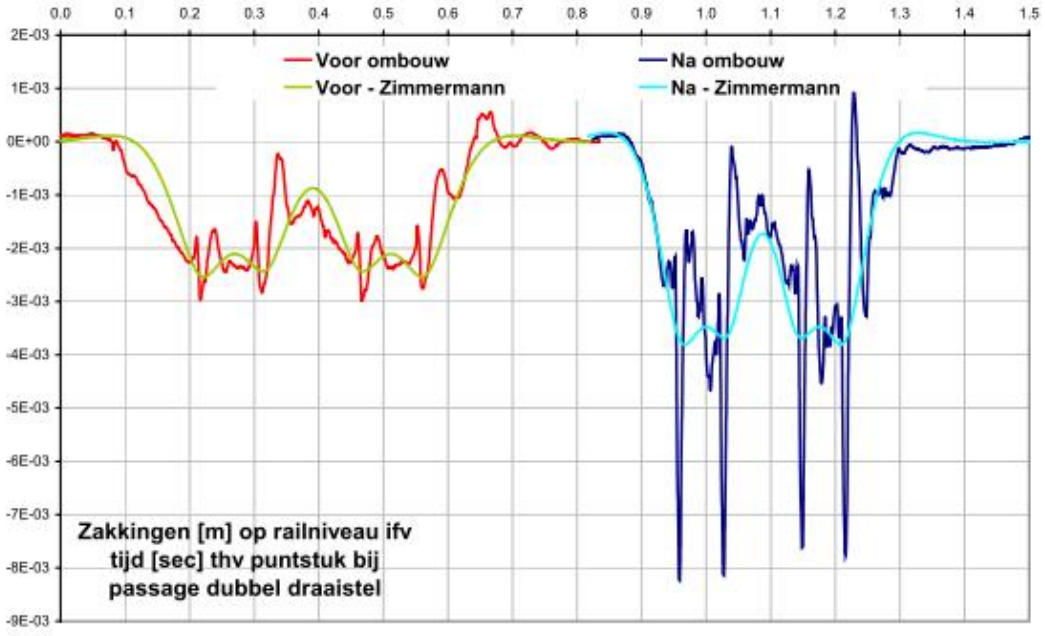

Figure 3.17: Dynamic deflection measurements of a double bogie at the frog before (left) and after renewal (right, with USP). [8]

3.4.3 Conclusions

- The old experiences of turnouts with USP show from measurements that the insertion loss can be considerable high. But the very soft USP (Cstat = 0.1 - 0.13) show different behavior (Baden, Stadelhofen, Testelt).

- Possibly not measured turnout parameters, e.g. maintenance status, play an important role in validation measurements.

- The emission spectra show for Cstat = 0.1 N/mm^3 and Cstat = 0.13 N/mm^3 a shift to lower frequencies: f(max after) ≅ 0.7 * f(max before). For Cstat=0.22 N/mm^3 no frequency shift is visible.

3.5 UNDER BALLAST MAT (UBM)

An under ballast mat (UBM) can reduce vibration significantly but normally above 40 Hz. For this reason a concrete baseplate is normally used additionally to reduce the low frequency emissions of the turnout (see Section 4.6 for concrete baseplate). The UBM is normally used to reduce the amplifications at higher frequencies of a baseplate. Normally, an under ballast mat needs a side support so that the ballast cannot move sideward.

SBB tested UBM for a turnout EW 300 without concrete plate in Rothrist on an open line [22]. The two turnouts on track 4 were installed around 1 month before the measurements. At the time of the measurements not every track was installed (track 2 and track 3 were missing), so the measurements could be done between track 1 and track 4 (see Figure 3.18).

Figure 3.18: Test site in Rubigen. Turnout 43 without UBM and measurement positions between the tracks. [22]

Figure 3.19 shows the insertion loss of a turnout with UBM to a turnout without UBM (track 4). For track 1, which is a normal track without turnouts, the UBM effect for normal track is shown. The track 4 results show an improved insertion loss for lower frequencies and a decrease of insertion loss for higher frequencies. So far, there is no physical reason known, why the UBM should have different performance under new turnouts. Measurements of the turnout-amplification of the two turnouts indicate that the seen difference in insertion loss for turnouts is due to the different dynamic behavior of the two turnouts. The exact reason for these effects is not known, as further turnout characterization measurements are not available. But it has to be considered that the turnout without UBM is fixed in straight direction and has not yet a connection to the parallel track as this was not yet built. So this turnout is more flexible and due to this flexibility the resonance of the turnout could be lower and higher frequencies could be reduced.

1. The measurements on the sleepers at the frog and at the switch part (not shown in this report, see [22]) do not show additional effects due to the UBM.
2. The UBM mitigation effect is probably similar for turnout than without turnout (for new turnouts no physical mechanism is known to change mitigation effects). The big differences measured in the turnout-amplifications of the two turnouts (see [22]) make it impossible to conclude directly from the measured UBM effect for turnouts.
3. The turnout-amplification can vary heavily even for new turnouts of the same type (EW 300).
4. It could be concluded for future turnout validation measurements: it is strongly recommended that the turnouts (with/without mitigation measure) have to show very similar turnout-amplifications. If this is not the case, results have to be regarded with caution.

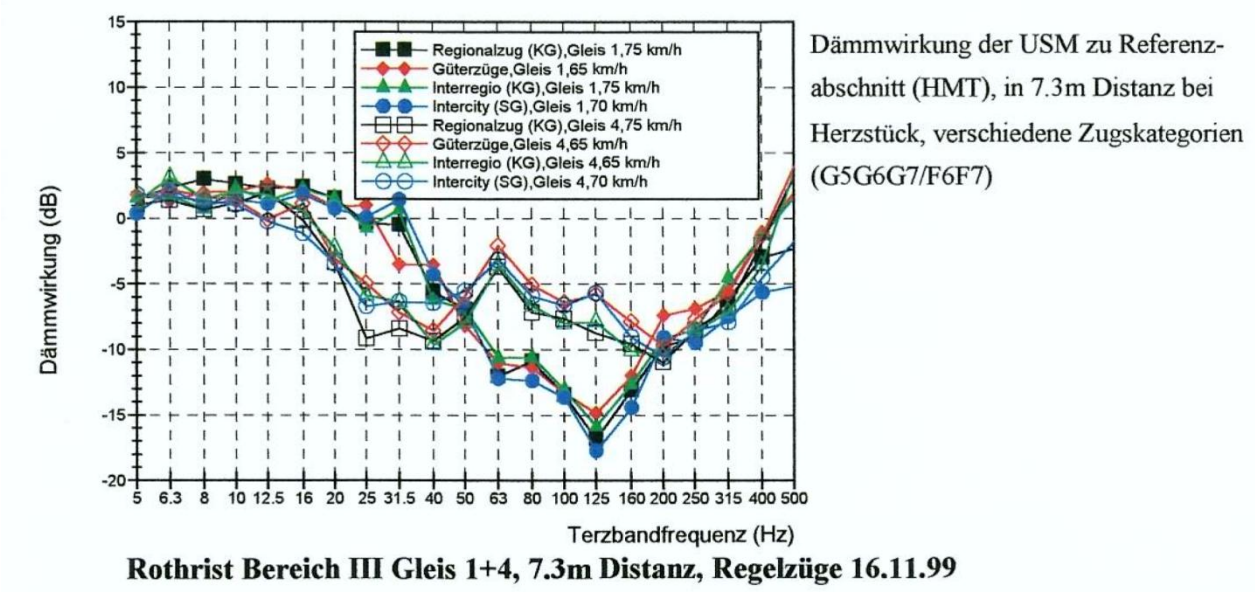

Figure 3.19: Rothrist measurements of insertion loss of UBM (track 1 without turnouts: lines with filled signs, track 4 with turnouts: lines with unfilled signs) [22]

Emission spectra for the two Rothrist turnouts EW300 see Section 2.5.

3.6 CONCRETE BASEPLATE AND UNDER BALLAST MAT

SBB installed a concrete baseplate together with an UBM in Visp for vibration protection of a turnout. Unfortunately, there is no real possibility to measure the insertion loss of the concrete baseplate incl. UBM in Visp because a suitable reference section is missing.

SBB studied concrete baseplate and soil stiffening in a literature study [32]. In Figure 3.20 the insertion loss of a concrete baseplate together with UBM in the low frequency range is illustrated. Between 8 Hz and 20 Hz maximum insertion loss of 5 dB is visible. Between 25 and 40 Hz nearly no mitigation effect can be seen. Attention: for a concrete baseplate a similar amplification above 40 Hz is normally produced when no UBM is installed.

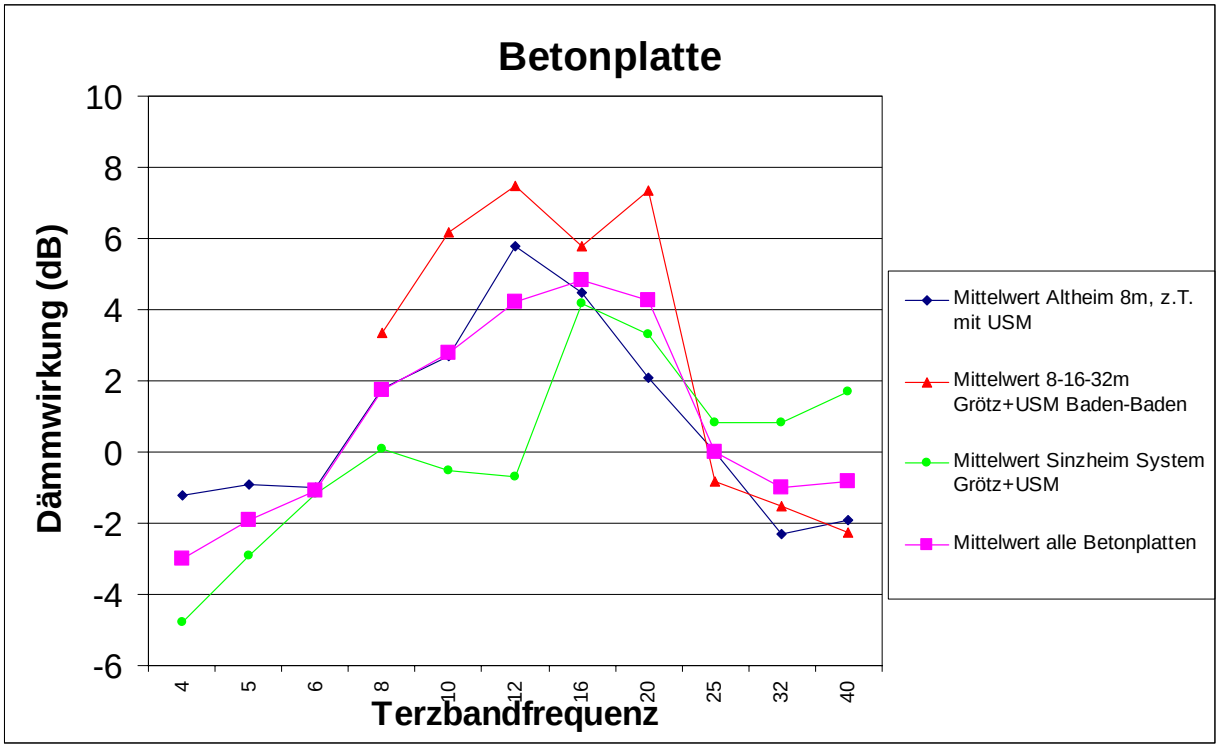

Figure 3.20: Insertion loss of concrete baseplate (incl. UBM= USM) of 3 tests in Germany [32]

With soil stiffening (see Figure 3.21) similar results can be obtained. Below 40 Hz small insertion loss of maximal 5 dB at 12 Hz and 16 Hz result from the soil stiffening. Vibration amplification due to the soil stiffening is produced at 50 Hz and at higher frequencies. This kind of mitigation measure obviously has to be improved with UBM or USP, otherwise groundborne noise amplification can be observed in buildings.

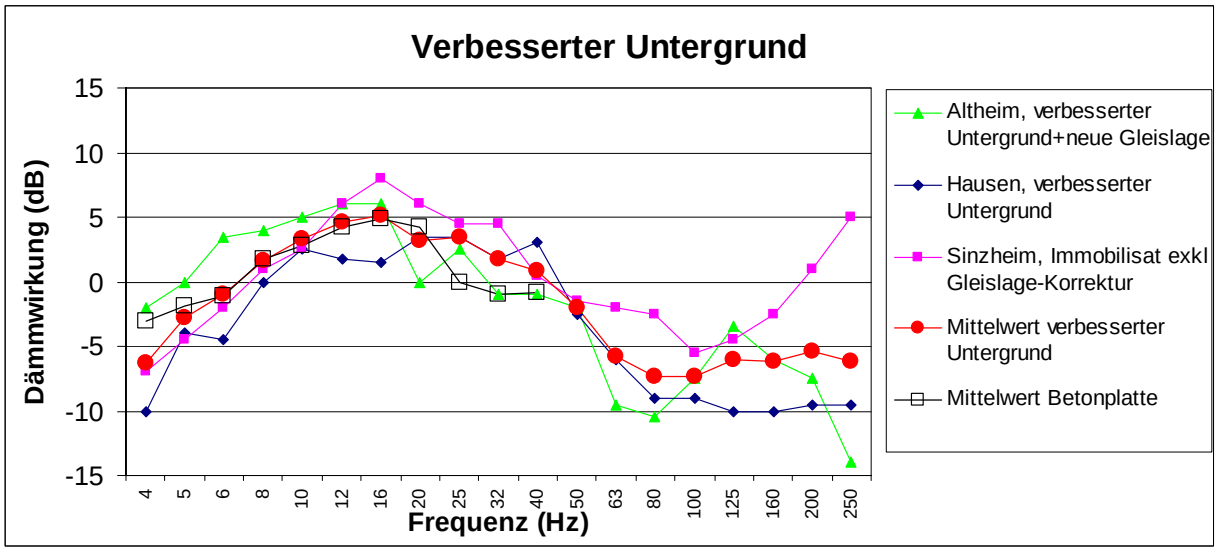

Figure 3.21: Insertion loss of soil stiffening (without UBM) of 3 sites. [32]

3.7 TURNOUT MAINTENANCE (RAIL GRINDING)

A test of rail grinding of the railway company BLS was not successful in Berne, Switzerland [33]. It even amplified the vibration emissions in some frequencies (see Figure 3.22). In 6 m distance some reduction at 31 Hz can be seen (see figure 3.23). The effect of a trench next to a turnout, on the other hand, seems very efficient.

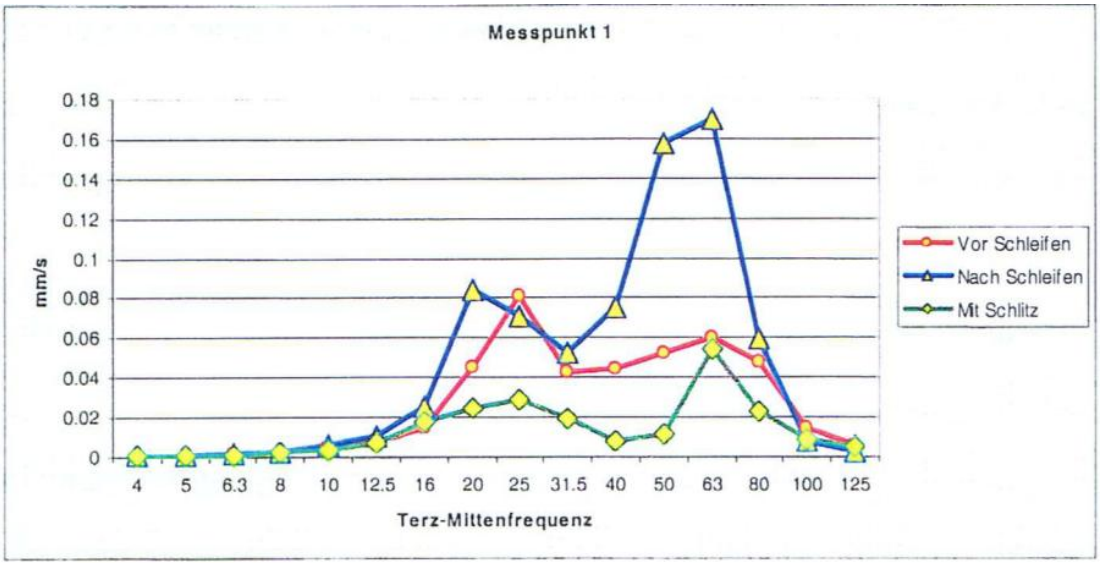

Figure 3.22: Berne, vibration measurement in a room before grinding, after grinding and after trench installation. [33]

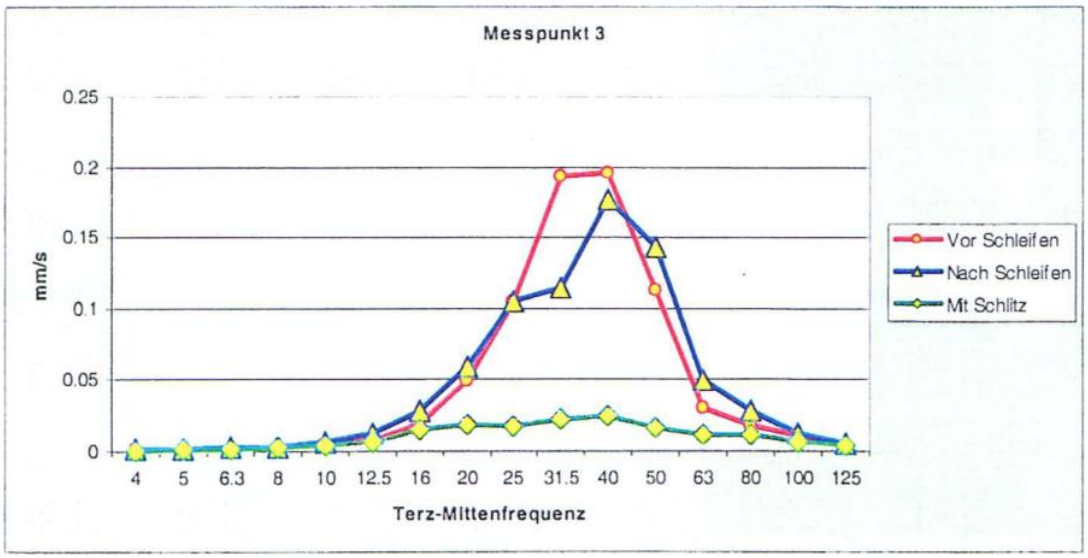

Figure 3.23: Berne, vibration measurement in the garden of the building (ca. 6 m from track) before grinding, after grinding and after trench installation. [33]

The turnout vibration emissions also normally increase on the long-term because of degradation of the maintenance status. So far it is not known how to characterize a turnout with respect to vibration emissions. This question will be investigated in WP3.3 in 2013.

3.8 OTHER NON-TRACK EXPERIENCE FOR TURNOUT MITIGATION MEASURES

Apart from track mitigation other mitigation measures have been tested. But mitigation measures at the turnout, which means at the source, are more interesting, because then also a lifecycle cost improvement of the turnout is expected.

For the influence of train velocity on switch vibration emission see Section 2.7.3.

3.8.1 Trench

A trench could be a solution for low frequency vibration reduction of a turnout. Two trenches have been built in Switzerland so far (results see Figures 3.22/3.23 for one case), both next to a switch. Both times the installation was a success with about a factor of two of improvement even in the lower frequencies. The trench will be studied further in WP4, but especially for turnouts the trench could be a solution if the installation in the ground is feasible.

3.8.2 Floor Stiffening

If only one building and one room of this building is having a resonance phenomenon with the turnout excitation also stiffening of the floor could be a possible mitigation measure. SBB made one test in 1997 in Bevaix [34], where an improvement of a factor of 2 could be attained by provisory stiffening with adjustable support. Normally a fixed support directly under the critical floor has to be installed, which is not yet tested and has feasibility restrictions, especially when there is a living room below the critical floor.

3.9 CONCLUSION

So far it is not possible to draw definitive conclusions from the existing tests which solution could be a cost-effective mitigation measure for a turnout. A chance to improve the vibration excitation of a turnout lies in softening the USP for better track behavior (unfortunately, it is unclear why softer USP should be better for track geometry than stiffer USP), to improve the turnout design (material and geometry of frog and geometry of turnout) and to soften the rail pad.

The development of the “SBB turnout 2015” could be a further option, see Section 5.5.

This state-of-the-art in Chapter 2 and Chapter 3 is partially based on experimental results. This empirical approach has been applied in the first month of the RIVAS project, to assess the mitigation effect of under sleeper pads in turnouts. The following chapter presents the results for 2 sites equipped by SBB. Each of these sites is composed of a modified turnout equipped with USP and a reference turnout unchanged in which ground vibrations have been measured.

4. TESTS OF USP INSTALLATION IN TURNOUTS FOR GROUND VIBRATION REDUCTION

In this chapter the measurements in Rubigen and Le Landeron (SBB sites) performed during the first 18 month of the RIVAS project are described. On the one hand there is a big lack of systematic vibration measurements to characterise turnout emissions. On the other hand it is not yet known how a turnout should be characterised by measurements. Experience has been gained on these two issues by measuring 8 turnouts, 4 with installed hard USP and 4 without USP.

4.1 VIBRATION MEASUREMENTS

Vibration measurements were performed in September 2011 in Rubigen (CH) and Le Landeron (CH) by the Federal Institute for Materials Research and Testing (BAM), Germany [35], and by Ziegler Consultants, Switzerland [36,37]. The goal of the investigation was to assess the effect of under sleeper pads (USP) on ground vibration levels from railway turnouts and ground vibration decay rates. Therefore, measurements were performed next to turnouts equipped with under sleeper pads and turnouts without under sleeper pads.

4.1.1 Measurement Location and Experimental Set-up

Measurements were performed in Rubigen and Le Landeron, Switzerland, (see Figure 4.1). In Rubigen, three different configurations were investigated: two turnouts with under sleeper pads, two turnouts without under sleeper pads and a reference case of a track without turnout (Ziegler investigated two reference cases [36]). In Le Landeron, two turnouts with under sleeper pads and two turnouts without under sleeper pads were investigated (Ziegler also invested the track without turnout [37]). The characteristics of the USP material is c_{stat}=0.022 N/mm^3).

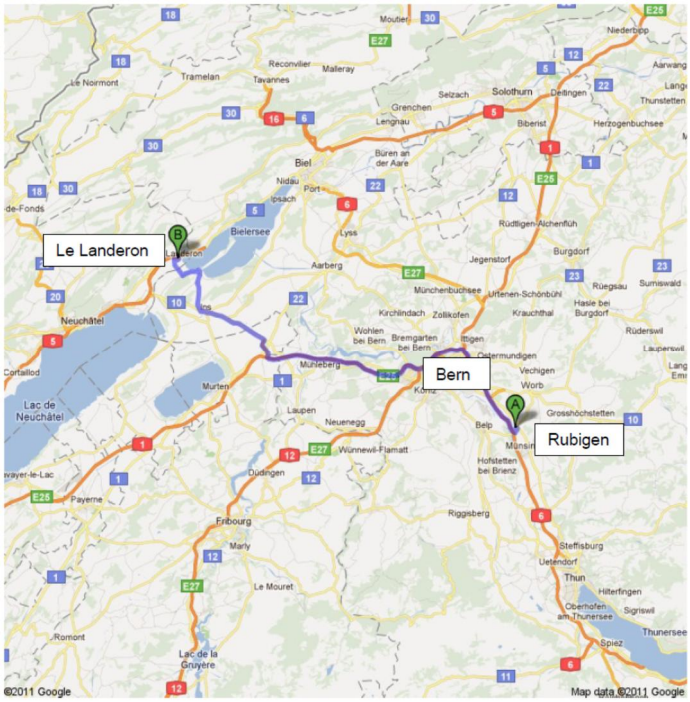

Figure 4.1: Measurement locations: A: Rubigen, B: Le Landeron [35]

The experimental set-up and equipment used by the Federal Institute for Materials Research and Testing, BAM is shown as well as for the measurements performed by Ziegler Consultants. BAM measured in Rubigen and Le Landeron also at the track (sleeper, railfoot), for results see [35]. BAM could not measure with their measurement equipment the same train at the turnout with/without USP whereas Ziegler could compare the same trains. In Section 4.2 DB acceleration measurements for turnout characterisation at sleepers and frog will be shown.

The site configuration in Le Landeron was very complex for distances over 4 m. It was decided therefore that measurements shall be performed only next to the track.

The measurement locations in Rubigen [35,36] are shown in Figure 4.2, Figure 4.3 and Table 4.1.

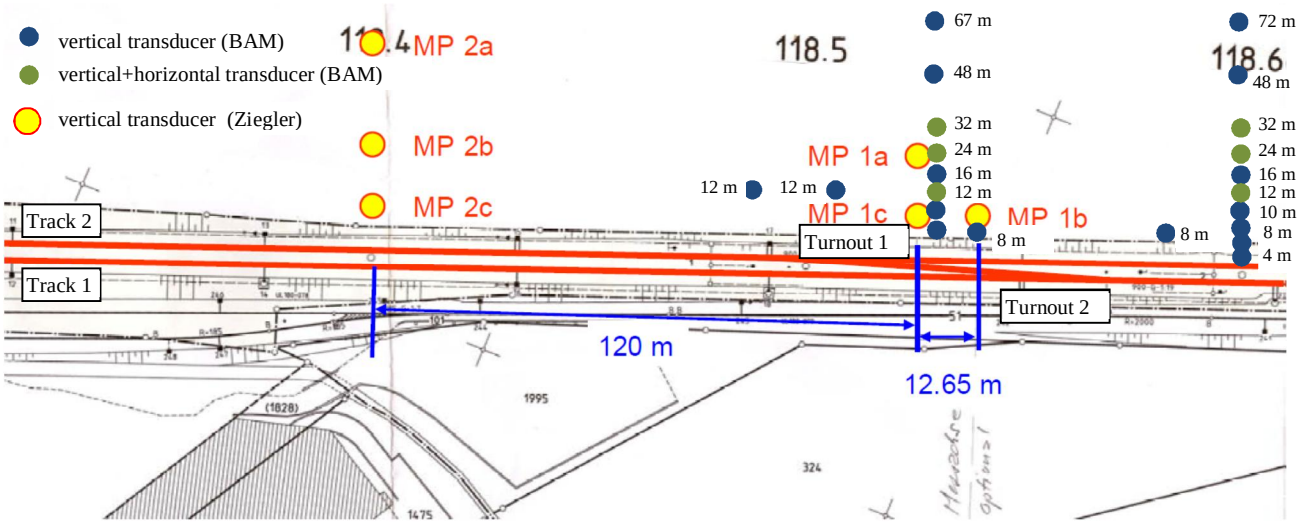

Figure 4.2: Rubigen, turnout 1 and 2 with USP, embankment with about 2 m height

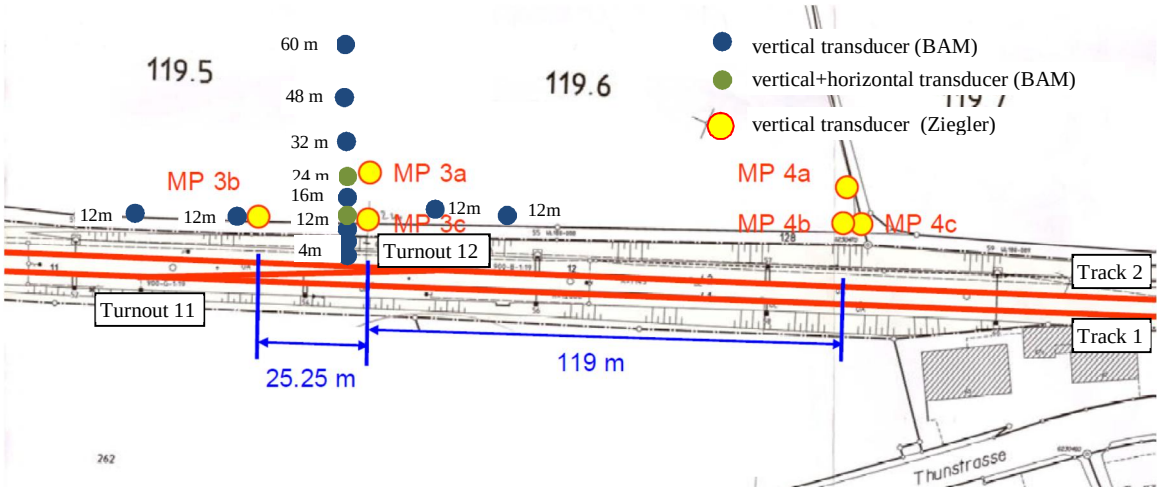

Figure 4.3: Rubigen, turnout 11 and 12 without USP, cut with about 2 m depth

The distance to the track for the different sensor positions is given in Table 4.1.

Measurement place	Sensor	Campaign	Measured Quantity	Distance to Track 2
Turnout 1 (EW900-G-1:19): Frog	MP 1a, 1c	Ziegler	Vertical vibration	23.9 m, 9.9 m
Turnout 1: Frog	8 sensors	BAM	Vertical velocity	8m,10m,12m, 16m, 24m,32m,48m, 67m.
Turnout 1: Frog	3 sensors	BAM	Horizontal velocity	12m,24m,32m
Turnout 1: mid turnout	1 sensor	BAM	Vertical velocity	12m
Turnout 1: switch	1 sensor	BAM	Vertical velocity	12m
Turnout 1: 4 sleepers at frog	4 sensors	DB	Vertical acceleration	At track
Turnout 1: At Frog	1 sensor	DB	Vertical acceleration	At track
Turnout 2 (EW900-G-1:19): Frog	MP 1b	Ziegler	Vertical velocity	9.6m
Turnout 2: Frog	1 sensor	BAM	Vertical velocity	8m
Turnout 2: switch	1 sensor	BAM	Vertical velocity	12m
Turnout 2: 4 sleepers at frog	4 sensors	DB	Vertical acceleration	At track
Turnout 2: At Frog	1 sensor	DB	Vertical acceleration	At track
Reference for turnout 1/2 (no turnout)	MP 2a,2b,2c	Ziegler	Vertical velocity	46.7m,23.7m,9.7m
Reference for turnout 1/2 (no turnout)	10 sensors	BAM	Vertical velocity	4m,6m,8m,10m,12m, 16m,24m,32m,48m,72m
Reference for turnout 1/2 (no turnout)	3 sensors	BAM	Horizontal velocity	12m,24m,32m
Turnout 12 (EW900-B-1:19): Frog	MP 3a, 3c	Ziegler	Vertical velocity	24.0m, 11.2m
Turnout 12: Frog	10 sensors	BAM	Vertical velocity	4m,7m,8m,10m,12m, 16m,24m,32m,48m,72m
Turnout 12: Mid turnout	1 sensor	BAM	Vertical velocity	12m
Turnout 12: Switch	1 sensor	BAM	Vertical velocity	12m
Turnout 12: 4 sleepers at frog	4 sensors	DB	Vertical acceleration	At track
Turnout 12: At Frog	1 sensor	DB	Vertical acceleration	At track
Turnout 11 (EW900-G-1:19): Frog	MP 3b	Ziegler	Vertical velocity	11.2 m
Turnout 11: Frog	1 sensor	BAM	Vertical velocity	12m
Turnout 11: Switch	1 sensor	BAM	Vertical velocity	12m
Turnout 11: 4 sleepers at frog	4 sensors	DB	Vertical acceleration	At track
Turnout 11: At Frog	1 sensor	DB	Vertical acceleration	At track
Reference for turnout 11/12 (no turnout)	MP 4a,4b,4c	Ziegler	Vertical vibration	24.0 m, 14.6m,14.6m

Table 4.1: Rubigen: Sensor position and distances

The measurement locations in Le Landeron are shown in Figure 4.4, Figure 4.5 and Table 4.2 [35,37)]. The site configuration in Le Landeron was very complex for distances over 4 m. It was decided therefore that measurements shall be performed only next to the track.

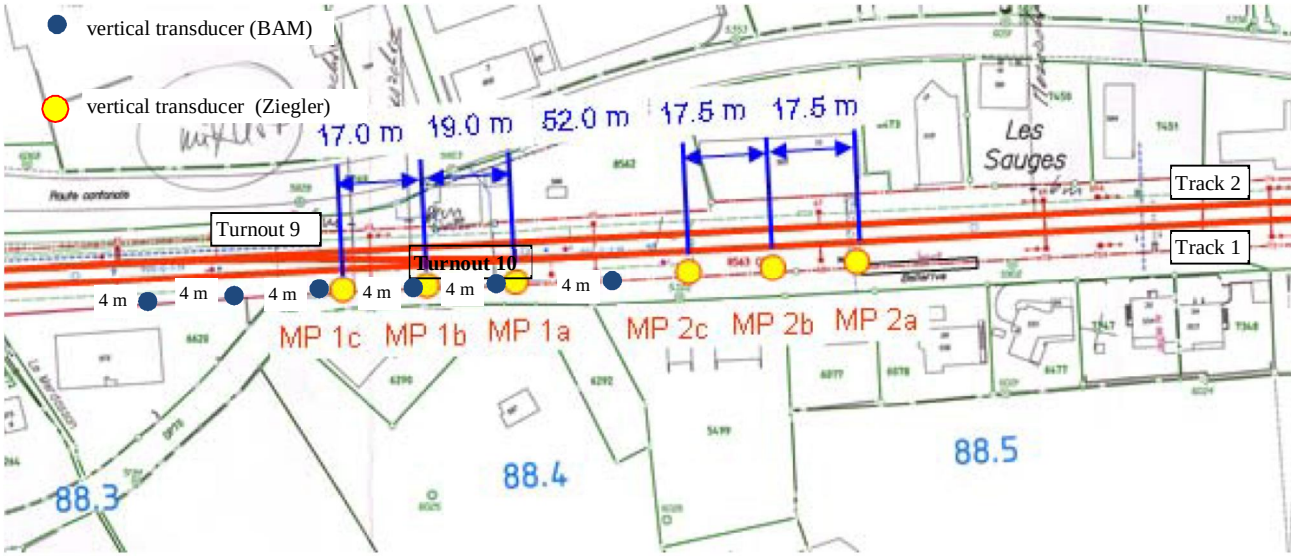

Figure 4.4: Le Landeron, turnout 9 and 10 with USP

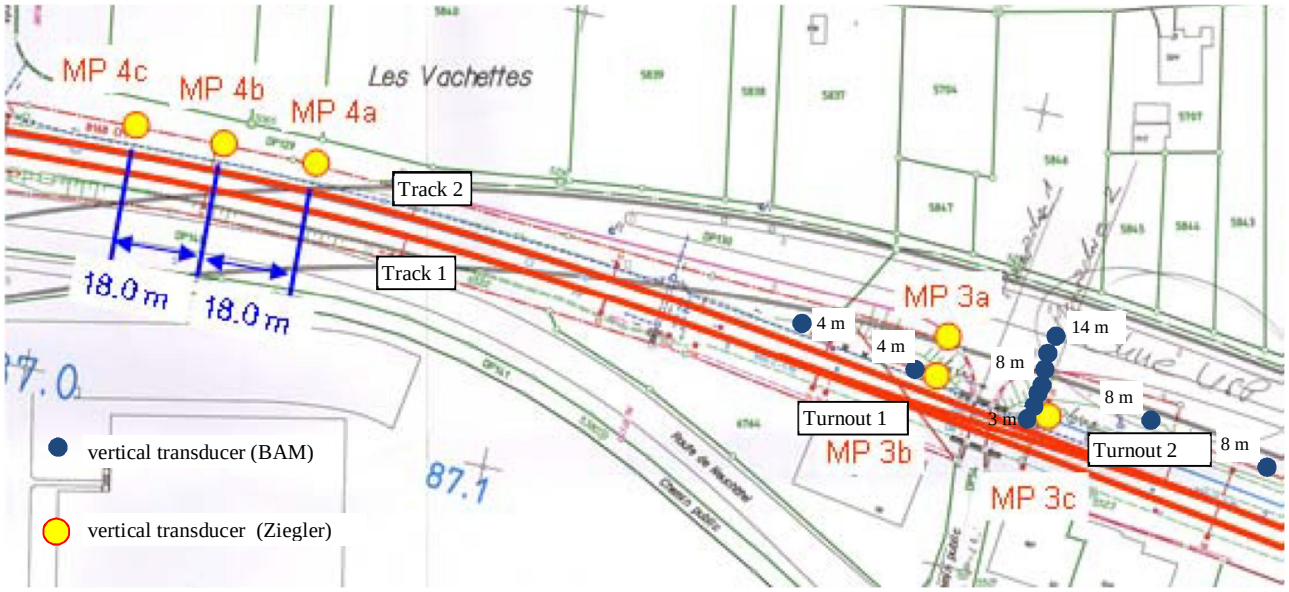

Figure 4.5: Le Landeron, turnout 1 and 2 without USP

The distance to the track for the different sensor positions is given in Table 4.2. The difficult measurement situation in Le Landeron was the cause that only measurements next to the track have been possible.

Measurement place	Sensor	Campaign	Measured Quantity	Distance to Track 2
Turnout 10 (EW900-G-1:19): Frog	MP 1b,	Ziegler	Vertical vibration	4.9m
Turnout 10: mid turnout	MP 1a	Ziegler	Vertical vibration	5.2m
Turnout 10: Frog	1 sensor	BAM	Vertical vibration	4m
Turnout 10: mid turnout	1 sensor	BAM	Vertical vibration	4m
Turnout 10: switch	1 sensor	BAM	Vertical vibration	4m

Turnout 9 (EW900-G-1:19): Frog	MP 1c	Ziegler	Vertical vibration	4.8m
Turnout 9: Frog	1 sensor	BAM	Vertical vibration	4m
Turnout 9: mid turnout	1 sensor	BAM	Vertical vibration	4m
Turnout 9: switch	1 sensor	BAM	Vertical vibration	4m
Reference Turnout 10/9	MP 2a,2b,2c	Ziegler	Vertical vibration	5.3 m,5.5m,5.4m
Turnout 1 (EW900-G-1:19): Frog	MP 3a,3b	Ziegler	Vertical vibration	11.5m, 4.8m
Turnout 1: Frog	1 sensor	BAM	Vertical vibration	4m
Turnout 1: switch	1 sensor	BAM	Vertical vibration	4m
Turnout 2 (EW900-G-1:19): Frog	MP 3c	Ziegler	Vertical vibration	6.5m
Turnout 2: Frog	7 sensors	BAM	Vertical vibration	3m,4m,6m,8m,10m,12m,14m
Turnout 2: mid turnout	1 sensor	BAM	Vertical vibration	8m
Turnout 2: switch	1 sensor	BAM	Vertical vibration	8m
Reference turnout 1/2	MP 4a,4b,4c	Ziegler	Vertical vibration	7.2m,6.5m,6.8m

Table 4.2: Le Landeron: Sensor position and distances

4.1.2 Measured Vibration Levels in the Time Domain

Rubigen site

The resulting maximum ground vibration levels, averaged over several train pass by events, for three different types of trains, Intercity (IC), freight train (GT) and regional train (RT), are summarized in Figure 4.6 – Figure 4.8. In the case of a turnout with under sleeper pads (Figure 4.6), regional trains resulted in lowest ground vibration velocity levels due to an average train speed below 100 km/h. Intercity and freight train caused similar ground vibration levels. Measured average train speeds for freight trains were of the order of 95 km/h and slightly above 150 km/h for Intercity trains.

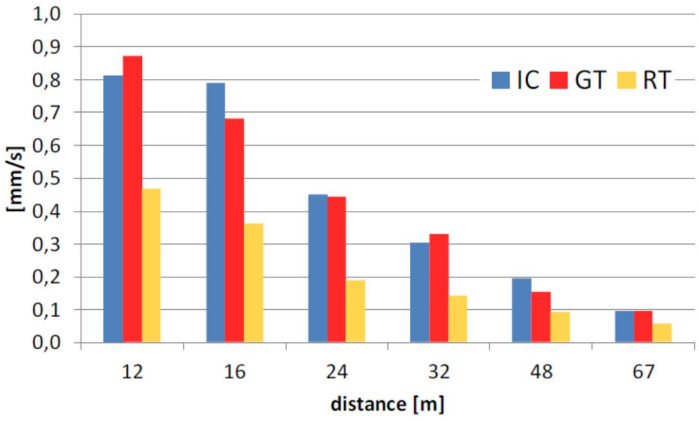

Figure 4.6: Rubigen, mean maximum value of ground vibration velocity, turnout 1 with USP [35]

Similar trends can be found in the case of a turnout without under sleeper pads, as illustrated in Figure 4.7 (included error bars of standard deviation. For IC there is small influence of traintype). Slow regional trains resulted in lowest ground vibration velocity levels. However, when compared to the turnout with under sleeper pads, the vibration amplitudes are smaller within the first 24 m

distance to the track. At a distance of 32 m and more, the turnout without under sleeper pads showed higher maximum ground vibration velocity levels compared to the turnout equipped with USP.

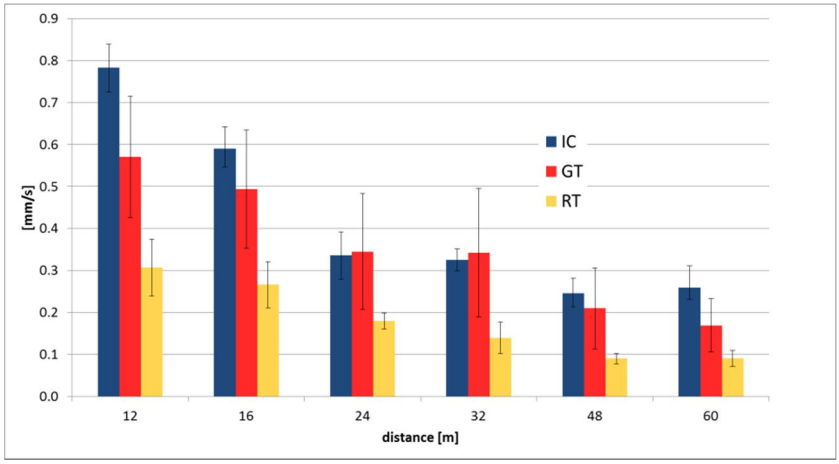

Figure 4.7: Rubigen, mean maximum value of vibration velocity, turnout 12 without USP [35]

Averaged maximum ground vibration velocity levels for a track without turnout, illustrated in Figure 4.8, showed amplitudes that are smaller by a factor of about 2 when compared to the test cases with turnout. The three different track set-ups had comparable train pass by velocities.

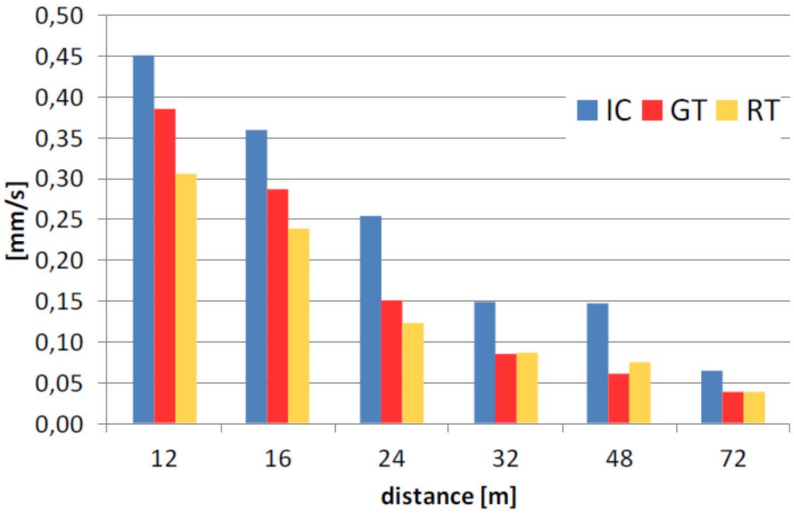

Figure 4.8: Rubigen, mean maximum ground vibration velocity, without turnout [35]

Additional measurements in Rubigen were performed by Ziegler Consultants. These measurements have the advantage that at the different sites it can be measured simultaneously and a huge number of trains were measured. Table 4.3-4.6 show a summary of 600 – 700 train pass by events in Rubigen for each turnout (v_{maxrms}).

Vibration velocity levels for a turnout without under sleeper pads are in the same range for MP 1a (turnout with USP) and MP 3a (turnout without USP). However, the turnout without under sleeper pads resulted in lower ground vibration velocity levels (in the order of a factor of 2) for the other two sensor positions (at the switch extremity and in front of the nose). Measurements next to the track without under sleeper pads in approx. 120 m distance to the turnout showed comparable

ground vibration velocity levels when compared to the track with under sleeper pads. The following tables for Rubigen show the mean values for all train types scaled for 10 m distance.

Track Nr.	Turnout USP MP 1		Regular track MP 2		Factor: Turnout-amplification	
	KBFt	v_{Leq}	KBFt	v_{Leq}	KBFt	v_{Leq}
1 (MP 1c / MP 2c)	0.405	0.175	0.138	0.054	**2.94**	**3.24**
2 (MP 1b / MP 2c)	0.349	0.150	0.094	0.042	**3.71**	**3.57**
1 (MP 1b / MP 2c)	*0.151*	*0.064*	*0.138*	*0.054*	*1.09*	*1.19*
2 (MP 1c / MP 2c)	*0.211*	*0.093*	*0.094*	*0.042*	*2.25*	*2.21*

Table 4.3: Rubigen, comparison (USP turnout-amplification) between MP 1 and MP 2 (all train types). (KBFt = average KBFmax value of all train passby. v_{Leq} = v-rms, average of Leq-value of vibration velocity.)

The turnout with USP and its turnout-amplification is high (Table 4.3) for the turnout 1 on track 1 and for the turnout 2 on track 2. The measurement point 1c which is 12.65 m next from the frog shows significant turnout-amplification of about a factor of 2.2.

The turnout without USP and its turnout-amplification is low (Table 4.4) for the turnout 1 on track 1 as well as for the turnout 2 on track 2. The same is true for the neighbouring measurement points 25.25 m next from the frog with no difference to the normal track.

Track Nr.	Turnout without USP MP 3		Regular track MP 4		Factor: Turnout-amplification	
	KBFt	v_{Leq}	KBFt	v_{Leq}	KBFt	v_{Leq}
1 (MP 3c / MP 4c)	0.224	0.102	0.208	0.091	**1.08**	**1.12**
2 (MP 3b / MP 4c)	0.148	0.073	0.153	0.073	**0.97**	**1.00**
1 (MP 3b / MP 4c)	*0.121*	*0.059*	*0.208*	*0.091*	*0.58*	*0.65*
2 (MP 3c / MP 4c)	*0.163*	*0.076*	*0.153*	*0.073*	*1.07*	*1.04*

Table 4.4: Rubigen, comparison (turnout-amplification) between MP 3 (Turnout without USP) and MP 4 (all train types)

In Table 4.5 it is obvious that both turnouts with USP have an amplification of a factor (v_{Leq}) of around 1.7 for track 1 and around 2.1 for track 2 in comparison with the turnouts without USP.

Track Nr.	Turnout with USP MP 1		Turnout without USP MP 3		Factor (USP mitigation effect, if smaller 1)	
	KBFt	v_{Leq}	KBFt	v_{Leq}	KBFt	v_{Leq}
1 (MP 1c / MP 3c)	0.405	0.175	0.224	0.102	1.81	1.72
2 (MP 1b / MP 3b)	0.349	0.150	0.148	0.073	2.36	2.06

Table 4.5: Rubigen, comparison (USP mitigation effect) between MP 1 and MP 3 (all train types)

In Table 4.6 it can be seen that the regular track at MP2 (embankment) is around a factor of 0.6 of MP4 (cut).

Track Nr.	Regular track MP 2		Regular track MP 4		Factor (track/subsoil effects)	
	KBFt	v_{Leq}	KBFt	v_{Leq}	KBFt	v_{Leq}
1 (MP 2c / MP 4c)	0.138	0.054	0.208	0.091	0.66	0.59
2 (MP 2c / MP 4c)	0.094	0.042	0.153	0.073	0.61	0.58

Table 4.6: Rubigen, comparison (influence of track and subsoil) between MP 2 and MP 4 (all train types)

Le Landeron site

Measurements by BAM (Figure 4.8 and Figure 4.9) show highest vibration velocity levels for the turnout with USP at 8 m distance in front of the frog. The three different types of trains, intercity, freight and regional train, show similar vibration levels at this sensor position. At 8 m from the track in front of the middle and in front of the switch point, the turnout with USP shows smaller vibration levels (by a factor of about 1.5 – 2 for freightand regional trains and by a factor of about 1.2 – 1.5 for intercity trains) when compared to the turnout without USP.

For the turnout without USP (Figure 4.9) the freight trains caused highest ground vibration velocity levels when compared to the intercity and regional trains. Differences in vibration levels between intercity trains and regional train are small. For the turnout with USP (Figure 4.8) the average maximum value of the ground vibration velocity level does not differ as significantly as for the turnout without USP for the three different types of trains.

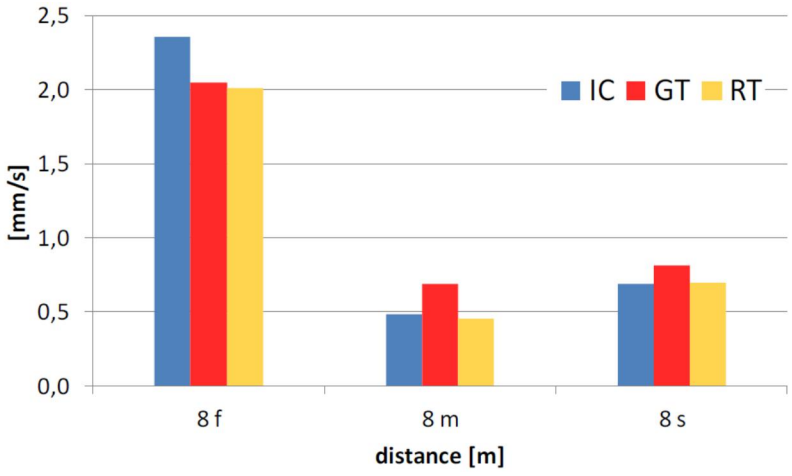

Figure 4.8: Le Landeron, mean maximum value of ground vibration velocity, turnout with USP, 8m, frog/middle/switch point, [36]

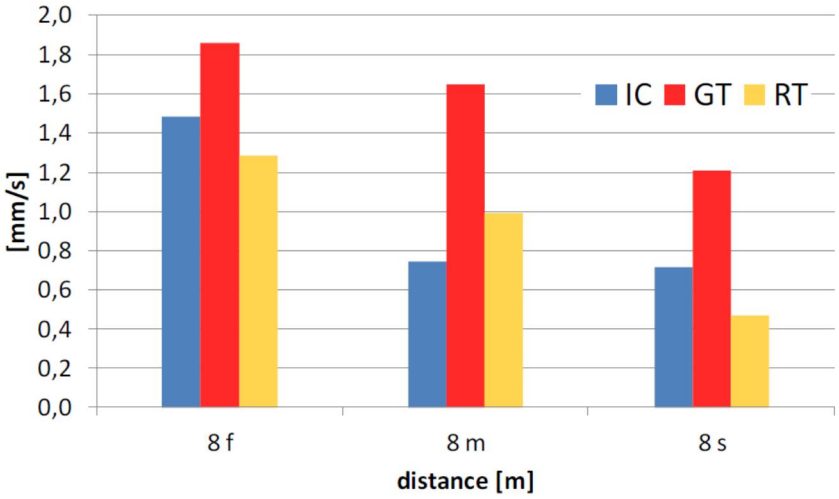

Figure 4.9: Le Landeron, mean maximum value of ground vibration velocity, turnout without USP, 8m, frog/middle/switch point, [36]

Table 4.7-4.10 show the measured mean vibration velocity values for all train types scaled for 6 m distance by Ziegler Consultants in Le Landeron for approx. 200 – 300 train pass-by events.

The turnout with USP and its turnout-amplification is quite low (Table 4.7) for the turnout on track 1 (factor 1.44) and for the measurement point 1c which is 17 m next from the frog shows no turnout-amplification (factor 0.58, which is a reduction in comparison to the reference). The turnout on track 2 has for the measurement point 1c directly before the frog a turnout-amplification (factor 1.64) and the measurement point 1b which is 17 m next from the frog shows also no significant turnout-amplification (factor 0.8).

The turnout without USP and its turnout-amplification is high (Table 4.8, factor 2.42) for the turnout on track 1 but lower (factor 1.89) for the turnout on track 2. The neighbouring measurement points 17 m next from the frog have lower turnout-amplification. (track 1 turnout: 1.26, track 2 turnout: 1.05).

Track Nr.	Turnout with USP MP 1		Regular track MP 2		Factor: Turnout-amplification	
	KBFt	v_{Leq}	KBFt	v_{Leq}	KBFt	v_{Leq}
1 (MP 1b / MP 2a,b,c)	0.858	0.363	0.600	0.253	**1.43**	**1.44**
2 (MP 1c / MP 2a,b,c)	0.685	0.273	0.336	0.167	**2.04**	**1.64**
1 (MP 1c / MP 2a,b,c)	*0.369*	*0.147*	*0.600*	*0.253*	*0.62*	*0.58*
2 (MP 1b / MP 2a,b,c)	*0.300*	*0.133*	*0.336*	*0.167*	*0.89*	*0.80*

Table 4.7: Le Landeron, comparison (USP turnout-amplification) between MP 1 and MP 2 (all train types). The MP2-measurement points have a relatively high scattering.

Track Nr.	Turnout without USP MP3		Regular track MP4		Factor: Turnout-amplification	
	KBFt	v_{Leq}	KBFt	v_{Leq}	KBFt	v_{Leq}
1 (MP 3b / MP 4a,b,c)	0.576	0.237	0.199	0.098	**2.89**	**2.42**
2 (MP 3c / MP 4a,b,c)	0.563	0.245	0.321	0.130	**1.75**	**1.89**
1 (M 3c / MP 4a,b,c)	*0.260*	*0.124*	*0.199*	*0.098*	*1.31*	*1.26*
2 (MP 3b / MP 4a,b,c)	*0.320*	*0.137*	*0.321*	*0.130*	*1.00*	*1.05*

Table 4.8: Le Landeron, comparison (turnout-amplification) between MP 3 (turnout without USP) and MP 4 (all train types). The MP4-measurement points have a low scattering.

In Table 4.9 it is seen that both turnouts with USP have an amplification of a factor (v_{Leq}) of around 1.53 for track 1 and around 1.11 for track 2 in comparison with the turnouts without USP.

Track Nr.	Turnout with USP MP 1		Turnout without USP MP 3		Factor	
	KBFt	v_{Leq}	KBFt	v_{Leq}	KBFt	v_{Leq}
1 (MP 1b / MP 3b)	0.858	0.363	0.576	0.237	1.49	1.53
2 (MP 1c / MP 3c)	0.685	0.273	0.563	0.245	1.22	1.11

Table 4.9: Le Landeron, comparison (USP mitigation effect) between MP 1 and MP 3 (all train types)

In Table 4.10 it can be seen that the regular track at MP2 is around a factor of 2.58 for track 1 and a factor of 1.29 for track 2 higher in amplitudes than MP4. The relatively low turnout-amplification for the USP turnout at track 1 has therefore to be regarded with caution.

Track Nr.	Regular track MP 2		Regular track MP 4		Factor	
	KBFt	v_{Leq}	KBFt	v_{Leq}	KBFt	v_{Leq}
1 (MP 2a,b,c/MP 4a,b,c)	0.600	0.253	0.199	0.098	3.02	2.58
2 (MP 2a,b,c/MP 4a,b,c)	0.336	0.167	0.321	0.130	1.05	1.29

Table 4.10: Le Landeron, comparison (influence of track and subsoil) between MP 2 and MP 4 (all train types)

4.1.3 Comparison of Third-Octave Band Spectra

Measured data were post-processed and plotted as third-octave band spectra. A comparison is done for the track with and without turnout, for different types of trains and for sleepers equipped or not with USP both in Rubigen as well as in Le Landeron.

Rubigen

Vibration emissions from intercity trains for track without turnout based on measurements performed in Rubigen by BAM are shown in Figure 4.10. The diagrams show five intercity train pass by events and the corresponding average.

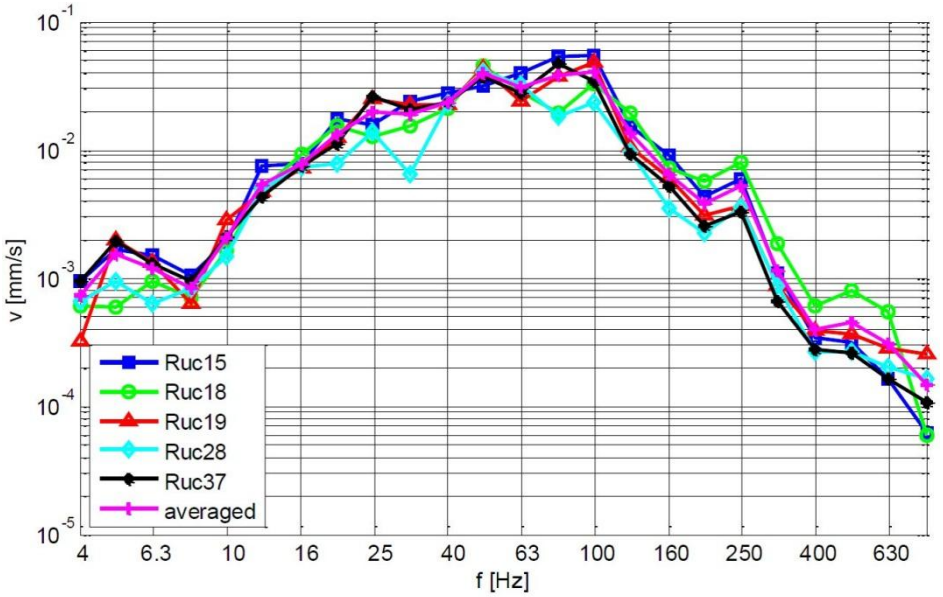

Figure 4.10: Rubigen, intercity train, third-octave band spectrum, 12 m, track without turnout, [35]

Measured vertical ground vibration velocity levels in Rubigen at 12 m distance to the track for a turnout with USP and for a turnout without USP are illustrated in Figure 4.11 for freight trains and in Figure 4.12 for regional trains. Installation of under sleeper pads in turnout tends to increase vibration levels in the 10 Hz – 25 Hz frequency band, keep constant the vibration levels between 25 Hz and 100 Hz and reduce the levels in the range above 100 Hz.

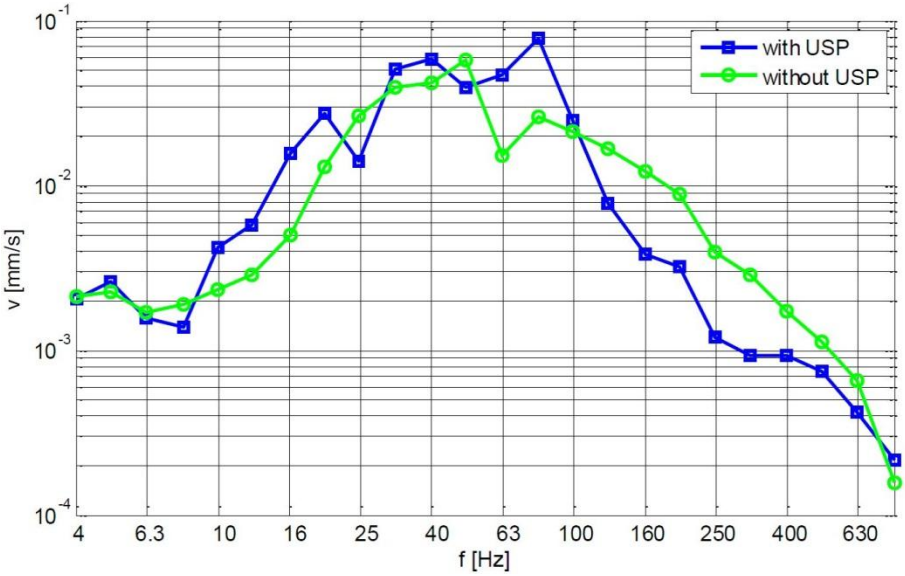

Figure 4.11: Rubigen, freight train, third-octave band spectrum, 12 m, turnout 1 with /turnout 12 without USP, [35]

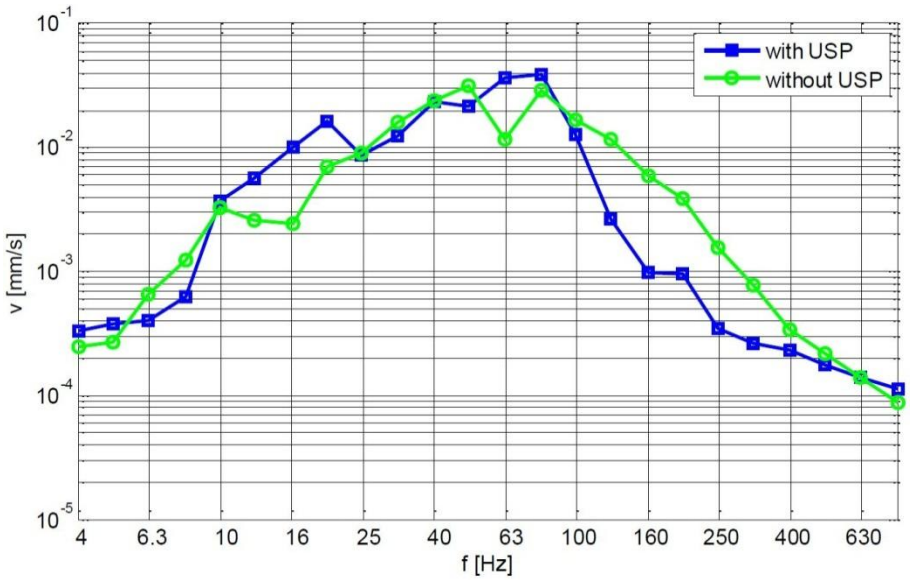

Figure 4.12: Rubigen, regional train, third-octave band spectrum, 12 m, turnout 1 with/turnout 12 without USP, [35]

Figure 4.13 shows the measured vibration levels relative to the baseline track without turnout for intercity trains, Figure 4.14 for regional trains and Figure 4.15 for freight trains.

The plots show averaged data from 12 m to 48 m distance of the sensor to the track and averaged over five train pass-by events.

Results show that a turnout with under sleeper pads causes vibration levels similar to the baseline track without turnout above the 100 Hz third-octave band. Turnouts without USP have a resonance frequency around 40 Hz and are quite similar for different train types. The intercity train seems to have additional impact for a turnout in comparison to regular track. Turnouts with USP have a resonance peak for intercity train around 31 Hz and around 50 Hz, for regional trains around 50 Hz and for freight trains around 63 Hz. The reason for this frequency shift is unclear; it could be the USP or the geometry of the turnout. Turnouts without USP tend to have higher turnout-amplifications which would indicate a positive effect of a turnout with USP at frequencies even below the USP resonance frequency.

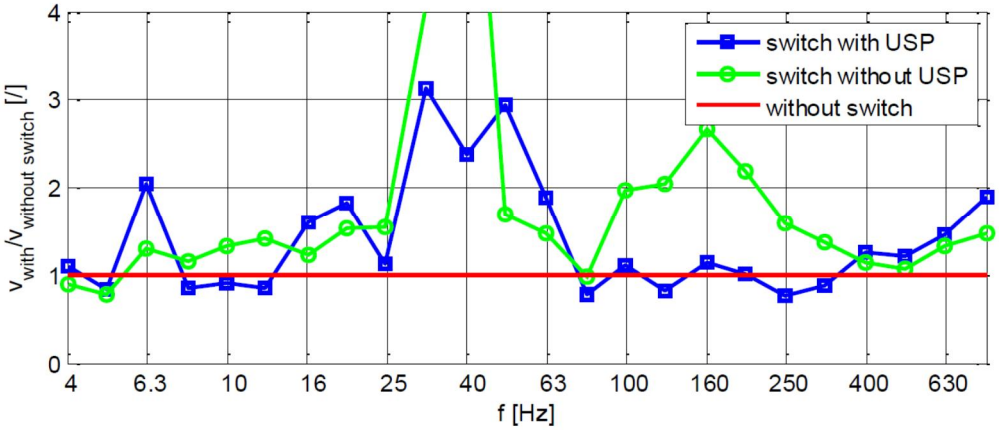

Figure 4.13: Rubigen, intercity train, turnout 1 with/turnout 12 without USP relative to track without turnout, [35]

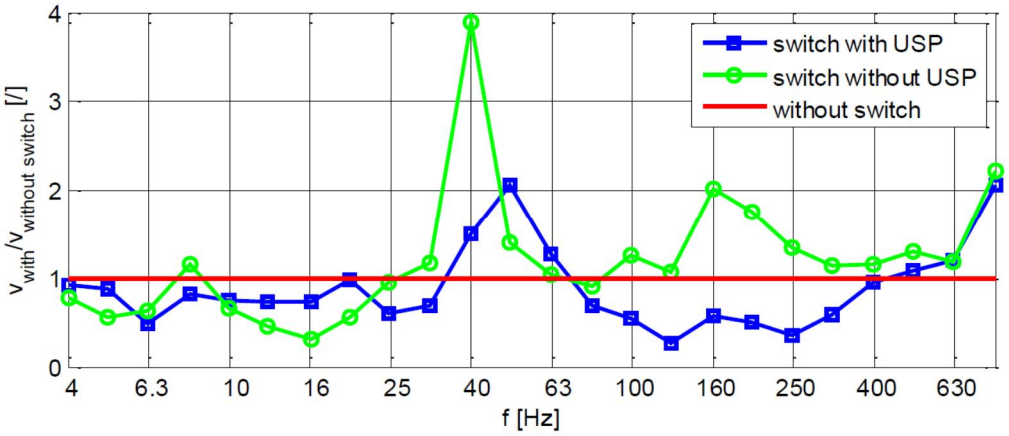

Figure 4.14: Rubigen, regional train, turnout 1 with/turnout 12 without USP relative to track without turnout, [35]

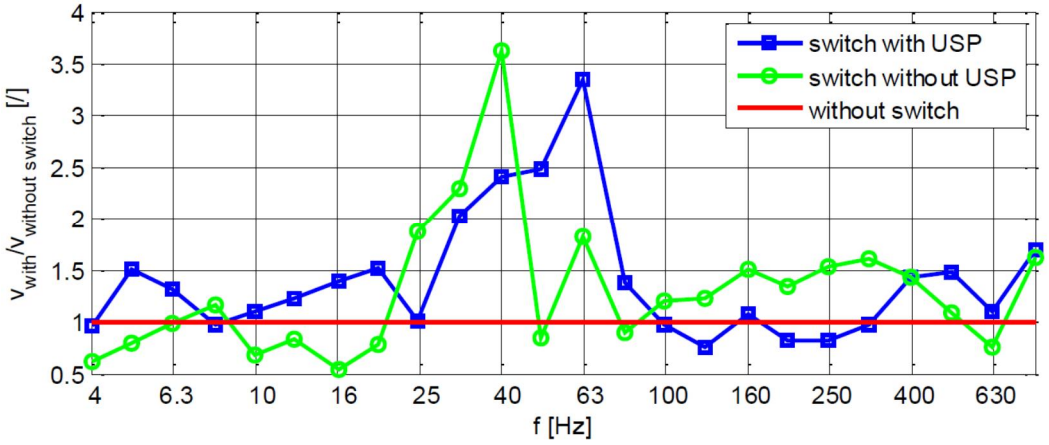

Figure 4.15: Rubigen, freight train, turnout 1 with/turnout 12 without USP relative to track without turnout, [35]

In the following diagrams (Figure 4.16- Figure 4.21) emission spectra and turnout-amplification spectra for intercity (IC), freight (GT) and regional (RT) trains are summarised for Rubigen from the measurement campaign of Ziegler.

In Figure 4.16 the turnout with USP shows maximum emission frequencies dependent on the train type between 32 Hz and 50 Hz. In Figure 4.17 the regular track is shown with much lower vibration and maximum emission frequencies between 50 Hz and 63 Hz.

In Figure 4.18 the turnout without USP shows maximum emission frequencies dependent on the train type between 32 Hz and 80 Hz. In Figure 4.19 the regular track is shown with similar vibration amplitudes as for the turnout and maximum emission frequencies at 32 Hz and 80 Hz. The form of the emission spectra is very different from the other regular track (Figure 4.17).

Figure 4.20 and 4.21 show the turnout-amplification factor. The behaviour of the turnouts is much different. Turnouts with USP seem to provoke more vibration than without USP (no correction for distance differences is applied). The reason for this difference is not obvious.

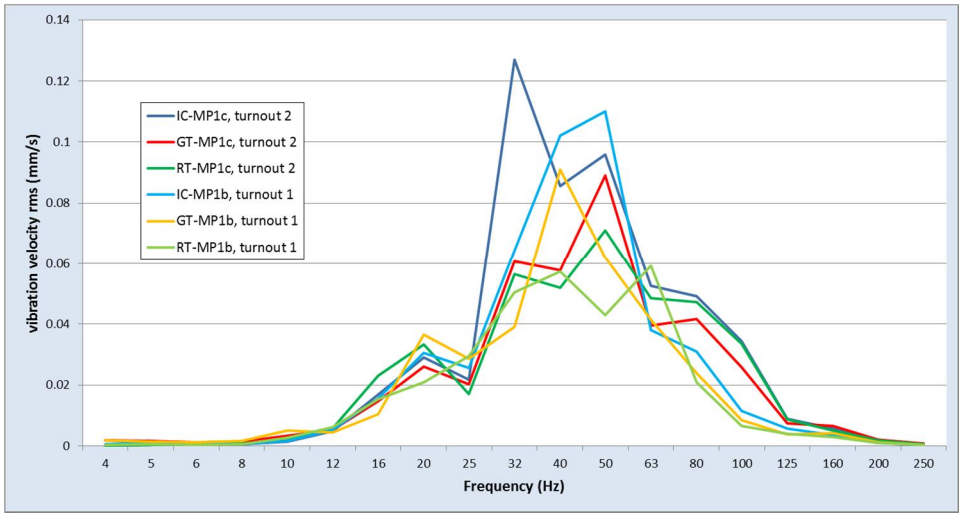

Figure 4.16: Rubigen, third-octave band spectrum, turnout with USP, turnout 2 and turnout 1.

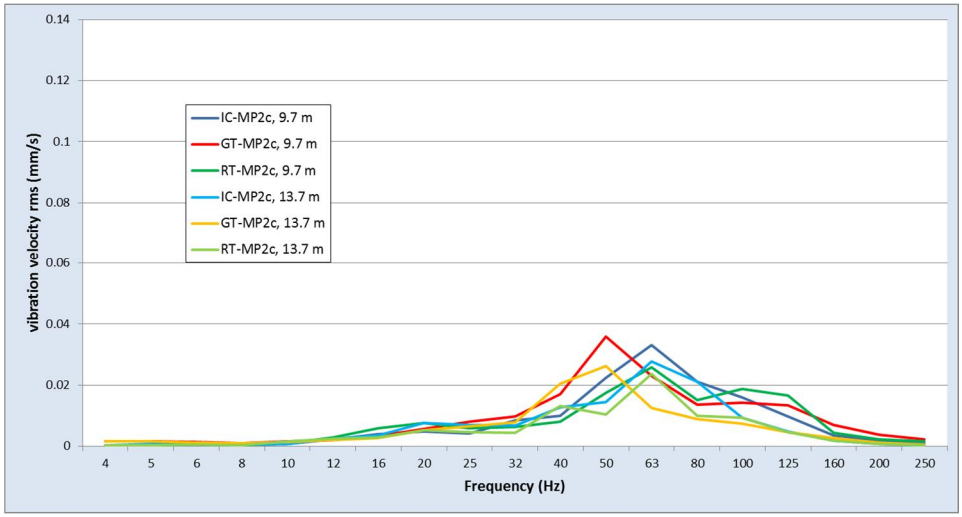

Figure 4.17: Rubigen, third-octave band spectrum, reference tracks for turnout 2 (9.7m) and turnout 1 (13.7 m).

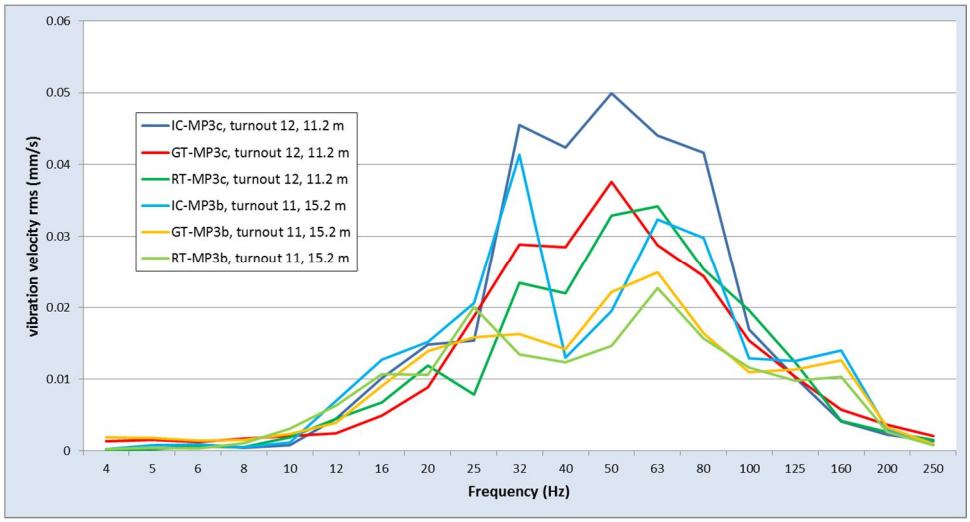

Figure 4.18: Rubigen, third-octave band spectrum, turnout without USP, turnout 12 and turnout 11.

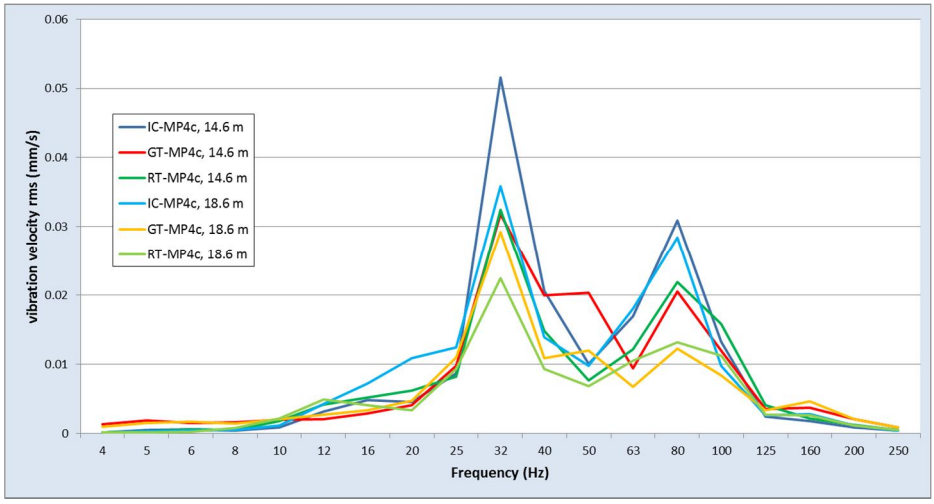

Figure 4.19: Rubigen, third-octave band spectrum, reference tracks for turnout 12 (14.6 m) and turnout 11 (18.6 m).

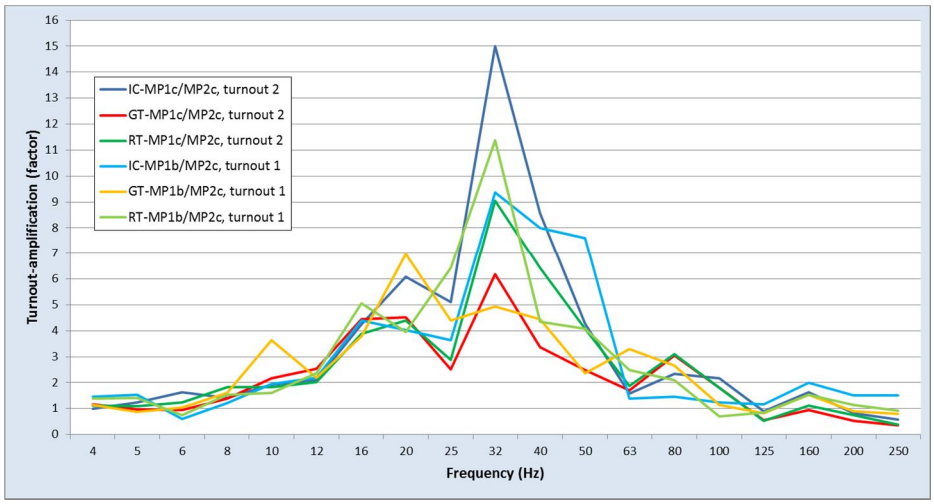

Figure 4.20: Rubigen, turnout-amplification for turnout 2 and turnout 1 with USP.

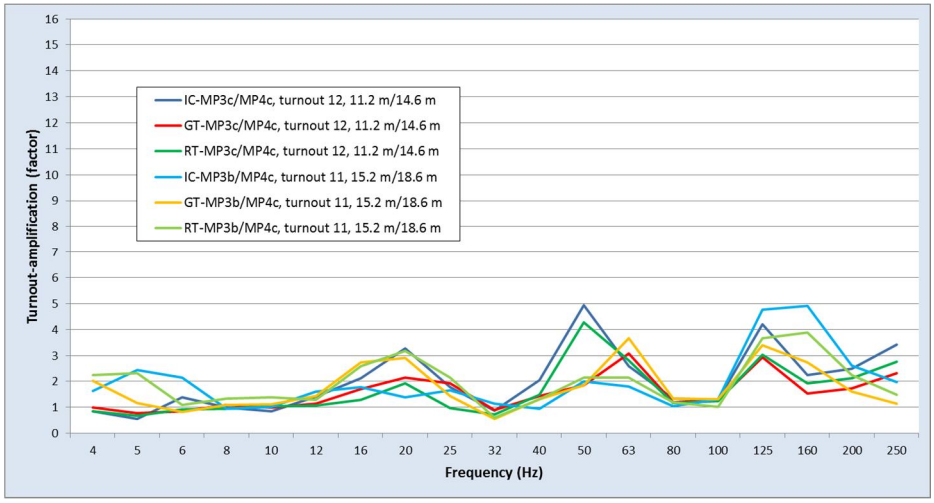

Figure 4.21: Rubigen, turnout-amplification for turnout 12 and turnout 11 without USP (no correction for distances)

Le Landeron

Results from measurements performed by BAM differ significantly when compared to results obtained for Rubigen. Figure 4.22 show the third-octave band spectra of vertical ground vibration velocities in 8 m distance to the turnout with and without under sleeper pads in front of the frog (Figure 4.22) for intercity train pass by events. Vibration levels are higher for the turnout without under sleeper pads in the frequency range below 20 Hz. Vibration levels are higher for the turnout with under sleeper pads in the frequency range from 20 Hz – 50 Hz. Third-octave band spectrum characteristics are similar for regional trains and freight train when compared to the characteristics for intercity trains.

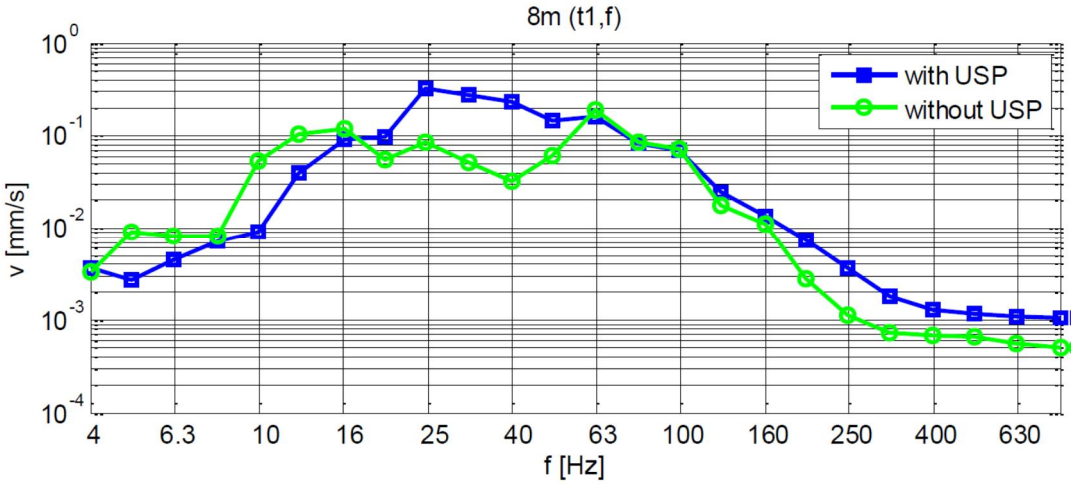

Figure 4.22: Le Landeron, intercity train, third-octave band spectrum, turnout with 10/turnout 2 without USP, 8m, frog, [36]

In the following diagrams (Figure 4.23 - 4.28) emission spectra and turnout-amplification spectra for intercity (IC), freight (GT) trains are shown from measurement campaign of Ziegler. Regional trains were not analysed because the velocity near the railway station is not constant.

In Figure 4.23 the turnout with USP shows maximum emission frequencies dependent on the train type between 16 Hz and 63 Hz. In Figure 4.24 the regular track is shown with much lower vibrations for 20 Hz – 80 Hz but with much higher emissions at frequencies 10 Hz and 12 Hz.

In Figure 4.25 the turnout without USP shows maximum emission frequencies dependent on the train type between 12 Hz and 63 Hz. The characteristics are similar and the amplitudes a little lower than for the turnouts with USP (Figure 4.23). In Figure 4.26 the regular track is shown with much lower vibration amplitudes as for the turnout and maximum emission frequencies at 12, 16 Hz and 63 Hz. The form of the emission spectra is much lower than (and very different in form), the other regular track (Figure 4.24).

Figure 4.67 and 4.68 show the turnout-amplification factor. The behaviour of the turnouts seems different at lower frequencies 4 Hz – 12 Hz. Turnout 1 and turnout 9 have a peak for freight trains at 25 Hz, 32 Hz and around 100 Hz.

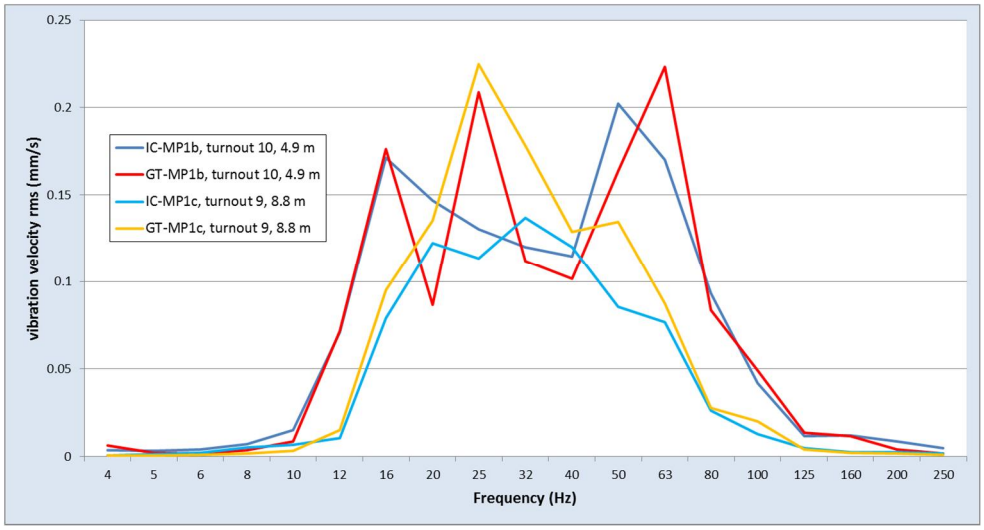

Figure 4.23: Le Landeron, third-octave band spectrum, turnout with USP, turnout 10 and turnout 9.

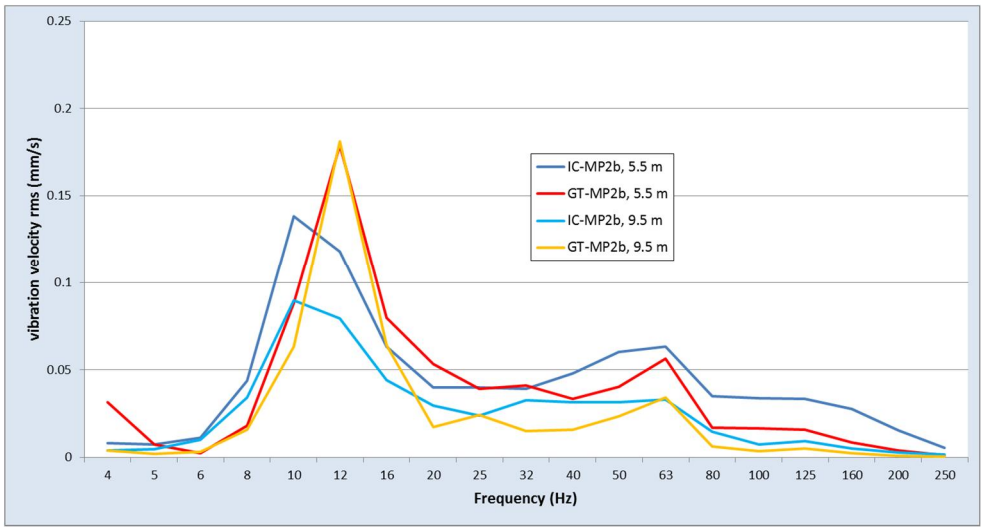

Figure 4.24: Le Landeron, third-octave band spectrum, reference tracks for turnout 10 (5.5 m) and turnout 9 (9.5 m).

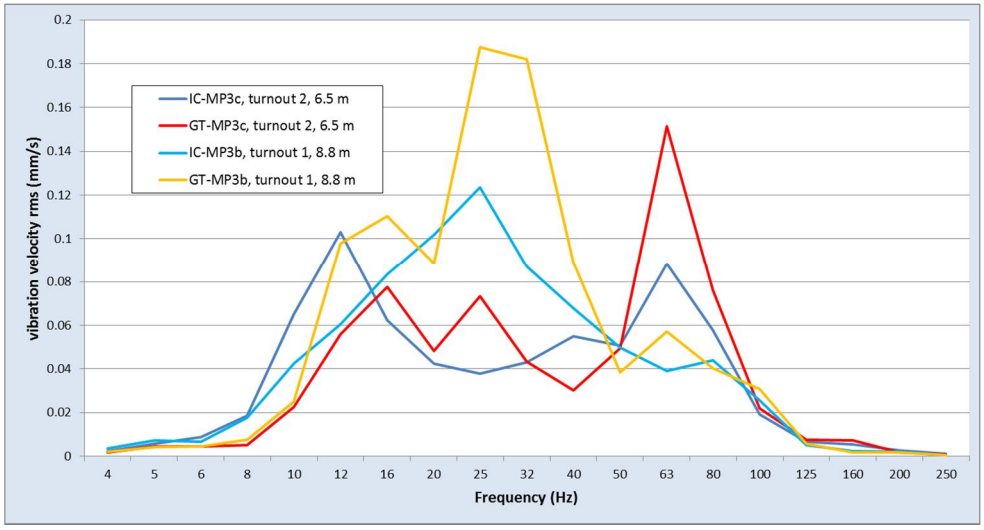

Figure 4.25: Le Landeron, third-octave band spectrum, turnout without USP, turnout 2 + turnout 1.

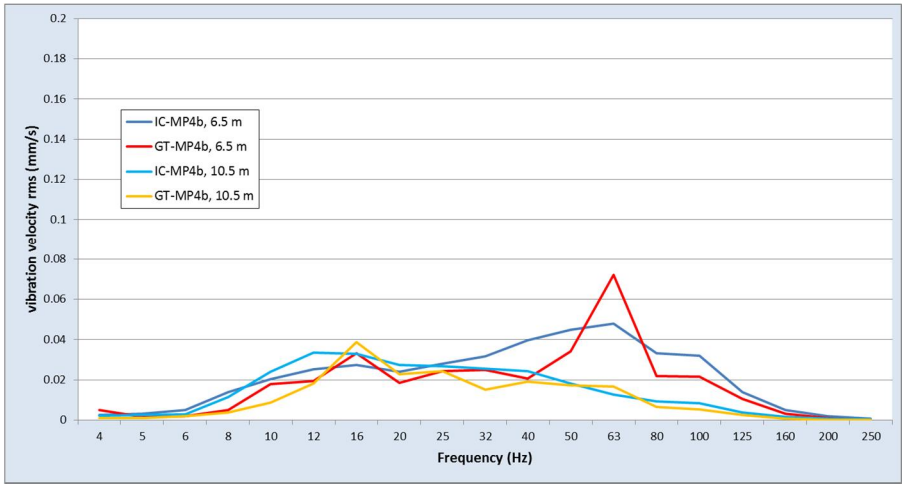

Figure 4.26: Le Landeron, third-octave band spectrum, reference tracks for turnout 2 (6.5 m) and turnout 1 (10.5 m).

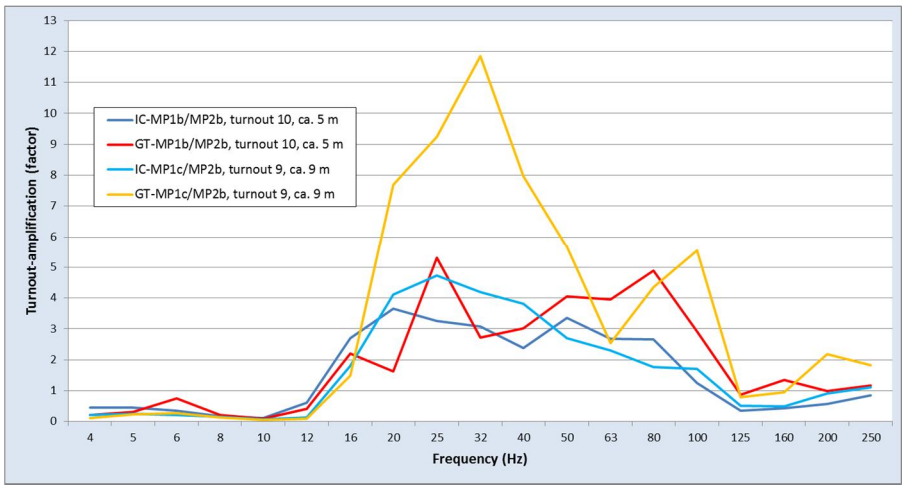

Figure 4.27: Le Landeron, turnout-amplification for turnout 10 and turnout 9 with USP (no correction for distances).

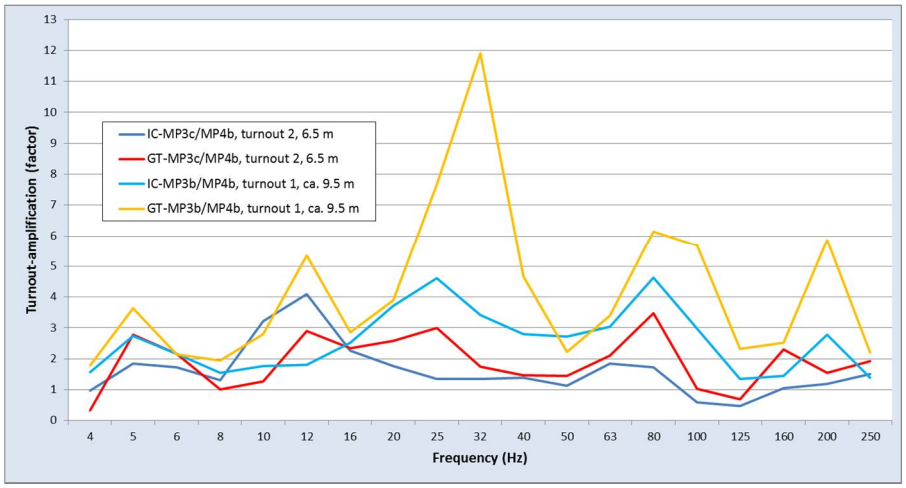

Figure 4.28: Le Landeron, turnout-amplification for turnout 2 and turnout 1 without USP (no correction for distances)

4.1.4 Summary and Concluding Remarks

Installations of 4 turnouts (two in Rubigen, two in Le Landeron) with under sleeper pads (c_{stat}=0.22 N/mm^3) have been tested by BAM and by Ziegler Consultants. Such under sleeper pads are used since a few years at SBB as vibration mitigation measures for turnouts, but so far never validated. 4 turnouts of the same type at the same cities are measured and used as reference turnouts.

Rubigen:

Results provided by BAM:

- vertical ground vibration velocity amplitudes in the time domain are the largest for the turnout with USP for most distances (see Figure 4.6-4.8) and the smallest for the track without turnout. Vibration levels for a track without turnout were smaller by about a factor of 2 when compared to a track with turnout.
- for a turnout with USP (Figure 4.6), regional trains resulted in the lowest vibration levels, intercity and freight trains cause similar vibration levels; similar trends were found for a turnout without USP (Figure 4.7).
- Installation of under sleeper pads in turnout tends to increase vibration levels in the 10 Hz – 25 Hz frequency band, keep constant the vibration levels between 25 Hz and 100 Hz and reduce the levels in the range above 100 Hz (Figure 4.11/4.12).
- third-octave band spectra show higher levels normally between 16 Hz and 63 Hz for the track with turnout than without turnout (e.g. Figure 4.13). Turnouts with USP show increased vibration levels between 50 Hz – 63 Hz, but lower levels for 31.5 Hz - 40 Hz and above 80 Hz compared to turnouts without USP (Figure 4.13-4.15). Turnouts without USP result in higher vibration levels above 80 Hz, because there is no mitigation effect by a USP and tend to show a second peak in the 160 Hz band. Below 31.5 Hz the turnout with and without USP and the regular track show similar vibration levels in the spectrum.

Results provided by Ziegler Consultants:

- vibration levels increase by a factor of more than 3 (Table 4.3) for a turnout with USP when compared to a track without turnout; for a turnout without USP levels increase only by a factor of about 1.05 (Table 4.4) when compared to a track without turnout (Distance 10 m).
- The behaviour of the turnout-amplification factor is much different for turnouts with than without USP. Turnouts with USP seem to provoke more vibration than without USP (Figure 4.20 and 4.21).

The two turnouts in Rubigen do have the same deflection radius of 900 m. For the turnout with USP the trains run over the facing point whereas for the turnout without USP the trains run over the trailing point. Comparison therefore has to be handled with care but tests (see Section 2.63) did not show big influences of the pass-by direction (and also for Le Landeron the effect could be much smaller). The reference tracks without turnout in the Ziegler set-up show significant technical/geological differences in the track structure and substructure (e.g. influence of embankment for turnout 1/2, and cut for turnout 11/12). A direct comparison is questionable. Results from BAM and Ziegler Consultants differ significantly, but often the measurement points are not at the same location. **Due to the poor reproducibility, results do not allow drawing definitive conclusions about the effect of USP on ground vibration velocity levels.**

Le Landeron:

Results provided by BAM:

- the highest vibration levels are observed for the turnout with USP at 8 m distance to the frog, the turnout without USP tends to show less vibration (Figure 4.22).

Results provided by Ziegler Consultants:

- vibration levels increase by a factor of about 1.6 for a turnout with USP when compared to a track without turnout; for a turnout without USP levels increase by a factor of more than 2 when compared to a track without turnout (see Table 4.7 and 4.8) but ground vibration levels are a little smaller for the turnout without USP when compared to the turnout with USP
- turnouts without USP show maximum emission frequencies dependent on the train type between 12 Hz and 63 Hz. The frequency characteristics are similar and the amplitudes a little lower than for the turnouts with USP (Figure 4.23 and 4.25).

The turnout with USP is run over the facing point whereas the turnout without USP is run over the trailing point, in opposite to Rubigen the effect cannot be seen in turnout-amplifications. The reference tracks without turnout in the Ziegler set-up show significant technical/geological differences in the track substructure. Therefore, a direct comparison is difficult but Le Landeron indicates a very small improvement by USP turnouts. **Results do not allow drawing definitive conclusions about the effect of USP on ground vibration velocity levels.**

4.2 TRACK MEASUREMENTS

The purpose of the track measurements was primarily to see if critical effects of the USP influence on track behaviour can be seen. On the other hand it was thought to get further insight on turnout behaviour for vibration excitation. Track measurements were performed by BAM, in Rubigen and in Le Landeron [35]. Vertical ground vibration velocity levels of sleepers were assessed with three sensors (next to the frog, in the middle of the turnout and next to the switch point). Tensile stress levels at the rail base were measured with strain gauges. Acceleration levels of the rail close to the frog, in the middle of the turnout and at the switch point were measured with accelerometers. These results are not discussed here, as they bring no additional information on the vibration situation of the turnouts. They showed no critical effects of the USP influence on turnout track behavior. Results were complemented by static track deflection measurements performed by the Swiss Railway, SBB [38,39]. The condition of the frog was investigated by the German Railways, DB [40].

4.2.1 Track Deflection

Based on static track deflection measurements [38,39], the vertical stiffness in the region of the turnout was compared with the track stiffness without turnout. Static track deflection measurement results of two turnouts with under sleeper pads performed in Rubigen are shown in Figure 4.29.

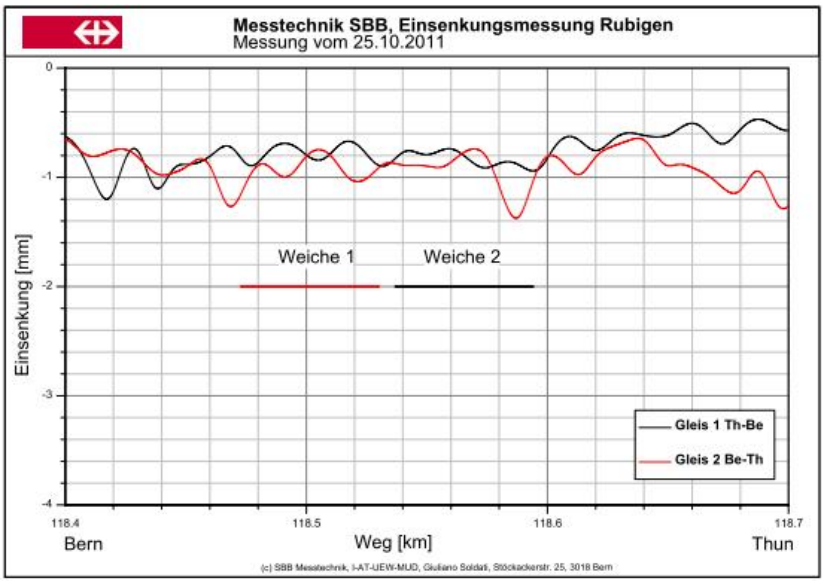

Figure 4.29: Rubigen, static track deflection measurement, turnout with USP, [38]

Static track deflections were assessed in Rubigen for two turnouts without under sleeper pads. Results are shown in Figure 4.30.

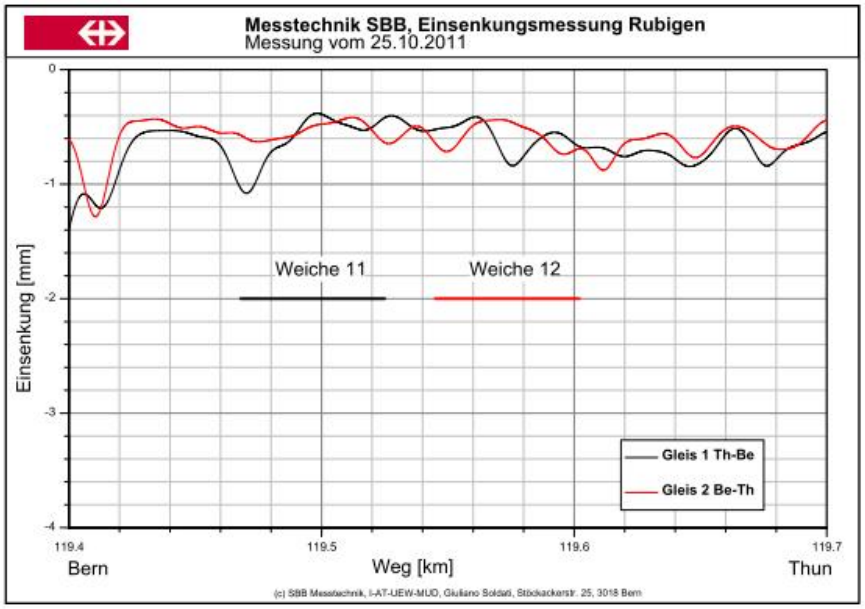

Figure 4.30: Rubigen, static track deflection measurements, turnout without USP, [38]

The use of under sleeper pads resulted in an increased static track deflection of the turnout by 0.29 mm. This can be explained by looking at the material properties of the under sleeper pads (0.22 N/mm^3). However, differences in the properties of the substructures are not accounted for in the comparison of the static track deflection levels for the turnouts with and without under sleeper pads. In both Figures 4.29/4.30 it can be seen that at the turnouts, when compared to regions before and after the turnouts, static track deflection measurements show insignificant influence of the turnout on track deflection levels. This means that no hanging sleepers are visible at the turnout.

Results from static track deflection measurements in Le Landeron for turnouts with and without under sleeper pads are illustrated in Figure 4.31 and Figure 4.32. The use of under sleeper pads resulted in a decrease of the static track deflection by 0.07 mm. This does not correspond to the under sleeper pad material properties (0.22 N/mm^3). Differences in the properties of the substructures are not accounted for in the comparison of the static track deflection levels for the turnouts with and without under sleeper pads. The effect of geology could be probably dominant on static deflection. Apparently, the property of the substructure affects the static track deflection significantly and therefore needs to be accounted for in the comparison of turnouts with and without under sleeper pads. When compared to regions before and after the turnouts, static track deflection measurements in Le Landeron show insignificant influence of the turnout on track deflection levels (no hanging sleepers).

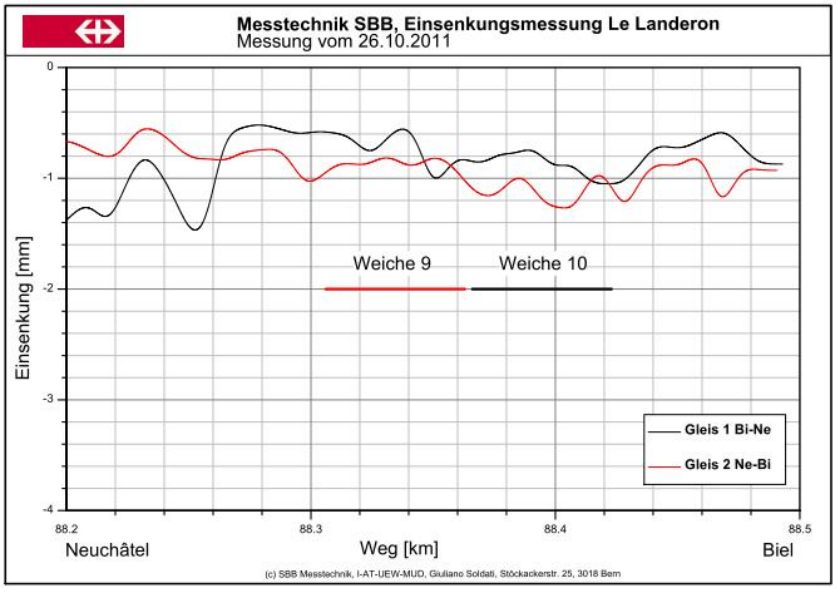

Figure 4.31: Le Landeron, static track deflection measurement, turnout with USP, [39]

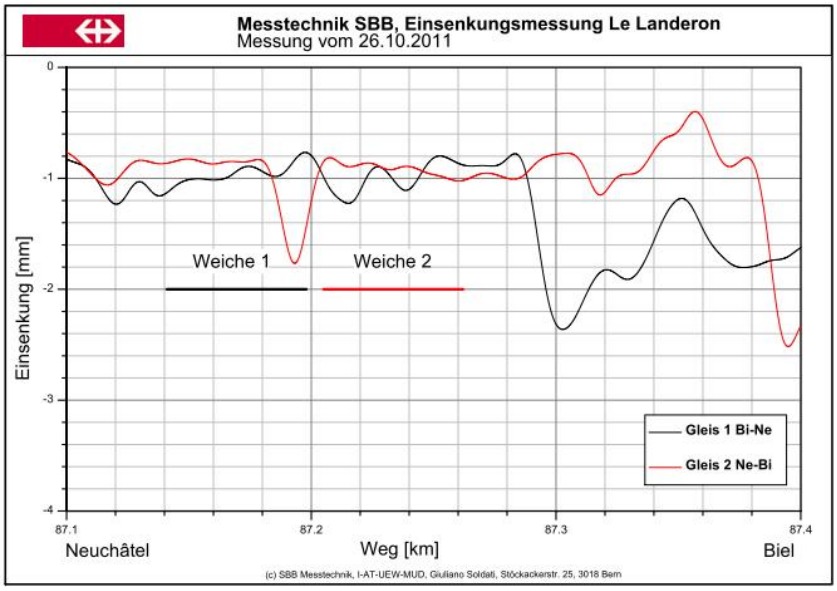

Figure 4.32: Le Landeron, static track deflection measurement, turnout without USP, [39]

4.2.2 Condition of Frog and Maintenance State of Turnout

For the assessment of the frog condition, measurements were performed by DB [40] using an ESAH-M measurement device at the same time as the BAM measurements. All the four turnouts were investigated in Rubigen, two with USP and two without USP. Sleeper accelerations were measured on four sleepers at the frog. Results are averages of several train pass-by events. Sleeper deflections are derived from a double integration of the local sleeper acceleration.

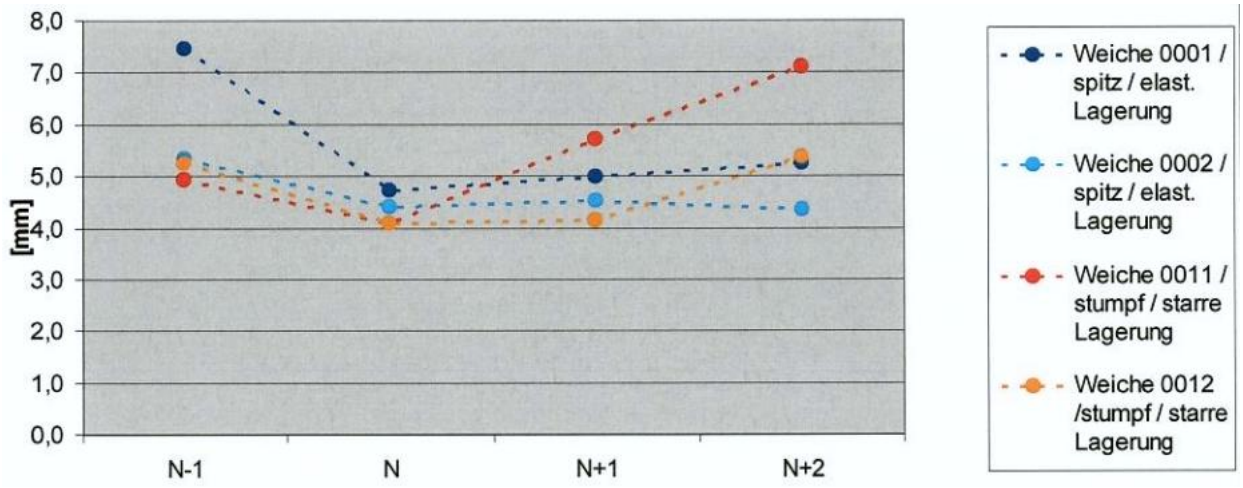

Figure 4.33: Rubigen, mean sleeper deflection for all turnouts, [40]

Figure 4.33 compares the means sleeper deflections (all train pass-bys are averaged) for all turnouts. No significant differences are visible. This is in accordance with the train deflection measurements.

Acceleration levels of the frog for the four different turnouts are illustrated in Figure 4.34. Turnouts No.1 and No.2 with under sleeper pads and turnout No. 11 without under sleeper pads show comparable acceleration levels for several train pass by events. However, turnout No.12 without under sleeper pads shows lowest acceleration levels by a factor of 3 and up to a factor of about 5. Turnout No.12 seems to be optimally installed. Turnout No.12 without under sleeper pads showed lowest acceleration levels measured at the frog. However, sleeper deflection levels for turnout No.12 did not differ significantly when compared to deflection levels of turnouts No.1 and No.2 with under sleeper pads and turnout No.11 without under sleeper pads, see Figure 4.33.

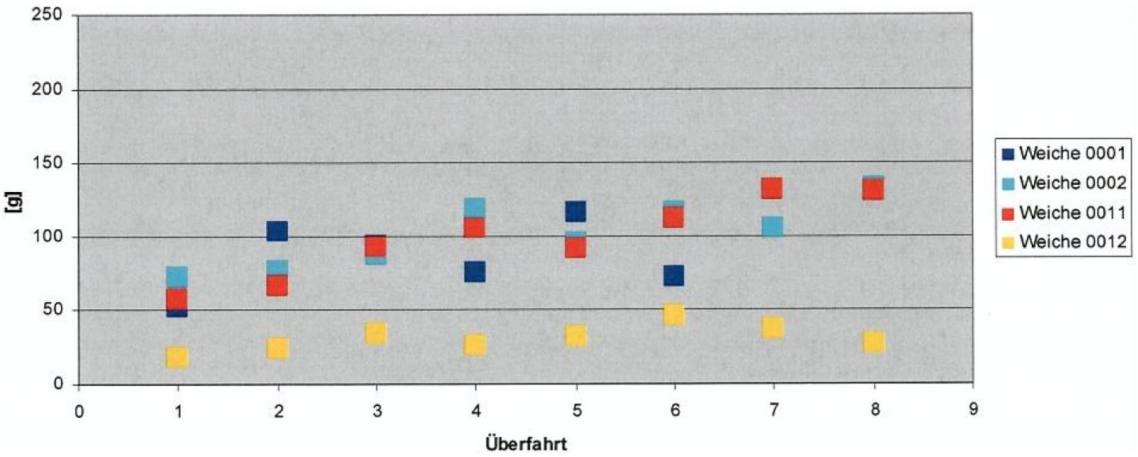

Figure 4.34: Rubigen, frog acceleration levels, turnout with/without USP, [40]

The turnouts in Rubigen were installed in 2005. Turnout maintenance was done in 2010 for all 4 turnouts. However, turnout No.12 obviously is in much better condition and therefore the measured accelerations at the frog were much lower when compared to turnout No.11 or the other turnouts.

As the deflection measurements (see Figure 4.29, 4.30) show no significant difference to the other turnouts, the difference in Figure 4.34 is probably due to geometry effects influencing wheel transitions.

4.2.3 Summary and Concluding Remarks

Static track deflection measurement for turnouts with under sleeper pads and turnouts without under sleeper pads showed no significant difference in deflection levels when compared to the track before and after the turnout. This indicates that the turnout has at the sites Rubigen and Le Landeron no hanging sleeper influence on vibration emissions.

The use of under sleeper pads resulted in an increased static track deflection in Rubigen by about 0.3mm. The material properties of the under sleeper pads ($0.22N/mm^3$) can explain the observed increase as well as the difference of sub-layer and ground conditions. The use of under sleeper pads resulted in a decreased static track deflection in Le Landeron by about 0.1mm. This does not correspond to the under sleeper pad material properties and the unexpected result is probably due to the track superstructure. This could have influence on vibration measurements next to the track.

The measurements in the turnouts (measurements at sleeper, frog, rail) cannot be properly compared: On the one hand not exactly the same train was running over the turnouts (no test trains, but comparison of same train category). On the other hand the turnouts with USP have train pass-by over the facing point whereas for turnouts without USP the pass-by is over the trailing point.

4.3 CONCLUSION

In Rubigen turnout Nr.12 showed low vibration impact on the frog. This could be an ideal turnout, but the parameters to result such an ideal turnout have to be investigated. The vibration measurements at turnout Nr.12 did not show relevant differences to turnout Nr.11 (see Figure 4.21). The vibration measurement results of Le Landeron and even more for Rubigen seem to be influenced by turnout condition and ground condition. The influence is too big to determine effects of USP in the low frequency range. Therefore conclusions cannot be obtained so far but there is a need of properly defining the turnout status, that means direct correlations of turnout parameters with vibration emission measurements. A first option could be the DB measurement method for turnout quality, the second is axle box measurements (see DB measurement car CTM in Section 2.7).

5. MITIGATION OPTIONS

Note: most of the mitigation measures found in literature reduce contact forces. The efficiency of the reduction should be pondered with the propagation in the ground by using an appropriate model. The following options shown are not yet tested or fully validated for vibration mitigation and could be mitigation options to decrease the turnout-amplification.

Reasons why a turnout could generate more vibrations are:

- Wheel transition over frog is not ideal because of vertical track geometry and vertical switching nose geometry (incl. maintenance state)
- Wheel transition over frog is not ideal because of horizontal track geometry and horizontal switching nose geometry (incl. maintenance state)
- Smaller radii of the turnout provoke more vibrations
- Not optimized elastic layers (baseplate stiffness and USP stiffness should be softened)

5.1 CONTROL OF GEOMETRY

The control of geometry is described in Section 2.4.1. The most promising solution from the INNOTRACK project was: Superelevation of the wing rail and profiling with a negative wheel shape to reduce the vertical wheel movement (MaKüDe).

It is known from track experts that the installation geometry of a turnout is not always perfect. This could be the reason for additional impact and faster wear of a turnout and hence for higher vibration emissions. So far this solution has not been tested with vibration measurements next to the track.

From tests with softer pads under the rail (see Figure 2.24) it is seen that the impact on the frog can be influenced by hanging sleepers at the frog.

Another approach could be to find out what is the difference between a good turnout behavior (“ideal turnout”, see Rubigen turnout nr. 12) and a turnout with normal and high impacts. It is important to identify the parameters provoking an ideal turnout.

Further modeling is needed to understand the wheel transition over the crossing nose and to see geometry parameter effects on this wheel transition. Further tests are needed to define the relevant geometry parameters influencing the turnout-amplification. If an improvement of the interaction of wheel transition and rail geometry can be obtained, then the turnout-amplification as well as the frog maintenance are improved.

5.2 SOFT USP

See the analysis in Section 3.4 of two softer USP tests for turnouts (Austria, Belgium). The experience for softer USP seems better than for the stiffer USP in Switzerland. Until now it is not

fully understood why softer USP should give much better results than stiffer USP, as both types should improve the track geometry of a turnout.

Therefore, SBB would like to test softer USP for vibration mitigation under controlled circumstances in the future. The same stiffness (c_{stat}=0.1 N/mm^3) as for open line curve test shall be used. Because of time reasons it will not be possible to have such results before the end of the RIVAS project.

5.3 SOFTER RAIL PADS

In Section 2.3.2 the softer rail pads are explained and give relevant reduction of impact forces.

So far this solution has not been tested with vibration measurements next to the track.

5.4 OTHER SOLUTIONS

Solutions such as stiffening of the track/turnout (stiffened turnout of Korus is not investigated, see INNOTRACK), concrete baseplate under the track and barriers directly next to the track are not studied in this report because they seem not to be enough cost-effective.

5.5 SBB PROJECT "TURNOUT 2015"

SBB has an innovation project ("Turnout 2015") to improve turnouts concerning maintenance. The impacts of the crossing nose of a turnout are also questioned and a combination of measures shall be tried to improve the situation. The point of view of this turnout innovation seems to be in line with the vibration mitigation perspective, as both perspectives pursue to have less load impact in the crossing nose of the turnout.

SBB started end of 2012 and installed 3 EW 900 turnouts. Further test installations are planned, see Figure below.

Year	Tests	Reason for test
2012	Installation Wichtrach W2: 26.10.2012 Installation Wichtrach W1: 28.10.2012 Installation Kloten W10: 11.11.2012	- Demonstration, feasibility - Improvements
2013	Further tests..	3-5 turnouts for IBAV Systems (Roll-systems.
2014	Further tests: 3-5 turnouts	- Definition of all components
2015	Start of normal installations	EW-900-1:19

Figure 5.1: Planning of SBB test installation "Turnout 2015"

The SBB "Turnout 2015", see Figure 5.2, has a manganese mono-bloc frog and is treated with explosive shock hardening (see also Section 3.2). The combination of layers below rail (softer baseplate) and sleeper (USP for the whole turnout) are optimized.

Figure 5.2: SBB “Turnout 2015”: manganese mono-bloc frog with explosive shock hardening left picture, sleeper with USP right picture

The rail inclination is continuous and 1:40. The rail profile is 60E2. The steal quality R350HT is stiffened but not the mono-bloc frog (Manganic)

From the future tests also indications should follow if further improvements are possible and needed for vibration mitigation (such as rail profiles, geometry, soft layers).

5.6 CONCLUSION

The best approach to improve the turnout-amplification is a system-approach where different parameters are changed and interact in a harmonic way. The SBB innovation “turnout 2015” could be such an approach and should be tested in 2013. From these tests also indications should follow if further improvements are possible and needed for vibration mitigation (such as rail profiles, geometry, soft layers).

Another approach could be to find out what is the difference between a good turnout behavior (“ideal turnout”, see Rubigen turnout nr. 12) and a turnout with normal and high impacts. It is important to identify the parameters provoking an ideal turnout.

Further modeling is needed to understand the wheel transition over the crossing nose and to see geometry parameter effects on this wheel transition. Further tests are needed to define the relevant geometry parameters influencing the turnout-amplification. If an improvement of the interaction of wheel transition and rail geometry can be obtained, then the turnout-amplification as well as the frog maintenance are improved.

6. CONCLUSIONS AND NEXT STEPS

Conclusions Chapter 2: From differences in vibration turnout-amplifications it could be concluded that there are possibilities to improve the switching nose part of a turnout. The wheel transition over a turnout shows that geometry is important for optimum and low energy impacts at the crossing nose. There is an influence of vertical and horizontal geometries.

Conclusions Chapter 3: So far it is not possible to draw definitive conclusions from the existing tests outside of RIVAS which solution could be a cost-effective mitigation measure for a turnout. A chance to improve the vibration excitation of a turnout lies in softening the USP for better track behavior (unfortunately, it is unclear why softer USP should be better for track geometry than stiffer USP), to improve the turnout design (material and geometry of frog and geometry of turnout) and to soften the rail pad.

Conclusions Chapter 4: The vibration measurement results of Le Landeron and even more for Rubigen seem to be influenced by turnout geometrical condition and ground condition. The influence is too big to determine effects of USP in the low frequency range. Therefore conclusions cannot be obtained so far but there is a need of properly defining the turnout status that means direct correlations of turnout parameters with vibration emission measurements. A first option could be the DB measurement method for turnout quality; the second is axle box measurements (see DB measurement car CTM in Chapter 2). In Rubigen a turnout showed low vibration impact on the frog and in total two turnouts showed low turnout-amplification. These could be “ideal” turnouts, but the parameters that lead to such an ideal turnout have to be investigated.

Conclusions Chapter 5: The best approach to improve the turnout-amplification is a system-approach where different parameters are changed and interact in a harmonic way. The SBB innovation “turnout 2015” could be such an approach and should be tested in 2013. From these tests also indications should follow if further improvements are possible and needed for vibration mitigation (such as rail profiles, geometry, soft layers). Another approach could be to find out what is the difference between a good turnout behavior (“ideal turnout”, see Rubigen turnout nr. 11, nr. 12) and a turnout with high impacts.

It is important to identify the parameters provoking an ideal turnout. Further modeling is needed to understand the wheel transition over the crossing nose and to see geometry parameter effects on this wheel transition. Further tests are needed to define the relevant geometry parameters influencing the turnout-amplification. If an improvement of the interaction of wheel transition and rail geometry can be obtained, then the turnout-amplification as well as the frog maintenance are improved. The following next steps are concluded:

Next steps:

Chalmers will simulate wheel–rail contact forces in turnouts and aim for an optimisation of crossing geometry that is robust for a range of nominal and worn wheel profiles. The magnitude and frequency content of the impact load at the crossing will be investigated. Sleeper velocities and/or forces in discrete springs modelling the ballast/subgrade stiffness could be predicted as an indication of the influence of crossing geometry on ground vibration.

End 2012, SNCF carried out a test campaign on a turnout trying to establish the contribution of each part of the turnout (joints, switch end, frog) and therefore of each excitation mechanism (impact load at the different joints and frog, parametric excitation) to the ground vibration velocity produced in the surrounding ground. First correlations will then be drawn between the excitation mechanisms, the contact force evolution along the turnout and the ground vibrations generated. Some parts of the measurement campaign will also allow validating Chalmers turnout-model. Results are planned to be delivered mid 2013.

The geometry influence on vibration excitation shall be studied for a few interesting turnouts by existing axlebox acceleration measurements over time (some years; SBB or DB has such data). This avoids an influence of differences in ground condition, turnout-type, passby direction, train velocity when looking at time histories. Correlations of the influence of frog geometry (maintenance status) with accelerations of wheelsets should be elaborated.

The new mitigation measure (SBB “Turnout 2015”) which is recently installed in Wichtrach between Bern and Thun shall be validated by ground vibration measurements if axlebox measurements in Spring 2013 indicate a positive geometry in comparison to normal turnouts on the same line.

REFERENCES

[1] E. Kassa, “Dynamic train-turnout interaction, Mathematical modelling, numerical simulation and field testing, Ph.D thesis,” Chalmers University of Technology, Gothenburg, Sweden, 2007.

[2] B. Palsson, “Towards Optimization of Railway Turnouts, Licenciate thesis,” University of CHALMERS, Gothenburg, Sweden, 2011.

[3] H. Steiger: Vorgang des Radüberlaufs bei Herzstücken mit starrer bzw. beweglicher Spitze, SBB internal report, 31.10.2005.

[4] Roland Müller: Aktuelle Probleme der Berührgeometrie. Glasers Annalen 10.10.2003.

[5] Bernhard Lichtberger: Handbuch Gleis. Tetzlaff Verlag 2003.

[6] V.L. Markine, M.J.M.M. Steenbergen, I.Y. Shevtsov, “Combatting RCF on switch points by tuning elastic track properties”, Wear, vol. 271 (1-2), pp. 158-167, 2011.

[7] B. Palsson and J. C. O. Nielsen, “Track Model Validation for Simulation of Train–Turnout Dynamics.”

[8] C. P., O. K., and B. H., “On the effects of high resilient undersleeper mats in turn-outs built in main line ballasted track, on ballast degradation, track stability and ground borne noise levels.,” in Proceedings of the 8th International Workshop on Railway Noise, Buxton, UK, 8-11, 2004.

[9] E. Kassa, J. C. O. Nielsen, and D. Nicklisch, Recommendation of, and scientific basis for, optimization of switches & crossings – part 1, INNOTRACK Guideline, Deliverable 3.1.5,. p. 27 pp+ 2 appendices.

[10] D. Nicklisch, E. Kassa, J. Nielsen, M. Ekh, and S. Iwnicki, “Geometry and stiffness optimization for switches and crossings, and simulation of material degradation,” Proceedings of the Institution of Mechanical Engineers Part F Journal of Rail and Rapid Transit, vol. 224, no. 4, pp. 279–292, 2010.

[11] J. Y. Zhu, “On the effect of varying stiffness under the switch rail on the wheel–rail dynamic characteristics of a high-speed turnout,” Proceedings of the Institution of Mechanical Engineers, Part F: Journal of Rail and Rapid Transit, vol. 220, no. 1, pp. 69-75, Jan. 2006.

[12] B. Pålsson and J. C. O. Nielsen, “Wheel – rail interaction and damage in switches and crossings,” Vehicle System Dynamics, vol. 50, no. February 2012, pp. 37–41, 2012.

[13] B. Pålsson and J. C. O. Nielsen, “Design optimization of switch rail profiles in railway turnouts. Proceedings,” in 9th International Conference on Contact Mechanics and Wear of Rail/Wheel Systems, pp. 655–665.

[14] A. Mirza, J. C. O. Nielsen, and P. Ruest, “Train Induced Ground Vibration – Influence of Rolling Stock - State-of-the-Art Survey - RIVAS D5.1,” 2011.

[15] J. C. O. Nielsen, “RIVAS D2.1 Classification of Track Conditions with Respect to Vibration Emission – Part 1: Classification of Track Irregularities and Numerical Simulations,” 2012.

[16] E. Kassa and J. C. O. Nielsen, “Dynamic interaction between train and railway turnout: full-scale field test and validation of simulation models,” Vehicle System Dynamics, vol. 46, no. sup1, pp. 521–534, Sep. 2008.

[17] Epp: Terzbandspektren-Analysen von VIBRA-3 Daten. SBB interner Bericht, 19.1.1998.

[18] F. Krüger: Schall- und Erschütterungsschutz im Schienenverkehr. 2001

[19] R. Müller, SBB-BahnUmwelt-Center: Emission und Weichenzuschlag für Weichentyp EW 1600/2600. Messung Rupperswil. Interner Bericht Mai 2000.

[20] R. Müller, SBB-BahnUmwelt-Center: Weichenzuschlag für EW 900. Messung Hindelbank. Interner Bericht Mai 2000.

[21] R. Müller, SBB-BahnUmwelt-Center: Bewegliche Weichenherzstücke. Erschütterungsmessungen Lenzburg. Interner Bericht Mai 2000.

[22] R. Müller, SBB-BahnUmwelt-Center: Dämmwirkung von Unterschottermatten. Rothrist Bereich III Weichen. Interner Bericht Mai 2000

[23] Rutishauser Ingenieurbüro: Bewegliche Herzstücke in Weichen, Erschütterungsmessungen, Nutzen und Kosten, Sicherheitsaspekte. Juni 1999

[24] Rutishauser Ingenieurbüro: Erschütterungsmessungen Bhf Othmarsingen, Weichen mit und ohne bewegliches Herzstück. 13.7.2000.

[25] R. Müller: Messbericht zu Erschütterungsmessungen in Rüschlikon, bewegliches Herzstück. SBB-BahnUmwelt-Center, internal report. 3.1. 2006

[26] W. Steinhauser: Eisenbahnerschütterungen-Emissionsmindeung durch den Einbau besohlter Schwellen und Weichen mit beweglichem Herz. DACH-Tagung, 2007.

[27] D. Leibundgut: Erschütterungsmessungen Altstetten. Versuchsweiche mit explosionsverfestigtem Manganguss-Herzstück. SBB measurement report. 19.08.2008

[28] J. Melke: Materialien 22 Erschütterungen und Körperschall des landgebundenen Verkehrs: Prognose und Schutzmassnahmen, 1995.

[29] K. Köstli: Messungen in Rubigen bei Weichen mit und ohne Schwellenbesohlungen. SBB analysis report. 2007.

[30] Rutishauser Ingenieurbüro: Messungen Spurwechsel Stadelhofen. Measurement report. 2007.

[31] F. Auer, R. Schilder: Technische und wirtschaftliche Aspekte zum Thema Schwellenbesohlung – Teil 1: Langzeiterfahrungen im Netz der ÖBB. ZEVrail 133, 4.4.2009.

[32] R. Müller: Betonplatte/Bodenverfestigung als Erschütterungsschutzmassnahme, Schotterfahrbahn auf offener Strecke. Literaturstudy. Internal paper. 29.9.2008.

[33] Gartenmann Engineering: Messbericht zu Schlitz bei einer Weiche (Fischmättelistrasse 7). Symposium Ziegler Consultants, Dübendorf, 2005.

[34] R. Müller, SBB-BahnUmwelt-Center: Messungen Bevaix Mai 97 mit Massnahmen. Internal report, 1997.

[35] S. Said, L. Auersch, E. Knothe: Mitigation measures for switches in Rubigen and Le Landeron, Switzerland. Part of Deliverable D3.12. Report December 2012. Respectively (S. Said: Messung der Ausbreitung der Bodenerschütterung ausgehend von Eisenbahnweichen mit und ohne Schwellenbesohlung in Rubigen und Le Landeron. BAM, 25.01.2012)

[36] A. Ziegler: „Erschütterungen Rubigen“, Ziegler Consultants. Measurement report 20.02.2012

[37] A. Ziegler: „Erschütterungen Le Landeron“, Ziegler Consultants. Measurement report 20.02.2012

[38] G. Soldati: Einsenkmessung Rubigen, Untersuchungsprogramm "elastisch gelagerte Weichen". SBB Mess- und Diagnosetechnik. Measurement report 25.10.2011

[39] G. Soldati: Einsenkmessung Le Landeron, Untersuchungsprogramm "elastisch gelagerte Weichen". SBB Mess- und Diagnosetechnik. Measurement report 26.10.2011

[40] Auswertebericht zu Messungen im Pilotprojekt der SBB “Erschütterungsschutz-elastische Weichenlagerung“. DB AG. Measurement report 2.11.2011